EVALUATING THE BIOGENICITY OF FLUVIAL-LACUSTRINE STROMATOLITES FROM THE MESOPROTEROZOIC COPPER HARBOR CONGLOMERATE, UPPER PENINSULA OF MICHIGAN, USA

by

Nicholas D. Fedorchuk

A Thesis Submitted in

Partial Fulfillment of the

Requirements for the Degree of

Master of Science

in Geosciences

at

The University of Wisconsin-Milwaukee

May 2014

ABSTRACT
EVALUATING THE BIOGENICITY OF FLUVIAL-LACUSTRINE STROMATOLITES FROM THE MESOPROTEROZOIC COPPER HARBOR CONGLOMERATE, UPPER PENINSULA OF MICHIGAN, USA

by

Nicholas D. Fedorchuk

The University of Wisconsin-Milwaukee, 2014
Under the Supervision of Professor Stephen Dornbos

The Mesoproterozoic (1.09 Ga) Copper Harbor Conglomerate represents alluvial fan, fluvial and lacustrine deposition in the Midcontinent Rift System. The formation outcrops in the Keweenaw Peninsula in the northwestern part of the Upper Peninsula of Michigan where it contains carbonate stromatolites preserved within both siltstone and conglomerate facies. The purpose of this study is to evaluate the biogenicity of these stromatolites, which lack direct microfossil evidence. The stromatolites were placed into their depositional context, their macro-scale features and thin section microfabrics were analyzed, and growth angles were measured of cobble-draping samples to determine if a phototrophic response existed. A methodology that uses magnetic susceptibility as a biosignature was also performed on these stromatolites. The results of these analyses reveal two distinct types of stromatolites. Stromatolites from the siltstone facies are interpreted as biogenic. They contain detrital laminae, hematite-rich micritic laminae, and fenestral fabrics. The stromatolites formed as microbial mats grew over a mudflat or sandflat with carbonate filled dessication cracks on an eroded topography. Stromatolites from the conglomerate facies are interpreted to have formed by a mix of chemical and

biological processes. They are microdigitate and have abiogenic features such as isopachous laminae with radial fibrous calcite fans and botryoids. They also lack a phototrophic response, suggesting that growth was not controlled by cyanobacteria. These stromatolites also have some biogenic signatures such as conical wavy laminae that have been separated by gas build-ups. These stromatolites are interpreted as having formed in a flooded braidplain setting with restricted circulation. Magnetic susceptibility tests yielded inconclusive results in this case because the stromatolites in question contain secondary hematite. This study supports previous studies of these stromatolites, as well as microbial structures and organic-rich paleosols that have suggested freshwater microbial communities were abundant in the Midcontinent Rift during the Mesoproterozoic. It also highlights how variable environmental factors can influence stromatolite growth, even in similar depositional settings and with a consistent microbial presence.

To my parents,
Robert and Rosemary Fedorchuk
and my aunt,
Mary K. Fedorchuk

TABLE OF CONTENTS

LIST OF FIGURES

ACKNOWLEDGMENTS

I would like to especially thank my advisor Dr. Stephen Dornbos for all of his expert input and encouragement throughout the course of this project. He helped me see this project through from start to finish and none of this would be possible without him. I would also like to thank Dr. Frank Corsetti for his advice and for using his equipment to photograph my samples. I would like to thank Dr. John Isbell, Dr. Julie Bowles, Dr. Mark Harris and Dr. Victoria Petryshyn for all of the time and energy that they have committed to helping me learn new techniques and providing me with invaluable guidance over the past two years. I would like to thank Dr. Thomas Hooyer for access to his laboratory equipment and Dr. Brent Briethaupt for his generous support. Dylan Wilmeth aided this project as an outstanding field assistant. Without Dylan's help my car may still be stuck in the Upper Peninsula of Michigan. Hanna Yousuf and my parents have supported me throughout the past two years and I would like to thank them as well. There is absolutely no way this project would exist without the help and encouragement of all of these people so I wish to express my sincere appreciation. This study was supported financially by the Institute on Lake Superior Geology, the Wisconsin Geological Society, and the University of Wisconsin-Milwaukee Department of Geosciences.

1. Introduction

Microbially induced sedimentary structures (MISS) and carbonate stromatolites found within the Mesoproterozoic (1.09 Ga) Copper Harbor Conglomerate of northern Michigan have been interpreted as evidence for freshwater microbial communities that colonized the failed Midcontinent Rift System (Elmore, 1983; Wilmeth et al., 2014). The purpose of this study is to better characterize the stromatolites preserved within the Copper Harbor Conglomerate and employ multiple methodologies to evaluate their biogenicity. There are other signs of microbial activity in the Midcontinent Rift System during the Mesoproterozoic as well. The Nonesuch Shale which directly overlies the Copper Harbor Conglomerate contains an abundance of organic carbon (Elmore et al., 1989; Pratt et al., 1991). Additionally, paleosols containing organic matter have been described within interflow deposits of the Portage Lake Lava Series which interfingers with the Copper Harbor Conglomerate (Mitchell and Sheldon, 2009, 2010; Sheldon, 2012). However, some of the stromatolites from the Copper Harbor Conglomerate exhibit characteristics of abiogenic structures. These characteristics include radial-fibrous calcite fans that form through the direct inorganic precipitation of calcite as opposed to microbially induced formation. Additionally, there is a lack of microfossil evidence in the Copper Harbor stromatolites that conclusively provide evidence of prokaryotes (Elmore, 1983). This highlights the need to explore new methods of evaluating stromatolite biogenicity in the absence of microfossil evidence. This study tests the hypothesis that the Copper Harbor Conglomerate stromatolites formed primarily through biogenic processes.

2. Previous Work

2.1 Stromatolites

Usage of the term stromatolite remains the subject of much debate. Difficulty defining stromatolites is based on the fact that they are both simultaneously fossils and sediment, containing biologic, stratigraphic and sedimentologic elements (Riding, 1999). However, stromatolites have been used extensively as evidence for the earliest life, as well as indicators of geochemical conditions, during the Precambrian (Grotzinger and Knoll, 1999). A stromatolite definition that is suitable to this study is "an attached, laminated, lithified sedimentary growth structure, accretionary away from a point or limited surface of initiation" (Semikhatov et al., 1979). This definition is broad enough to allow for the role of both abiogenic and biogenic processes in forming the stromatolites relevant to this study.

2.1.1 Biogenic Formation

The defining laminae of stromatolites are created through the episodic processes of sediment trapping and binding and/or mineral precipitation (e.g., Walter, 1976; Grotzinger and Knoll, 1999; Riding, 2000; Riding, 2011). Trapping occurs due to the blockage of grain movement (baffling) or adhesion to the extracellular polymeric substance (EPS) produced by microbes (Riding, 2000). The trapping of sediments occurs in conjunction with the binding of sediment as organic matter overgrows the trapped material. Trapped, detrital grains form a new substrate on which microbial growth can occur and a new succession of trapping can begin (Riding, 2000). Early lithification of stromatolite laminae provides the rigid structure and the stability of the structure to grow

upright. It allows stromatolites to take on domal or columnar morphologies and to outpace the deposition of surrounding sediment (Riding, 2000). The precipitation of minerals out of alkaline waters can be induced by the presence of microbes. The photosynthetic uptake of CO_2 by cyanobacteria results in a local increase in alkalinity ($H_2O + CO_2 \rightleftharpoons H_2CO_3$) that drives the equilibrium reaction ($CaCO_3 \rightleftharpoons Ca^{2+} + CO_3^{2-}$) towards the precipitation of calcium carbonate (Schneider and Le Campion-Alsumard, 1999; Kamennaya et al., 2012). However, an increasing number of studies have highlighted the importance of heterotrophic communities, such as sulfate reducing bacteria, in the biomineralization of microbial mats (e.g. Zavarzin, 2002; Dupraz et al., 2004; Visscher and Stolz, 2005; Dupraz et al., 2009). The degradation of EPS by heterotrophic communities releases Ca^{2+} ions which can drive the production of calcium carbonate in an alkaline setting (Dupraz et al., 2009).

2.1.2 Abiogenic Formation

There is also evidence that encrusting cements are capable of forming stromatolites and associated morphologies without a biogenic component (e.g., Grotzinger and Rothman, 1996; Knoll and Semikhatov, 1998; Grotzinger and Knoll, 1999). Grotzinger and Rothman (1996) used the Kadar-Parisi-Zhang (KPZ) equation to demonstrate that some stromatolite forms such as domal morphologies can be created abiotically. Additionally, a diffusion limited aggregation (DLA) model in which particles (sediment, ions, and nutrients) arrive at an aggregate through a path similar to Brownian motion (diffusion) can be coupled with episodic sedimentation to create columnar branching stromatolite morphologies (Grotzinger and Knoll, 1999). Evidence of

abiogenic precipitation includes very fine laminations, oscillating Ca/Mg ratios between laminae, and compositional differences between stromatolites and the surrounding sediment. For example, when calcareous stromatolites are entirely surrounded by siliciclastic sediment it suggests that trapping and binding were not involved in stromatolite formation (Grotzinger and Knoll, 1999). In addition, a number of different cement textures within stromatolites have been recognized as indicators of direct precipitation. These include textures such as radial fibrous, herringbone calcite, radiaxial fibrous, and fascicular optic calcite or dolomite (Sumner and Grotzinger, 1996; Grotzinger and Knoll, 1999).

2.2 The Copper Harbor Stromatolites

The Copper Harbor Conglomerate stromatolites were initially described by Hedlund (1953) and Cornwall (1954). Since then, they have been described or mentioned numerous times (e.g. Elmore, 1983; Elmore, 1984; Nishioka et al., 1984; Kalliokoski, 1986; Elmore et al., 1989; Ojakangas et al., 2001; Wilmeth et al., 2014). Elmore (1983) offered the most detailed description of the stromatolites as contorted beds in mudstone and as laterally linked hemispheroids that drape over cobbles. He interpreted the stromatolites to be biogenic in origin based on their general morphology and microfabrics. For example, he points out that there are detrital grains trapped on the highly inclined sides of cobble-draping hemispheroids that must have been stabilized by microbes. Elmore (1983) also mentions the possible abiogenic characteristics of some stromatolites such as radial-fibrous calcite fans superimposed on the stromatolite laminae and calcite pseudomorphs after gypsum within the stromatolites. Nishioka et al. (1984)

observed copper occurrences within the stromatolite and offered detailed observations of the stromatolite microfabrics. They supported Elmore's (1983) claim of a biogenic origin based on observations of possible tubular microfossils within vugs, although identification of these microstructures was not definitive.

Elmore (1983) interpreted the stromatolites to have formed in ponded, abandoned fluvial channels within an alluvial fan system. He contended that the abandoned channels must have been large in order to facilitate the production of ooids and oncoids that are seen in the stromatolite bearing units. Elmore (1983, 1984) pointed out that the alluvial fan has characteristics of both wet and dry alluvial fans but dessication cracks and calcite pseudomorphs after gypsum suggest an arid or semi-arid climate (Elmore, 1984). Kalliokoski (1986) also supported an arid or semi-arid climate based on caliche horizons within the Copper Harbor Conglomerate and a paleolatitude of ~30º N. In order to explain standing water in abandoned channels, Elmore (1983, 1984) suggested that there were seasonal climate fluctuations that re-flooded abandoned channels and created the large standing ponds in which the stromatolites formed. Additionally, the nearby rift lake may have experienced an elevated water table and encroached on the distal alluvial fan, providing one method of re-filling the abandoned channels in an otherwise arid setting (Elmore, 1983).

3. Geologic Setting

The Copper Harbor Conglomerate is a Mesoproterozoic (1.09 Ga) freshwater succession located within the upper peninsula of Michigan, northern Wisconsin and on Isle Royale in Lake Superior. It ranges from 200 m to approximately 2,000 m in

thickness and fines upward (White and Wright, 1960). It is comprised of fluvial and alluvial fan derived volcanogenic sandstone and conglomerate that was infilling the Keweenawan Trough (Elmore, 1984). This basin is part of the Midcontinent Rift System which extends from Canada to Kansas and, before failing, threatened to split the North American Craton (Van Schmus and Hinze, 1985). The Copper Harbor Conglomerate represents the base of the Mesoproterozoic (Middle and Upper Keweenawan) Oronto Group and the earliest infilling of the Keweenawan Trough after the cessation of volcanic activity (Fig.1) (Dickas, 1986). Clast imbrications within the conglomerate suggest that sediment was being transported north, towards the center of the basin (Elmore, 1984). The conglomerate overlies and interfingers with a thick, mafic volcanic sequence known as the Portage Lake Lava Series. The Portage Lake Lava Series rests unconformably on the more felsic North Shore Volcanic Group (Wolff and Huber, 1973). U-Pb dating of zircons within the Portage Lake Lava Series has yielded ages of 1096.2 ± 1.8 Ma and 1094 ± 1.5 Ma. However, dating of clasts in the Copper Harbor Conglomerate shows an age of 1104 ± 2 Ma (Davis and Paces, 1990). This suggests that a lower Keweenawan source was the primary contributor of sediment to the Copper Harbor Conglomerate that was deposited during the middle Keweenawan (Davis and Paces, 1990).

The Copper Harbor Conglomerate is conformably overlain by the siltstones and mudstones of the Nonesuch Shale, which is upper Keweenawan in age. These green and black siltstones and mudstones represent a perennial lacustrine environment (Paleo-lake Nonesuch) that was contemporaneous with deposition of the Copper Harbor Conglomerate (Elmore et al., 1989). The conglomerate and overlying shale were

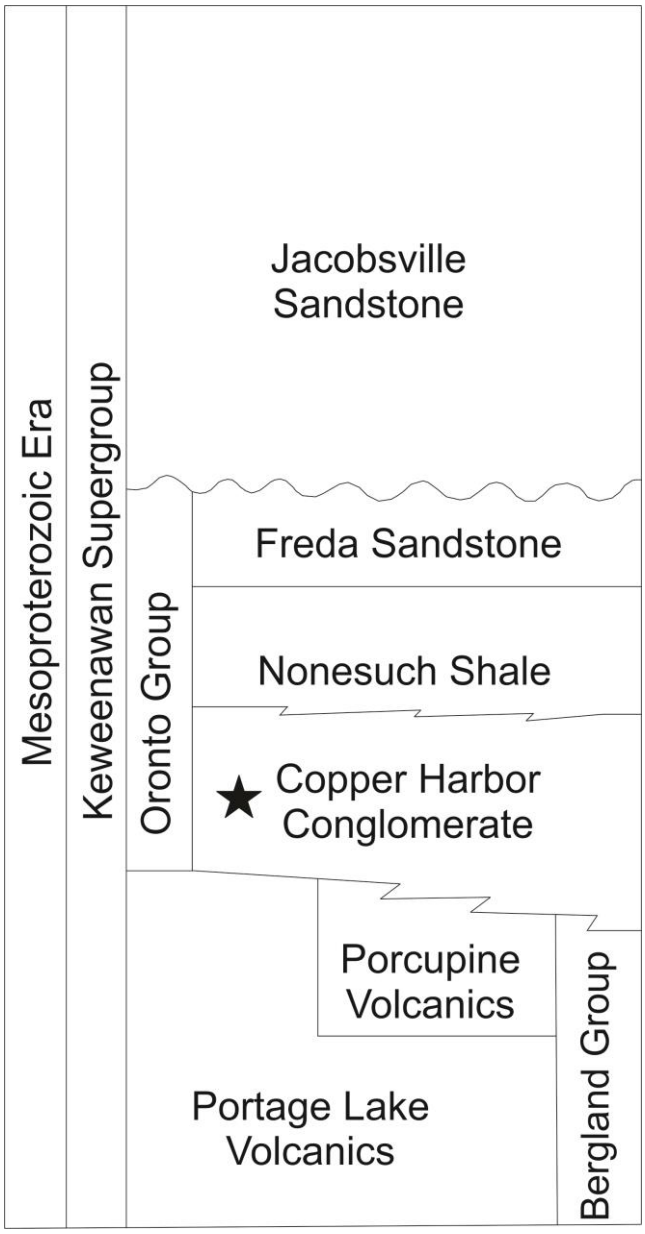

Fig. 1. General stratigraphy of Midcontinent Rift System in Michigan. Location of Copper Harbor Conglomerate marked with star. (Modified from Schmidt and Williams, 2003).

deposited as part of a transgressive-regressive sequence that has been interpreted to be controlled by subsidence and sediment supply (Elmore, 1984). Cyclical alluvial fan, fluvial and lacustrine sedimentation that is driven by subsidence is common in rift basin settings around the world such as the Permo-Triassic North Minch Basin of Scotland and the Jurassic-Cretaceous southern Gulf of Mexico Basin (i.e. Steel and Wilson, 1975; Blair, 1987). The overall pattern of subsidence within the Keweenawan Trough led to the Nonesuch Shale transgressing over the top of the Copper Harbor Conglomerate. The Nonesuch Shale is then overlain by red sandstones and shale of the Freda Sandstone which represents the final stage of basin infilling (Wolff and Huber, 1973; Elmore, 1984). This entire sequence dips ~30-40° to the northwest on the Keweenaw Peninsula in the upper peninsula of Michigan.

This study focuses on two localities on the northeastern tip of the Keweenaw Peninsula that were described by Elmore (1983, 1984). These localities are on the southern shore of Lake Superior and are approximately 13 km apart (Fig. 2). They correspond to two distinct facies where stromatolites occur within the Copper Harbor Conglomerate. The first locality is known as Horseshoe Harbor and is ~7 km east of the town Copper Harbor. The second locality is known as Dan's Point and is located ~6 km to the west of the town Copper Harbor.

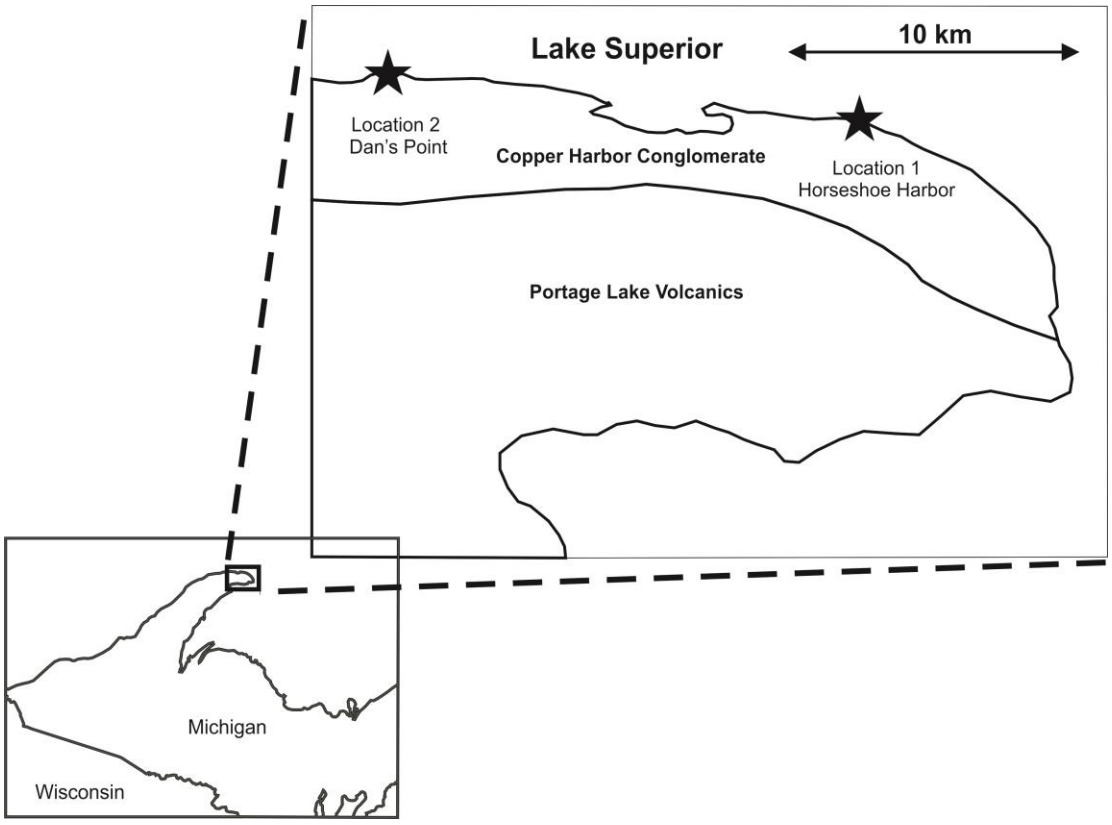

Fig. 2. Locality map of Keweenaw Peninsula in Upper Peninsula of Michigan. Two study localities are marked as stars: Location 1 corresponds to Horseshoe Harbor and Location 2 corresponds to Dan's Point. Horseshoe Harbor is located at 47°28.348' N and 87°48.130' W. Dan's Point is located at 47°28.781' N and 87°58.244' W.

4. Methods

Several different field and laboratory methods were used to evaluate the biogenicity of the Copper Harbor Stromatolites. In the field, stratigraphic sections were measured and described at both the Horseshoe Harbor and Dan's Point localities. Stromatolites were placed in their depositional context at both locations and their macro-scale features were noted. Stromatolites and associated sedimentary structures were photographed and large-scale outcrop photos were captured using a GigaPan robotic head to record facies changes. Eleven large (10-15 kg) stromatolite samples were collected from the two localities for laboratory analyses. Six were collected from Horseshoe Harbor and 5 were collected from Dan's Point. In the laboratory, stromatolite samples were serially sectioned into 30 slabs (~2 cm thick) and polished. Seven large (50 mm x 75 mm) petrographic thin sections, 4 from Horseshoe Harbor and 3 from Dan's Point, were made from internal stromatolite slabs. These sections were used for standard petrographic analyses such as Alizarin Red-S staining and reflected light. Photomosaics of entire thin sections were also created in order to better visualize the microfabrics. These photos allowed for the characterization of the gross morphology, microfabrics, and mineralogy of the stromatolites.

Petryshyn and Corsetti (2011) developed a method of evaluating stromatolite biogenicity using growth angles of individual stromatolite heads. They measured the growth angles of digitate cobble-draping stromatolites in Walker Lake, Nevada to determine if a preferential growth direction towards sunlight occurred (Fig. 3). This method is based on the assumption that stromatolite columns on all the sides of boulders will branch towards the direction of sunlight if a phototrophic response exists. On the

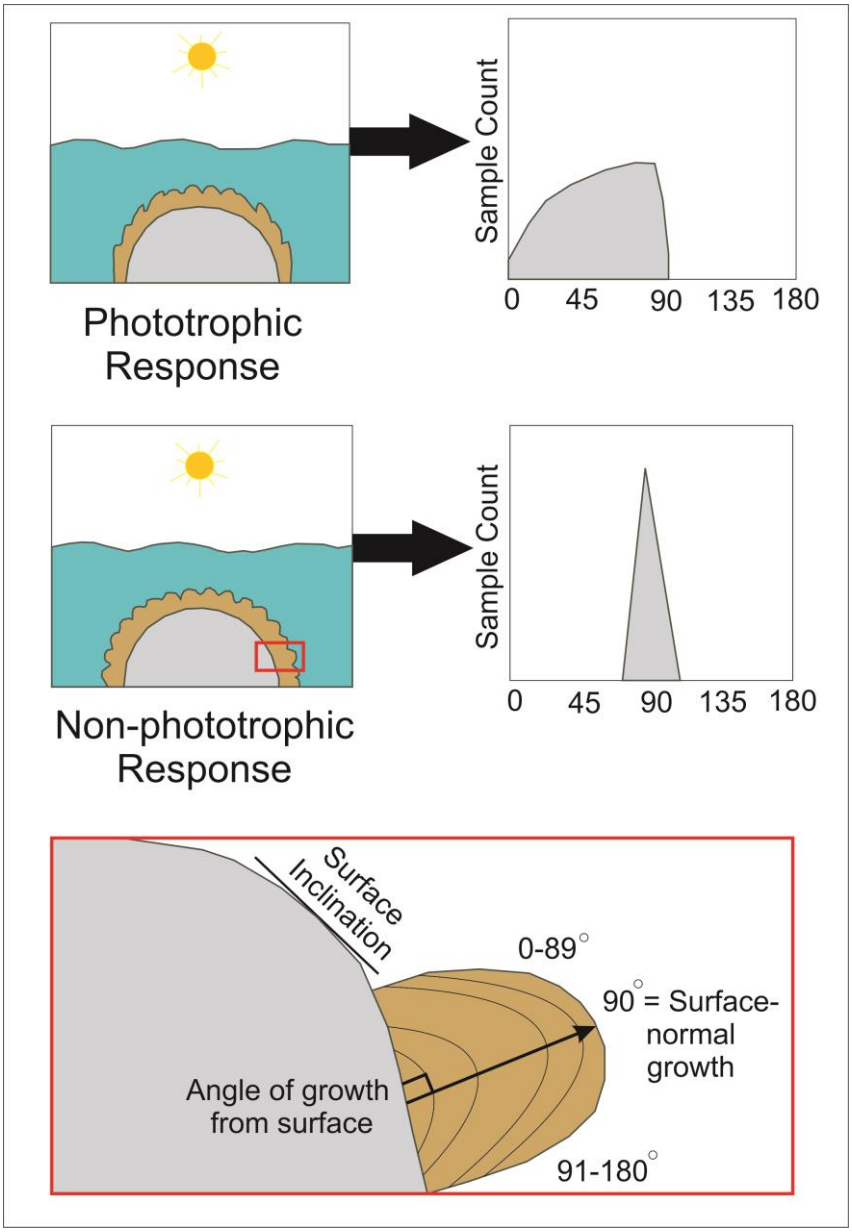

Fig. 3. Expected distribution of stromatolite growth angles from phototrophic response and non-phototrophic response. Surface normal growth is 90º while upwards growth is less than 90º and downwards growth is greater than 90º. (Modified from Petryshyn and Corsetti, 2011).

other hand, if stromatolite growth is dominated by abiogenic or non-phototrophic processes, then stromatolite columns will grow out approximately ninety degrees perpendicular from surface normal (the sides of the boulder) (Petryshyn and Corsetti, 2011).

This test alone cannot determine stromatolite biogenicity but it provides important evidence into whether or not growth was controlled by a phototrophic response. Additionally, the test is only applicable to cobble or boulder draping stromatolites so it was only used on the Dan's Point digitate cobble-draping stromatolites. The Horseshoe Harbor stromatolites are not cobble-draping, so this test could not be applied to them. To employ this method, 5 Dan's Point cobble-draping stromatolite slabs with 46 individual digitate stromatolites were analyzed. The growth angle of each stromatolite was measured relative to surface normal (Fig. 3) so that growth perpendicular to surface normal would measure at 90°. Stromatolites that branched upwards towards the top of the cobble or boulder would then measure less than 90°. Growth angles would only measure greater than 90° if the stromatolite branched downwards towards the substrate. The stromatolite growth angles were evaluated as a whole and also grouped according to the initial inclination of the growth surface to assure no bias.

Another method for testing stromatolite biogenicity uses magnetic susceptibility (Petryshyn et al. 2010). Magnetic susceptibility (χ) is a physical property that is the ratio of an induced magnetization to the inducing magnetic field. χ typically varies with the type and concentration of magnetic material. In most stromatolites, magnetic susceptibility is based on the distribution of detrital material, including magnetic grains, trapped within the stromatolite. Therefore, by measuring the magnetic susceptibility

along single laminae we can assess the amount of magnetic detrital material versus the depositional angle. The theory behind this methodology is that biogenic stromatolites are better at trapping sediment (including magnetic minerals) than abiogenic stromatolites because of the adhesive nature of microbial mats. For this reason, if there is a relatively high magnetic susceptibility on the high angle sides of stromatolites we would hypothesize that there was a microbial presence involved in trapping and binding the sediment in place. Support for this methodology has been found in both laboratory experiments and the measured susceptibility of ancient stromatolites (Fig. 4; Petryshyn et al., 2010). Elmore (1983) invoked detrital grains trapped at high depositional angles as possible evidence for his biogenic argument. This description was based on petrographic analysis so this study will attempt to use magnetic susceptibility to quantify Elmore's (1983) observation.

The methodology of Petryshyn et al. (2010) was followed to conduct this paleomagnetic test on Copper Harbor stromatolite samples. Two large slabs from Horseshoe Harbor stromatolites and 3 large slabs from Dan's Point stromatolites were used. The slabs were micro-drilled along transects that followed the contours of single laminae using a 1 mm diamond bit to collect ~20 mg of powder for each sample. A total of 45 samples were collected from 11 laminae transects. Eleven samples were collected from Horseshoe Harbor stromatolites and 34 samples were collected from Dan's Point stromatolites. For each sample, the depositional angle relative to the substrate was recorded. Samples from the very top of stromatolites were recorded at 0º and samples collected from the side (perpendicular to the substrate) were recorded at 90º. The powder was placed into 1 cm^3 plastic cubes for magnetic susceptibility analysis using a MFK1

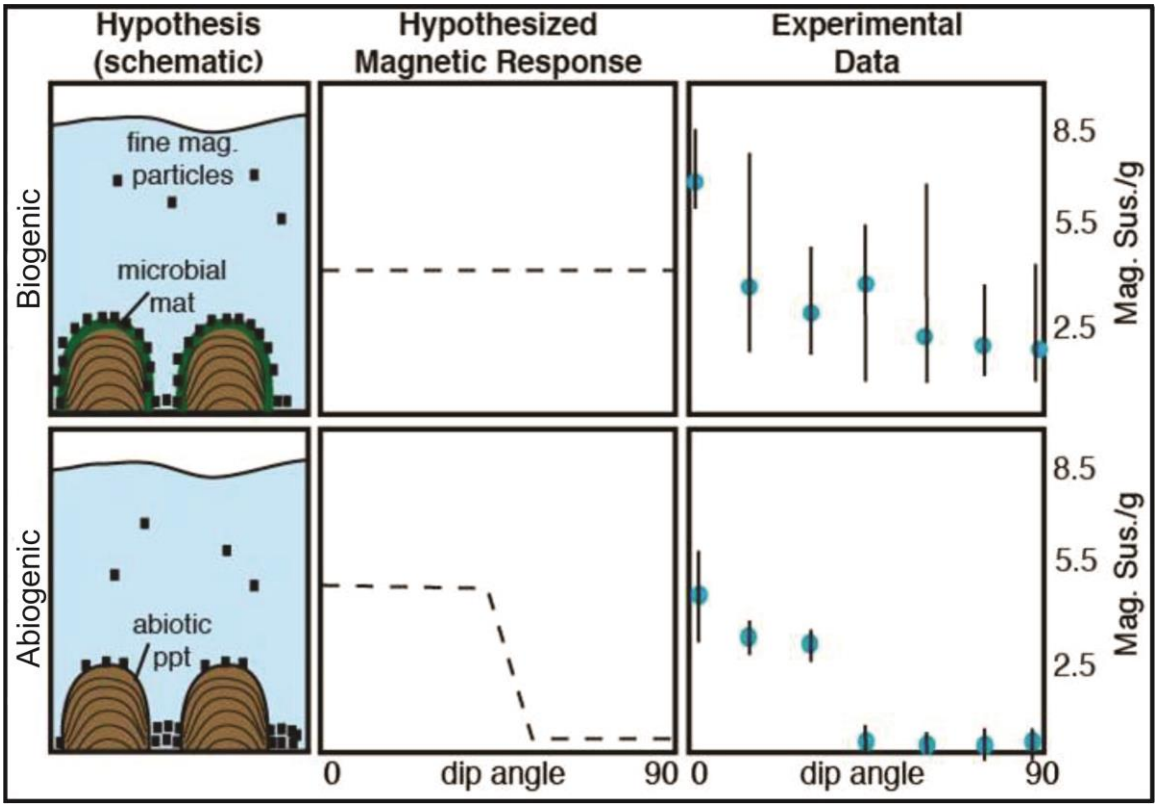

Fig. 4. Hypothetical and measured distribution, recorded by Petryshyn et al. (2010), of magnetic susceptibility versus laminae dip angle in biogenic and abiogenic structures. (Modified from Petryshyn et al., 2010).

Kappabridge. The measured mass normalized susceptibility was then compared to the depositional angle from which the samples were taken. In order to better understand the magnetic properties of the stromatolites, samples were heated using the MFK1 Kappabridge to identify the Curie temperature of the magnetic minerals. The natural remanent magnetization (NRM) was demagnetized via alternating field (AF) demagnetization. To further constrain magnetic mineralogy, isothermal remnant magnetization (IRM) acquisition was carried out in fields up to 1 T, followed by a back field 0.3 T IRM ($IRM_{-0.3T}$) to calculate the "hard" IRM (HIRM). The HIRM (e.g. Thomson and Oldfield, 1986) is calculated as 0.5 ($IRM_{1.0T}$ + $IRM_{-0.3T}$) and gives us the magnetization arising from high-coercivity minerals like hematite. We report HIRM/ $IRM_{1.0T}$ which then ranges from 0 for samples with only low-coercivity ($\leq$ 0.3 T) minerals like magnetite to 1.0 for samples dominated by high-coercivity (>0.3 T) minerals like hematite.

5. Results

5.1 Sedimentology and Field Observations

The Copper Harbor Conglomerate occurs on the Keweenawan Peninsula as a wedge of volcanogenic sediment that ranges from clay to boulder sized (0.5 m) grains. Volcanic rock fragments make up approximately 50-75% of the conglomerate and include basalt, andesite, trachyte, latite, quartz latite, and rhyolite (Wolf and Huber, 1973). Felsic rock types are more prevalent over mafic types. There are three major facies that can be observed at both Horseshoe Harbor and Dan's Point. These are a conglomerate facies, a siltstone facies and a trough-cross stratified sandstone facies.

Stromatolites are located in the siltstone facies and overlying the conglomerate facies (Fig. 5).

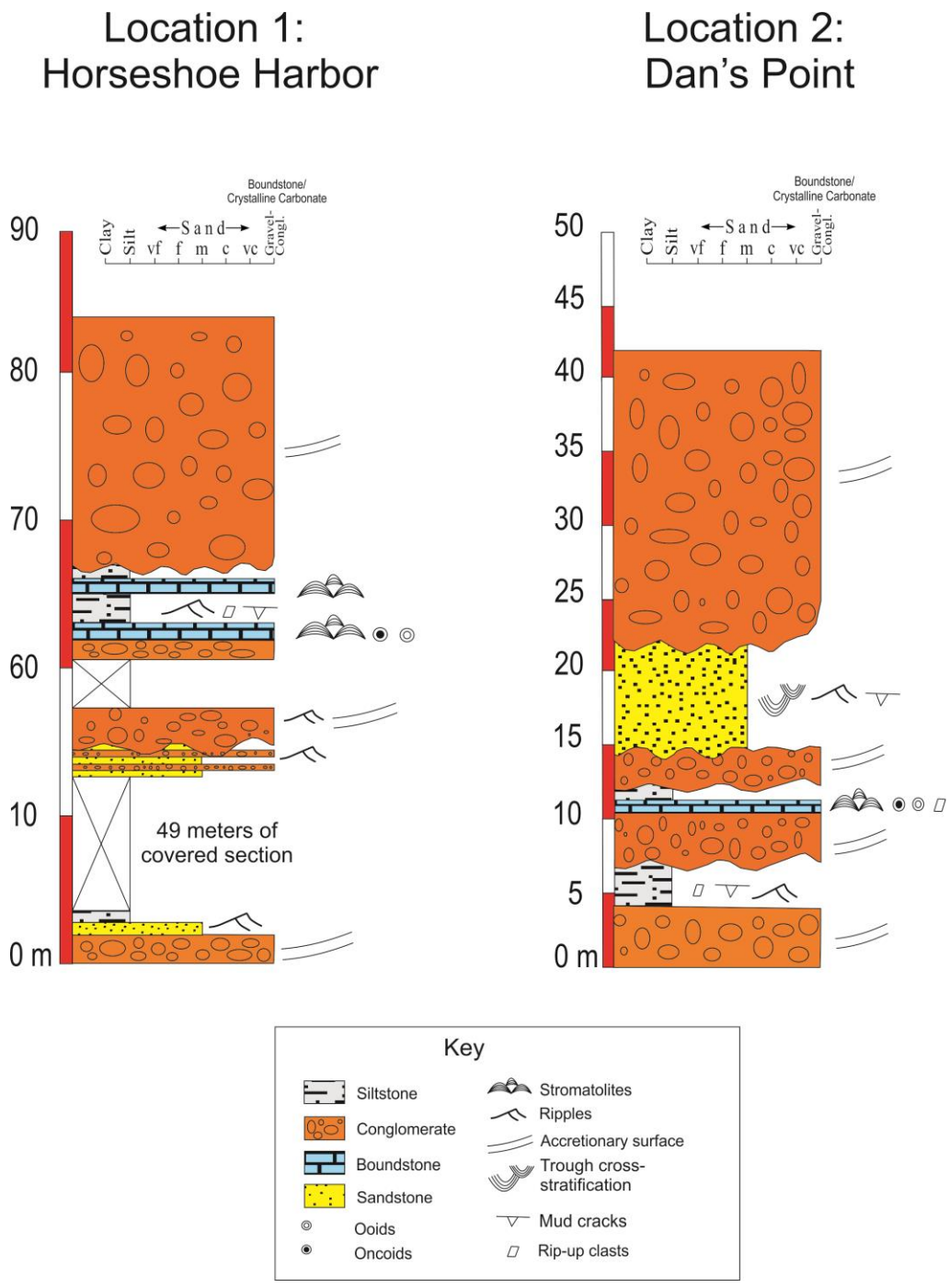

Fig. 5. Measured stratigraphic sections from Horseshoe Harbor and Dan's Point localities. Stromatolites occur above conglomerate facies and within siltstone facies.

5.1.1 *Conglomerate Facies*

The conglomerate facies is the most common facies at both Horseshoe Harbor and Dan's Point. Beds range from approximately 3-20 m in thickness. It is poorly sorted and contains well-rounded pebble to boulder sized clasts. The clasts are imbricated and indicate flow directions north towards the center of the basin (Elmore, 1984). The conglomerate matrix is a mixture of sand, silt, and clay sized grains and it alternates between intervals of grain support and matrix support. The conglomerate contains a diagenetic calcite and laumontite cement and has an erosional base (Elmore, 1984). It contains cross-bedded sandy channel fills with lateral and downstream accretion. The channels are approximately 2-15 m in width and lenticular in form. Thin discontinuous (2-10 m long and <5 cm thick) carbonate crusts can be found within the conglomerate facies and have been interpreted as caliche horizons formed by an evaporative arid or semi-arid setting (Kalliokoski, 1986).

The alteration between grain-support and matrix-support conglomerates indicates shifts between fluvial, sheet flow, and mass-gravity flow deposition on an alluvial fan. The massive, matrix-support beds in are the result of mass-gravity flows. The conglomerate contains northward dipping accretionary surfaces indicate progradation of fan lobes basinward. The grain-supported comglomerate beds often contain crudely graded beds that fine upward, indicating waning flow during channelized and sheet-flow sedimentation (Fig. 6). Mass-gravity flow conglomerate beds that are matrix supported are commonly seen on alluvial fans that lack vegetation, dip steeply, and have subaqueous terminations (often sublacustrine) (e.g. Bull, 1977; Nemec and Steel, 1984).

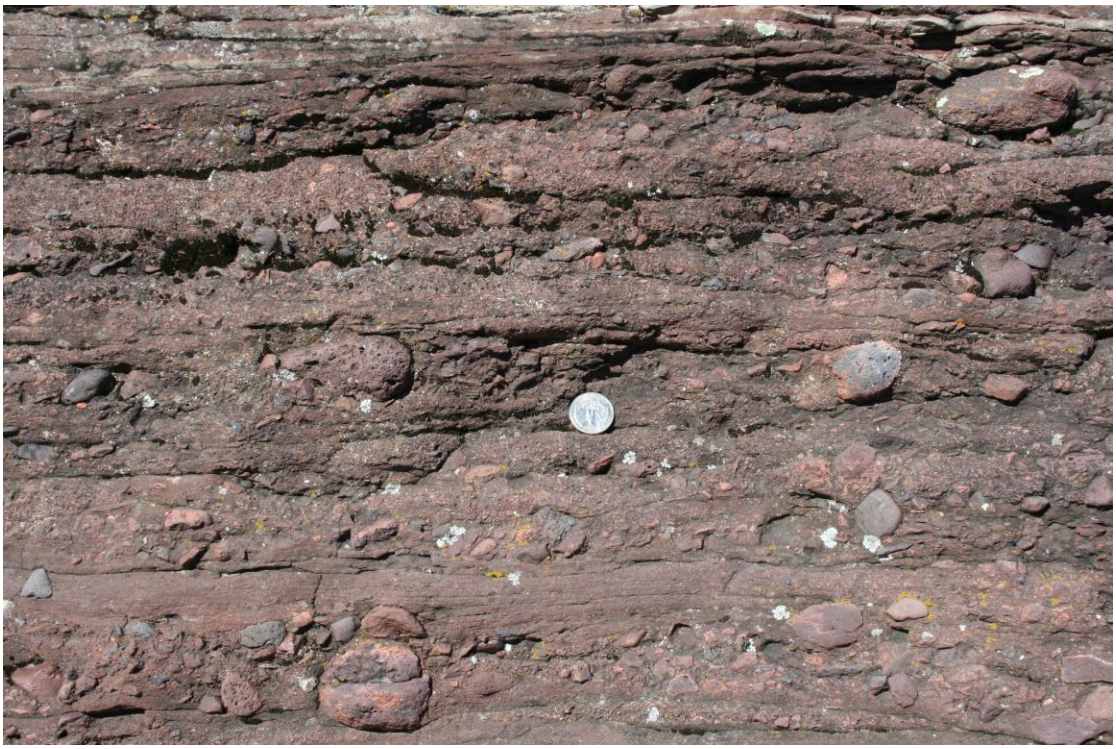

Fig. 6. Interstratified sandstone, clast-supported conglomerate and matrix-supported conglomerate beds resulting from espisodic sheet-flow and debris flow deposition. Located within conglomerate facies at Horseshoe Harbor ~53 m above base of measured section.

Stromatolites are found overlying the conglomerate facies at both Horseshoe Harbor and Dan's Point. However, they are much more common at the Dan's Point locality and are referred to here as the Dan's Point stromatolites. They are observed to drape over the top of cobbles as laterally linked hemispheroids. The stromatolite beds are ~0.3 m thick, laterally continuous, and appear similar to carbonate crusts. They are conformably overlain by a siltstone unit (Fig. 7a). The stromatolites have a microdigitate structure in which each cobble-draping hemispheroid consists of multiple 2 mm to 3 cm wide individual domes (Fig. 7b). Together, the collection of individual domes gives each hemispheroid a bulbous mound-like appearance with individual mounds ranging from 0.1-1 m in diameter (Fig. 7c). The stromatolite bearing carbonate bed also contains an abundance of ooids, oncoids, and aggregate grains. Stromatolites extend over the top of these coated grains but grains are also often observed trapped within stromatolite laminae and in the spaces between individual stromatolite heads. Cemented collections of ooids (grapestone) are coated to form botryoidal lumps (Fig. 7d).

Grapestone and aggregate grains typically form in moderate energy, $CaCO_3$ rich inner platform settings where circulation is restricted (Fabricius, 1977). Microbial binding of oolitic sediment and reworking by storm activity or flashy discharge are considered to be crucial steps in the formation of grapestone and botryoidal lumps (Fabricius, 1977). Grapestone and aggregate grains have been described from a similar rift basin (playa-lacustrine) shoreline depositional setting in the Late Triassic Mercia Mudstone Group of southern Britain (Milroy and Wright, 2002).

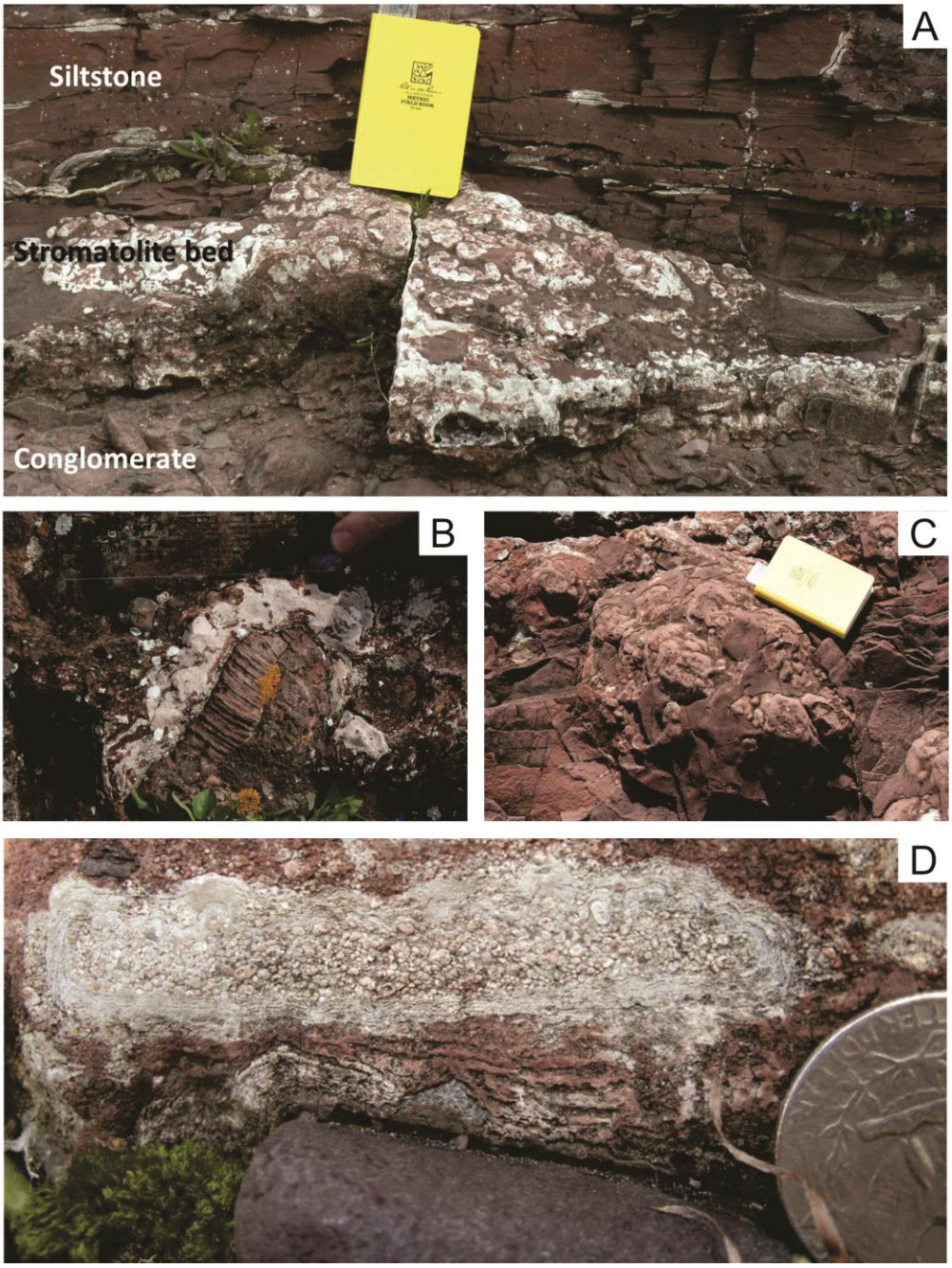

Fig. 7. Stromatolite bed and associated features from conglomerate facies at Dan's Point ~11 m above base of measured section. (A) Carbonate stromatolite bed draping over conglomerate facies and overlain by siltstone facies. (B) Example of microdigitate stromatolite coating cobble-sized clast from conglomerate facies. (C) Large bulbous stromatolite mound with siltstone drapes. (D) Collection of ooids cemented together and coated by calcite laminae to form botryoidal lump.

5.1.2 Siltstone Facies

The siltstone facies is the other stromatolite-bearing facies. This facies outcrops at both the Horseshoe Harbor and Dan's Point localities. It consists of clay, silt, and fine sand sized sediment that occurs in thin (cm-scale) horizontal beds. It has a conformable base and is observed draping onto the underlying conglomerate. Siltstone packages range from approximately 0.5 to 3 m in thickness. The siltstone shows signs of subaerial exposure in the form of carbonate-filled desiccation cracks. Small bidirectional wave ripples can also be seen in some siltstone beds. Elmore (1983) also reports rain drop impressions from within this facies. Rip-up clasts from the exposure cracks can be seen floating in overlying mudstone beds.

An undulating, laterally continuous, stromatolite bed can be seen within the siltstone facies at the Horseshoe Harbor locality (Fig. 8a and 9). These are referred to here as the Horseshoe Harbor stromatolites. The bed is typically between 0.10 and 0.30 m in thickness. The stromatolites overlie an erosional topography within the siltstone unit that is associated with carbonate filled exposure cracks (Fig. 8b). Stromatolite growth over the erosional surface likely gives the stromatolite bed a contorted appearance, sometimes resulting in mushroom-shaped morphologies (Figs. 8c and 8d). Hedlund (1953) interpreted these stromatolites as original growth forms that experienced slight deformation. Elmore (1983) thought they experienced deformation from either tectonic activity or loading. However, no evidence of deformation in the overlying and underlying siltstone beds was observed, which suggests that the stromatolites did not undergo post-depositional deformation. Additionally, there are no detachment blocks of

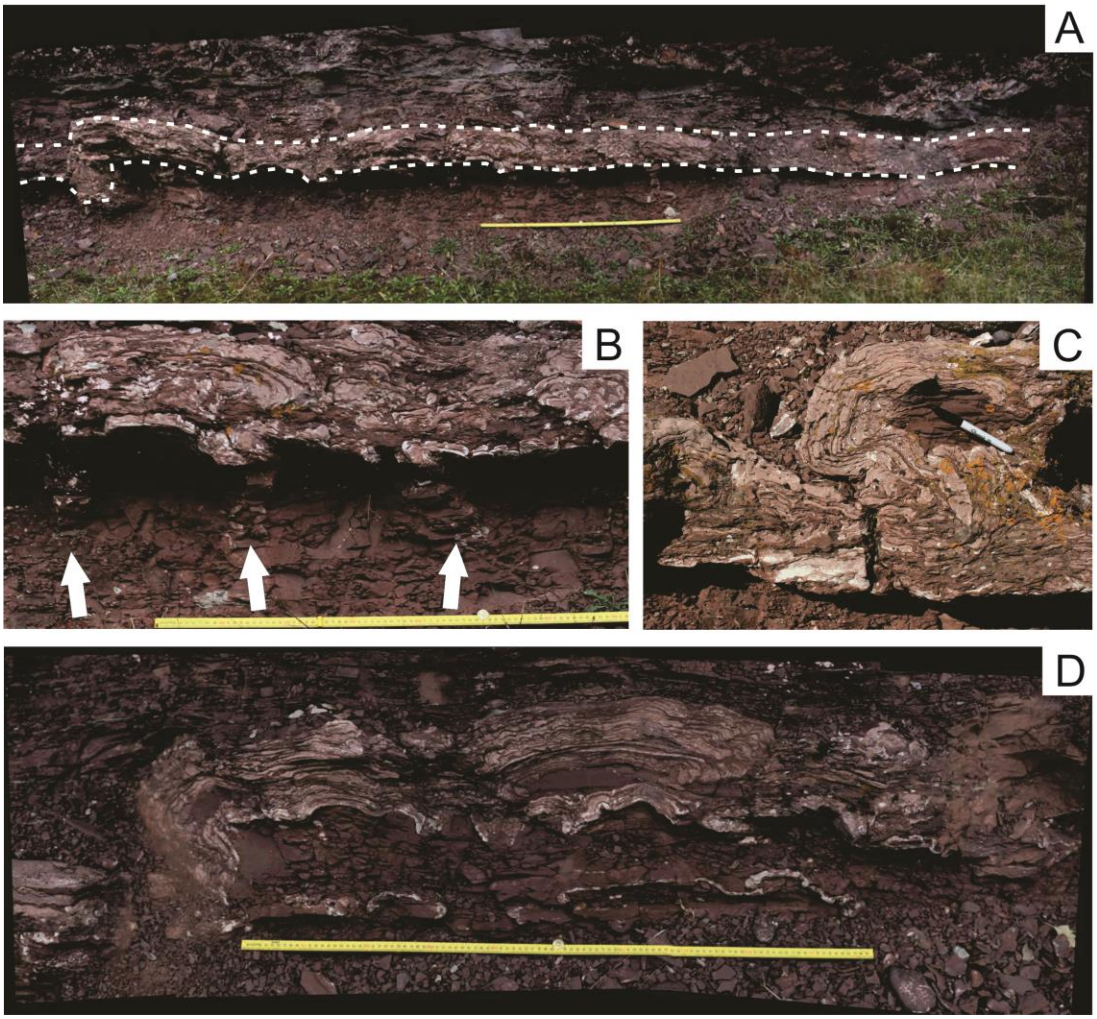

Fig. 8. Stromatolite bed and associated features from siltstone facies at Horseshoe Harbor ~64 m above base of measured section. (A) Location of stromatolite bed within siltstone facies highlighted by dashed lines. (B) Carbonate filled mud cracks indicated by white arrows beneath stromatolite bed. (C) Contorted appearance of stromatolite bed as it grows on the bottom of a siltstone overhang. (D) Contorted stromatolite bed overlain and underlain by undeformed siltstone beds.

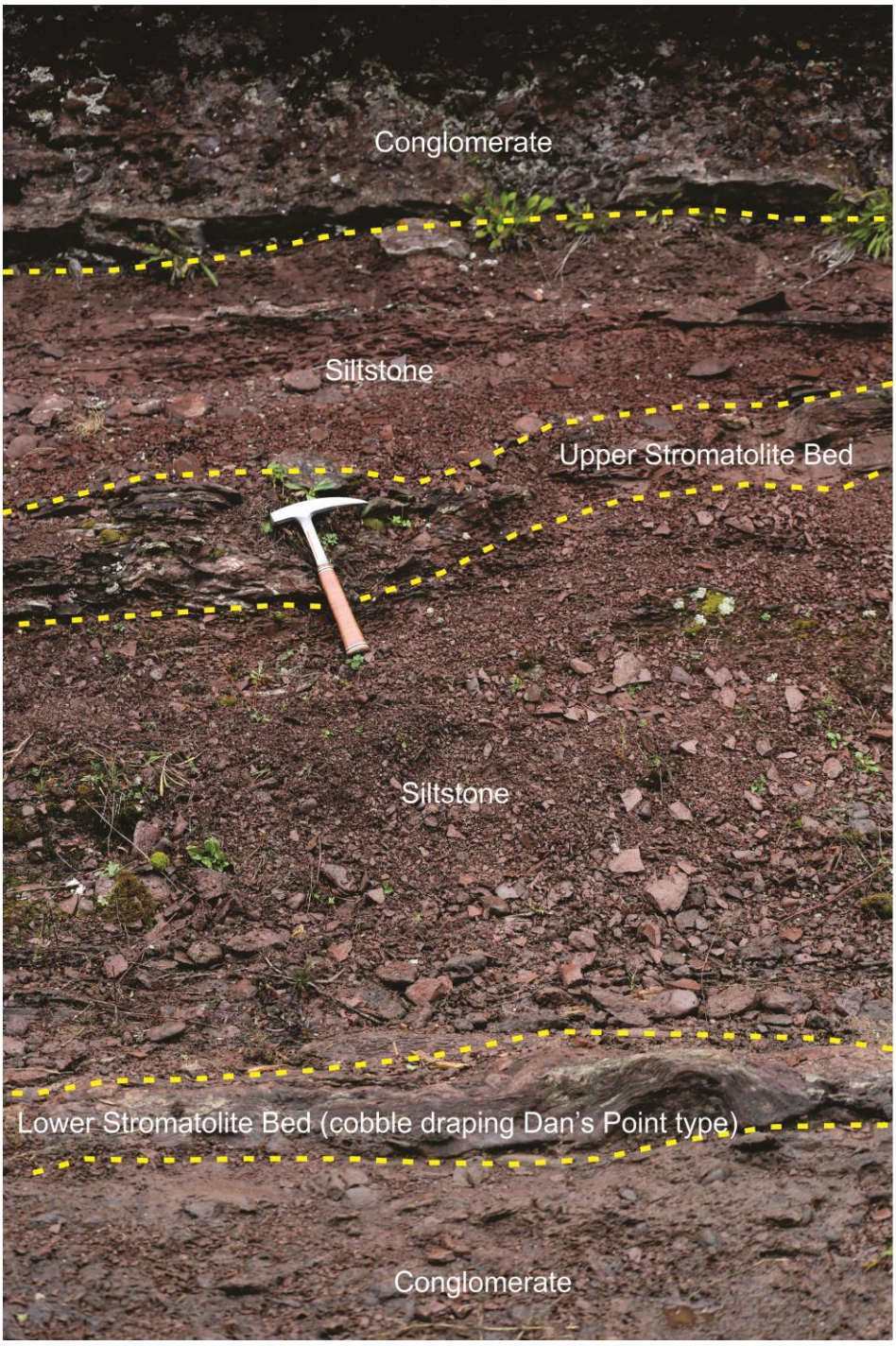

Fig. 9. Stratigraphic position of the two stromatolite beds at Horseshoe Harbor locality between 63-66 m above base of measured section.

the stromatolite bed, which indicates that the contorted appearance does not reflect syndepositional slumping. These stromatolites are therefore interpreted as representing original growth forms. The erosional surface likely formed during flashy discharge conditions across the alluvial fan and the stromatolite bed grew on top of the eroded substrate. Rip-up clasts of siltstone are sometimes found incorporated into the stromatolite laminae. Rip-up clasts of the stromatolite itself can also be seen floating in the overlying siltstone beds indicating that the stromatolite bed was at least partially lithified during subsequent flooding episodes.

5.1.3 Trough-Cross Stratified Sandstone Facies

The trough-cross stratified sandstone facies does not contain stromatolites. It occurs only at the Dan's Point locality as a 9 m thick package of cross-bedded and trough-cross bedded sandstone that is found in between mass gravity flow conglomerate beds (Fig. 10). It is comprised of medium sand with mud intraclasts and contains occasional mud drapes with polygonal desiccation cracks. It has a sharp erosional base and contains small pebble sized lags within the sandstone. The trough-cross stratified sandstone facies contains both current ripples and wave ripples.

Elmore (1984) suggested that the trough-cross stratified sandstone may represent a combination of fluvial and aeolian deposition in channels and on small longitudinal bars. Specifically, there is evidence within this facies of episodic flooding and desiccation. The trough-cross stratification represents the migration of dunes while the ripples are often characteristic of both current flow and shallow standing water conditions. Small cycles that start with small conglomerate lags and trough-cross

stratified sandstone and fines upwards to small ripples and mud drapes represents gradual abandonment of channel complexes (Elmore, 1984) or episodic flow on the fan surface. Mud drapes may indicate the settling out of fine sediment in small pools after episodes of flooding.

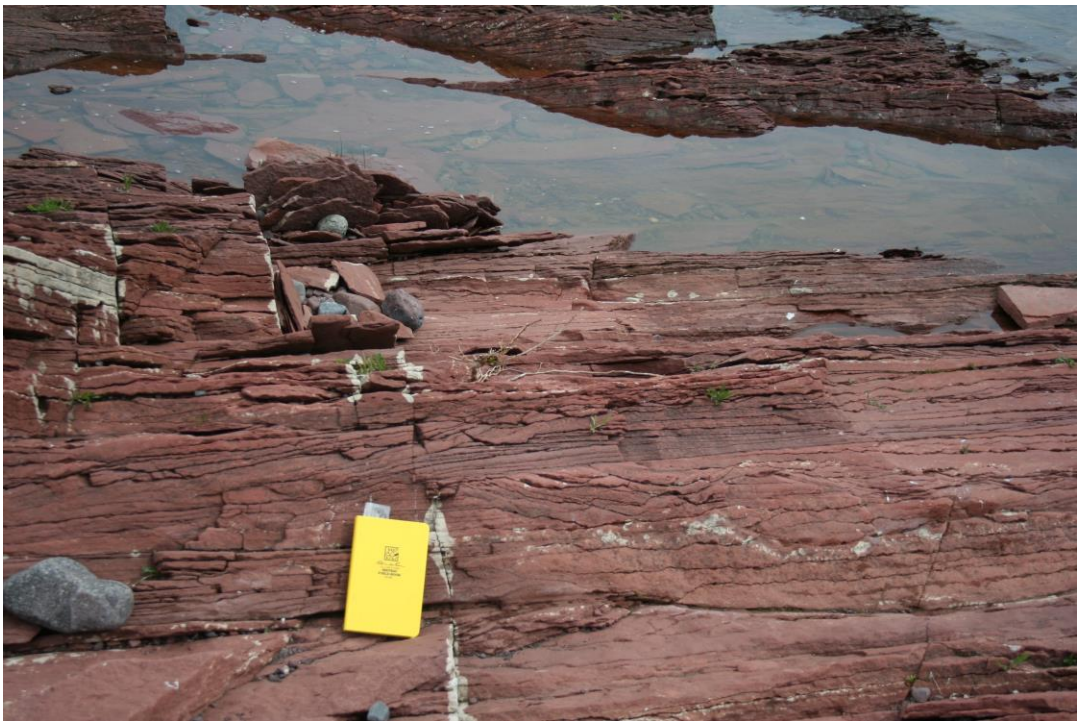

Fig. 10. Outcrop of trough cross-stratified sandstone facies at Dan's Point ~17 m above base of measured section.

5.1.4 Interpretation of Depositional Environments

Typical rift-basin depositional settings include alluvial fans, fan deltas and submarine fans along graben margins (Fig. 11). Fluvial plain and playa environments are expected to form on lake margins during the early stages of sedimentation into the basin. Meanwhile, drainage catchment is focused into the center of the basin, assuming the graben is not tilted, causing the formation of shallow rift lakes (Gawthorpe and Leeder, 2000). Liesa et al. (2006) describe transitions between alluvial, fluvial and lacustrine environments controlled by extensional faulting in the Cretaceous Galve sub-basin of Spain. This is similar to the facies patterns seen in the Copper Harbor Conglomerate. The conglomerate facies described above alternates between sheet flow and mass-gravity flow sedimentation. This is consistent with and alluvial fan environment that is proximal to the graben margin in a rift basin. Additionally, a siltstone facies and trough cross-stratified sandstone facies with evidence of exposure in the form of dessication cracks and rip-up clasts is suggestive of a fluvial plain and mudflat setting on the margins of a rift lake. While not observed in the measured sections, the Nonesuch Shale has been interpreted as lacustrine sediment from a rift lake.

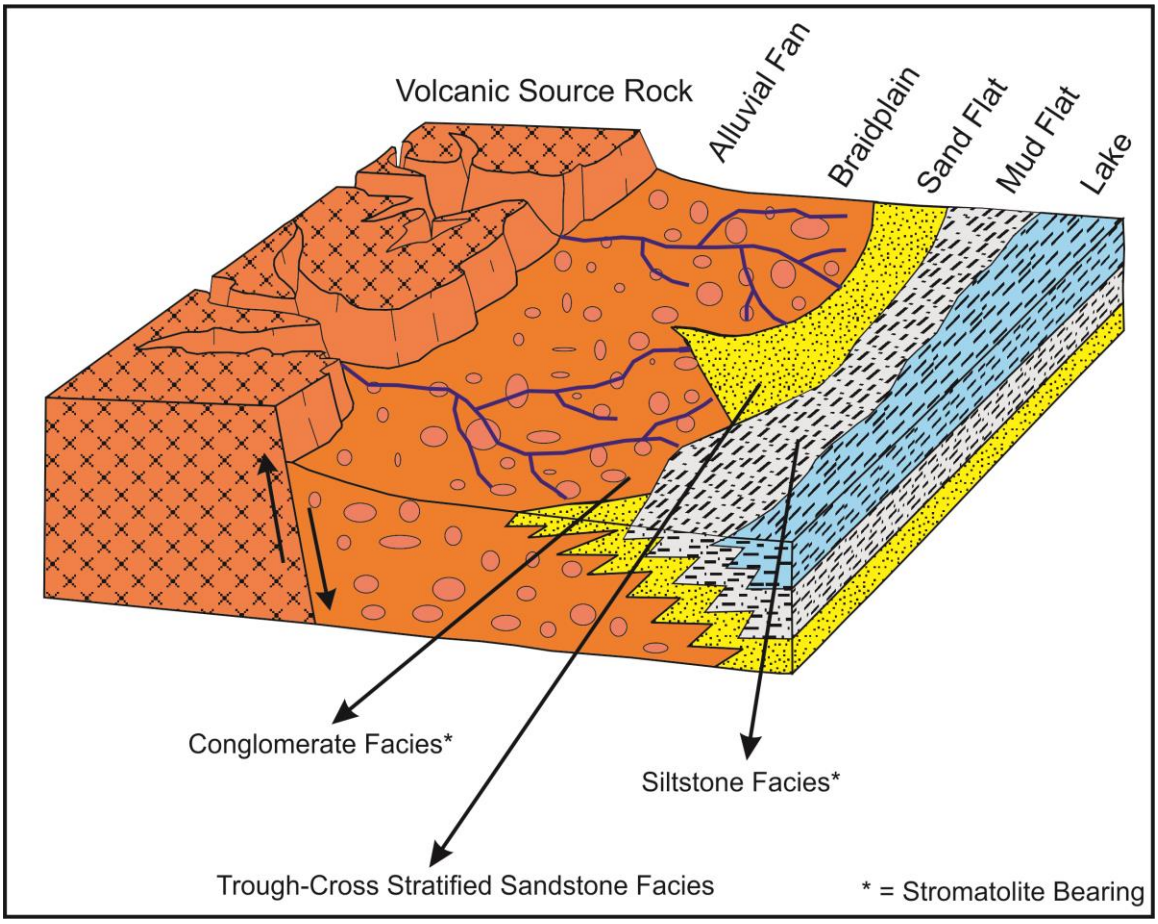

Fig. 11. Location of facies within a simple depositional model for the Copper Harbor Conglomerate. Stromatolites are located within mudflat/sandflat setting and braidplain setting. (Modified from Elmore, 1984).

5.2 Stromatolite Microfabrics

5.2.1 Horseshore Harbor Stromatolites

Stromatolites from the Horseshoe Harbor locality have the microfabric characteristics of structures that form due to microbial mat trapping and binding of sediment in conjunction with the precipitation of calcite. Alizarin Red-S staining shows that their laminae and cement is mostly comprised of calcite. The stromatolites consist of alternating dark (approximately 50 μm to 1 mm thick) and light laminae (approximately 0.5-3 mm thick) which are wavy and crinkled in character (Fig. 12a). The light laminae contain detrital (silt and clay-sized) grains, spar, and microspar while the dark laminae are micritic and hematite rich. The light laminae have more variable thicknesses than the dark laminae. They pinch and swell as detrital material fills in underlying depressions. The dark micritic layers have a clotted texture that is sometimes formed by the calcification of EPS (Riding, 2000). They appear opaque under plane light and crossed polarizing filters. However, an abundance of hematite can clearly be seen under reflected light (Fig. 12c). Hematite appears widespread throughout the stromatolites but especially concentrated in the dark wavy laminae (Fig. 12d).

The Horseshoe Harbor stromatolites also have an abundance of fenestral fabrics. Observations of the fenestrae show that the boundaries between the void space and

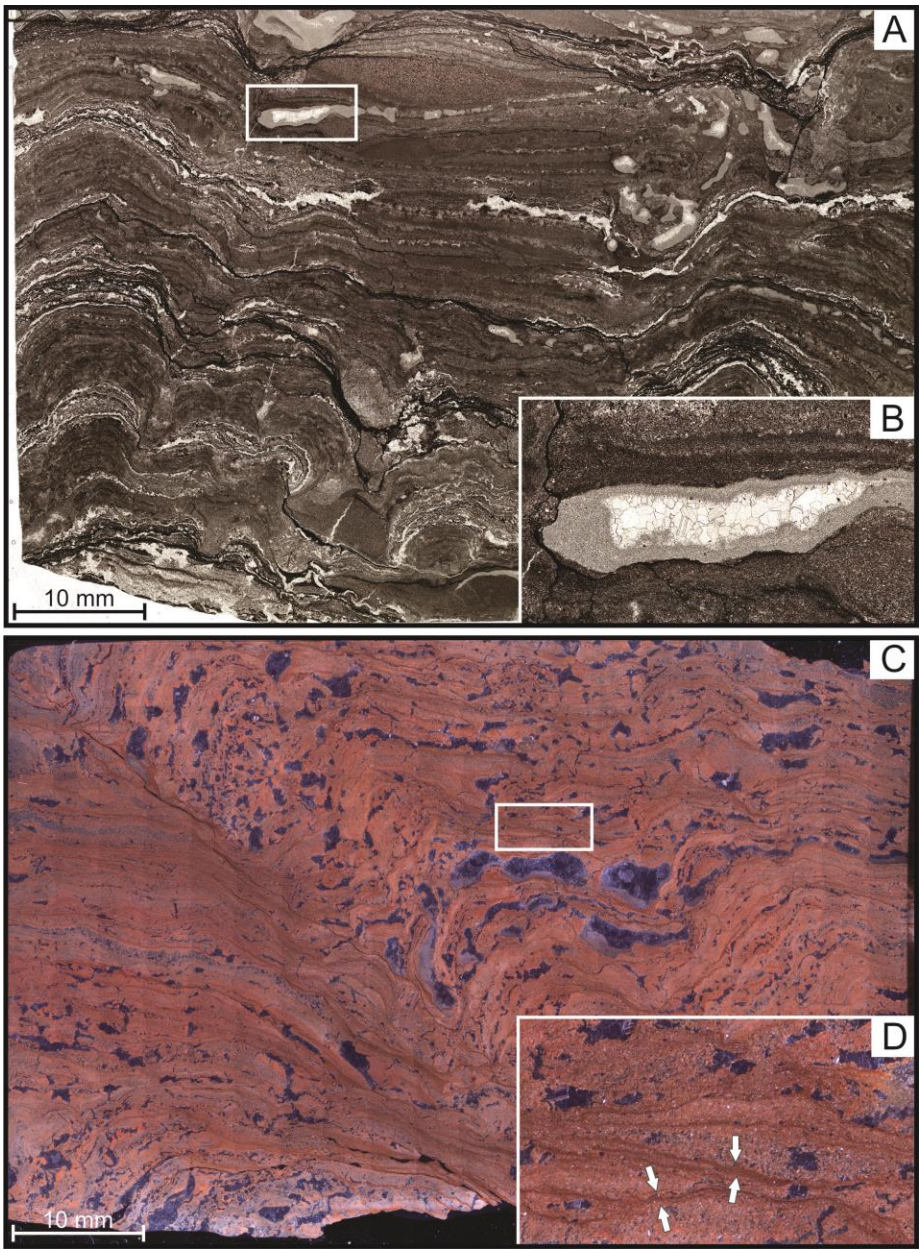

Fig. 12. Thin section photomosaics of Horseshoe Harbor-type stromatolite microfabrics. (A) Wavy and crinkled laminae and thin opaque laminae under plane polarized light. (B) Calcite filled fenestrae with microspar coating and blocky spar in center indicating inwards calcite growth. (C) Photomosaic taken under reflected light showing abundance of hematite that gives orange-red color. (D) Opaque laminae under plane polarized light appear dark red and hematite rich under reflected light (white arrows).

detrital grains are coated with microspar, which nucleated on the sediment and grew inwards, filling the center of the void space with blocky calcite (Fig. 12b). This suggests that the sediment overlying the fenestrae must have been present before calcite grew inwards, confirming that the fenestrae are secondary features that were created within the mat instead of primary features that were created on the surface of the mat.

The detrital sediment was likely deposited on top of the mat, trapped by EPS and then bound by overgrowth and calcite precipitation. During pauses in sedimentation the mat would have grown and stabilized the substrate (Noffke, 1998). The spar and microspar within the light laminae may either reflect *in-situ* carbonate precipitation from microbial degradation or abiogenic binding of the trapped sediment from direct precipitation. *In-situ* carbonate precipitation induced by microbial degradation is often associated with zones containing heterotrophic bacteria (Gerdes, 2007). The presence of hematite within the dark laminae is consistent with a microbially induced formation in which heterotrophic bacteria create strongly reducing conditions below the mat surface as they decompose organic matter (Gerdes et al., 1985, 2000). The reducing conditions lead to the formation of pyrite or siderite within the stromatolite which can later be oxidized to form the dark hematite or goethite rich laminae like those observed in the stromatolites from Horseshoe Harbor (e.g. Hofmann and Grotzinger, 1985; Noffke et al., 2006; Druschke et al., 2009).

Fenestral fabrics are associated with a build-up of gas from decaying organic matter within a microbial mat (Noffke et al., 2003; Gerdes, 2007). The fenestrae are secondary voids that are produced once the pressure of gas overcomes the resistance of the sedimentary grains (Gerdes, 2007). The fenestrae also serve as geopetals in which

there is a thicker accumulation of microspar at the bottom of the void space compared to the top of the void space (Nishioka et al., 1984). Nishioka et al. (1984) also describe putative algal filaments within the void spaces which they describe as branching and tubular in morphology. However, we found no direct evidence of microfossils within the Horseshoe Harbor stromatolites.

5.2.2 *Dan's Point Stromatolites*

The stromatolites from the Dan's Point locality have some distinctly different microfabrics than those at Horseshoe Harbor. They exhibit the characteristics of a mix between both biogenic and abiogenic modes of formation. Most of the laminae are either a sparry microdigitate carbonate crust or a hybrid sparry fine-grained crust. Individual stromatolite domes range from 2 mm to 3 cm in width (Fig. 13a). The laminae are isopachous (between 20-200 μm thick) and sometimes alternate between dark and light. The dark laminae are comprised of clotted micrite while the light laminae are mostly comprised of microspar. Very fine (clay and silt sized) detritus can be found dispersed evenly across both light and dark laminae. Radial-fibrous calcite fans and botryoids (typically <1 mm wide) are superimposed across multiple laminae and oriented perpendicular to the laminae (Figs. 13b and 13c). The Dan's Point stromatolites drape over ooids, oncoids or, large clasts. Ooids and oncoids are often incorporated into the stromatolite laminae or are located in between individual stromatolite columns.

Microdigitate stromatolites are formed by the direct in-situ precipitation of calcite on the substrate, essentially making them evaporite deposits although they may be microbially mediated (Grotzinger and Knoll, 1999; Pope et al., 2000). They are typically

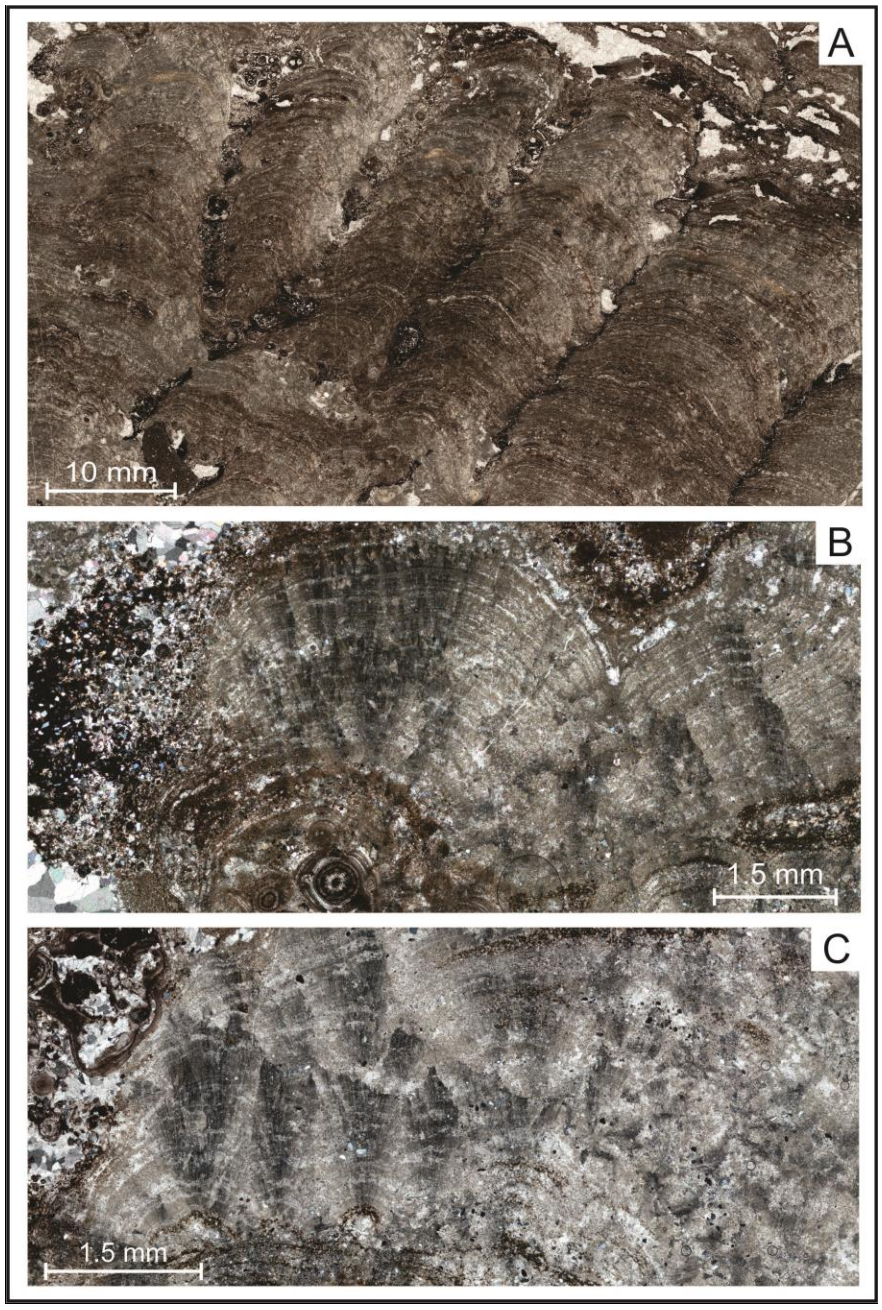

Fig. 13. Thin section photomosaics of Dan's Point-type stromatolite microfabrics. (A) Microdigitate stromatolite composed of individual small domes. (B) Microdigitate stromatolite domes under cross-polarized light exhibiting interference growth with radial fibrous calcite fans superimposed across laminae. (C) Radial fibrous botryoids under cross-polarized light within Dan's Point-type stromatolite.

found in high energy settings that experience exposure and they often exhibit a radial fibrous fabric like that described here (Riding, 2008). Radial fibrous calcite fans, botryoids and isopachous laminae are all considered strong evidence of abiogenic stromatolite formation (Grotzinger and Knoll, 1999). The columns and individual calcite fans also exhibit interference growth in which they grow in to each other but do not join together and become laterally linked as a microbial mat typically would (Fig. 13b). This is another feature indicative of abiogenic stromatolite growth (Grotzinger and Knoll, 1999; Corsetti and Storrie-Lombardi, 2003).

However, some laminae within the Dan's Point stromatolites appear to have a biogenic origin. Trapped grains can be observed on the high angle sides of stromatolite domes, possibly indicating stabilization from a microbial mat (Fig. 14a). Towards the top of the stromatolites, the laminae transition from being sparry and isopachous with calcite fans to more micritic, wavy, and variable in thickness. Individual stromatolite domes become irregular and conical in shape (Fig. 14b). Small cone-shaped morphologies are described in modern microbial mats as cyanobacteria grow towards sunlight (Bosak et al., 2009). There are also large calcite-filled void spaces in between laminae which are suggestive of gas build-up within a microbial mat. This feature is also commonly observed within small conical stromatolites as a gas build-up lifts and separates the stromatolite laminae from adjacent sediment (Gerdes, 2007; Bosak et al., 2009).

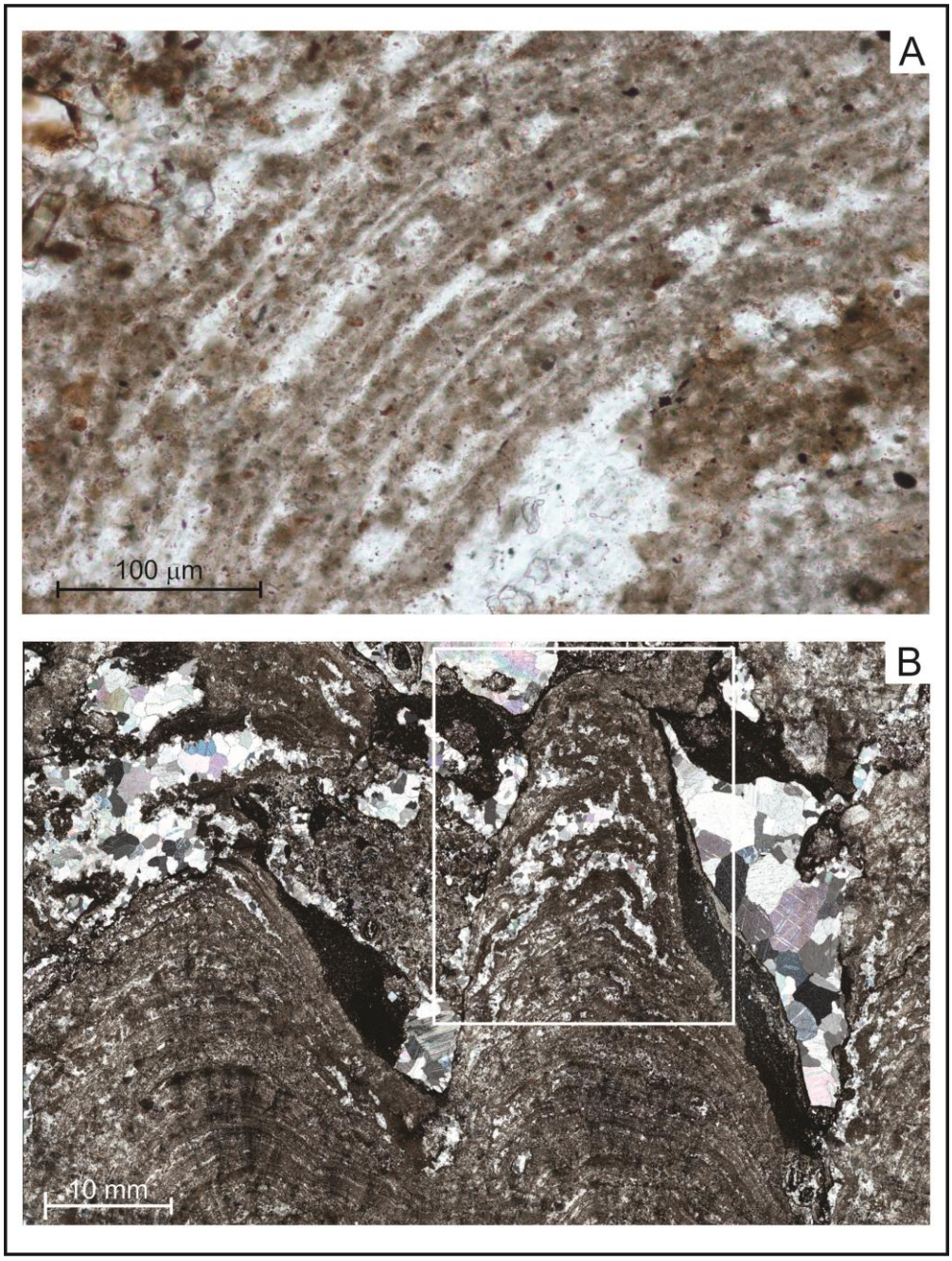

Fig. 14. Thin section photomosaics of Dan's Point-type stromatolite microfabrics. (A) Detrital grains trapped within laminae on high angle sides of individual stromatolite dome. (B) Mixed biogenicity stromatolite dome under cross-polarized light. Note transition from isopachous laminae with radial fibrous fans at base to conical morphology with wavy laminae separated by blocky calcite at top (within boxed area).

5.3 Growth Angle Analysis

A growth angle analysis was performed on 46 cobble and boulder-draping stromatolites from the Dan's Point locality to determine if a phototrophic response existed (Fig. 15a). Stromatolite samples were binned according to three groups (0-20°, 20-50° and 50-90°) based on the inclination of the surface they grew on. Nineteen samples were analyzed that grew on an initial inclination between 0-20°. These samples had a mean growth direction of 87.9 with a standard deviation of ± 14.5° (Fig. 15b). Eighteen samples were measured that initiated on surfaces inclined between 20-50º. Samples in this bin exhibited a mean growth direction of 87.8 ± 8.1º (Fig. 15c). Nine samples were measured that nucleated on substrates with an inclination between 50-90º. These yielded a mean growth direction of 86.7 ± 11.4° (Fig. 15d). All three bins showed similar mean growth angles, suggesting that the initial inclination did not affect stromatolite growth. Finally, a total growth angle analysis of all 46 samples yielded a mean growth direction of 87.6 ± 11.5°. In comparison, the 305 stromatolites from Walker Lake, Nevada that were measured by Petryshyn and Corsetti (2011) exhibited a mean growth direction of 83.6 ± 12.5° and were interpreted to lack a phototrophic response. Of the 46 samples measured here, a total of 71.7% (33 samples) fall within one standard deviation of surface-normal growth (90°) which is not suggestive of a phototrophic response. In a phototrophic response, we would expect to see stromatolites branch towards a particular direction of maximum incident light. The total growth angle analysis may show a small (~2.5°) bias towards upwards growth. Petryshyn and Corsetti (2011) found a similar (~6°) bias towards upwards growth in their samples and suggested this may be related to sediment availability rather than incident light.

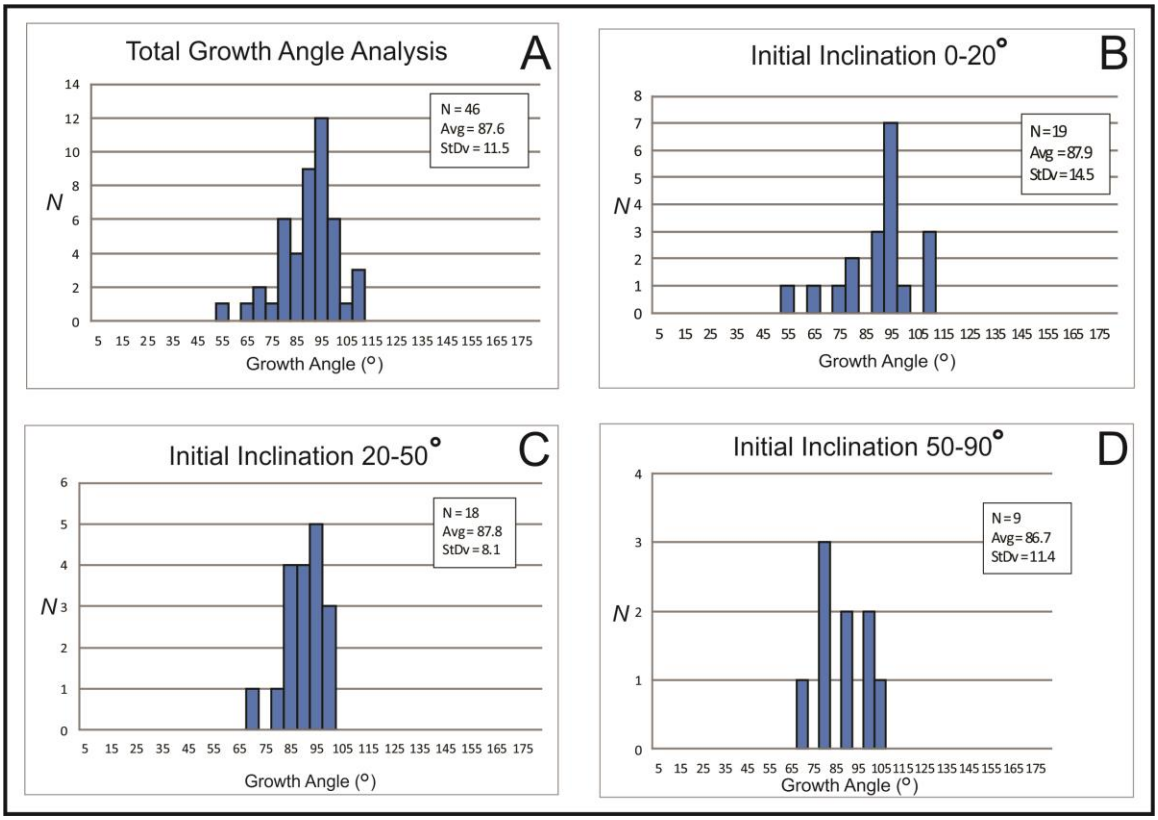

Fig. 15. Distribution of total stromatolite growth angles grouped according to angle of accretion surface. (A) Growth angle distribution of all stromatolite samples analyzed. (B) Growth angle distribution of stromatolites nucleated on a surfaces inclined between 0-20º. (C) Growth angle distribution of stromatolites nucleated on surfaces inclined between 20-50º. (D) Growth angle distribution of stromatolites nucleated on surfaces inclined between 50-90º.

5.4 Magnetic Susceptibility as a Potential Biosignature

Mass normalized susceptibility was measured from 45 powdered samples that were collected in 11 laminae transects. Machine noise with empty 1 cm^3 plastic cubes was measured to be ~6E-9 m^3/kg and results were found to be repeatable. Results revealed that the Horseshoe Harbor stromatolites had variable susceptibility values between 6.2E-7 m^3/kg and 2.0E-6 m^3/kg. Susceptibility values between 4.30E-7 m^3/kg and 2.70E-6 m^3/kg were found for the cobble-draping stromatolites from Dan's Point. No correlation between the mass susceptibility and angle of laminae dip was found in either the Horseshoe Harbor or Dan's Point stromatolites (Fig. 16). The independence of susceptibility from the angle of deposition was found in all 11 transects across different laminae.

These results are not consistent with the description of abiogenic stromatolites by Petryshyn et al. (2010). In abiogenic structures we would expect the susceptibility to drop sharply to almost zero once the angle of repose was reached, as detrital magnetic grains would be swept off the high angle sides. Therefore, these results may suggest a microbial presence that was trapping and binding sediment to the high angle sides of the stromatolite domes. However, the high variability in the mass susceptibility called into question what magnetic minerals were present in the stromatolite samples and whether they were authigenic or deposited as fine-grained detritus.

Samples were heated in order to determine the Curie temperature of the magnetic grains present. Heating revealed a large and irreversible increase in susceptibility between ~450ºC and 500ºC for samples from both Horseshoe Harbor and Dan's Point which is consistent with the creation of magnetite due to the thermal decomposition of

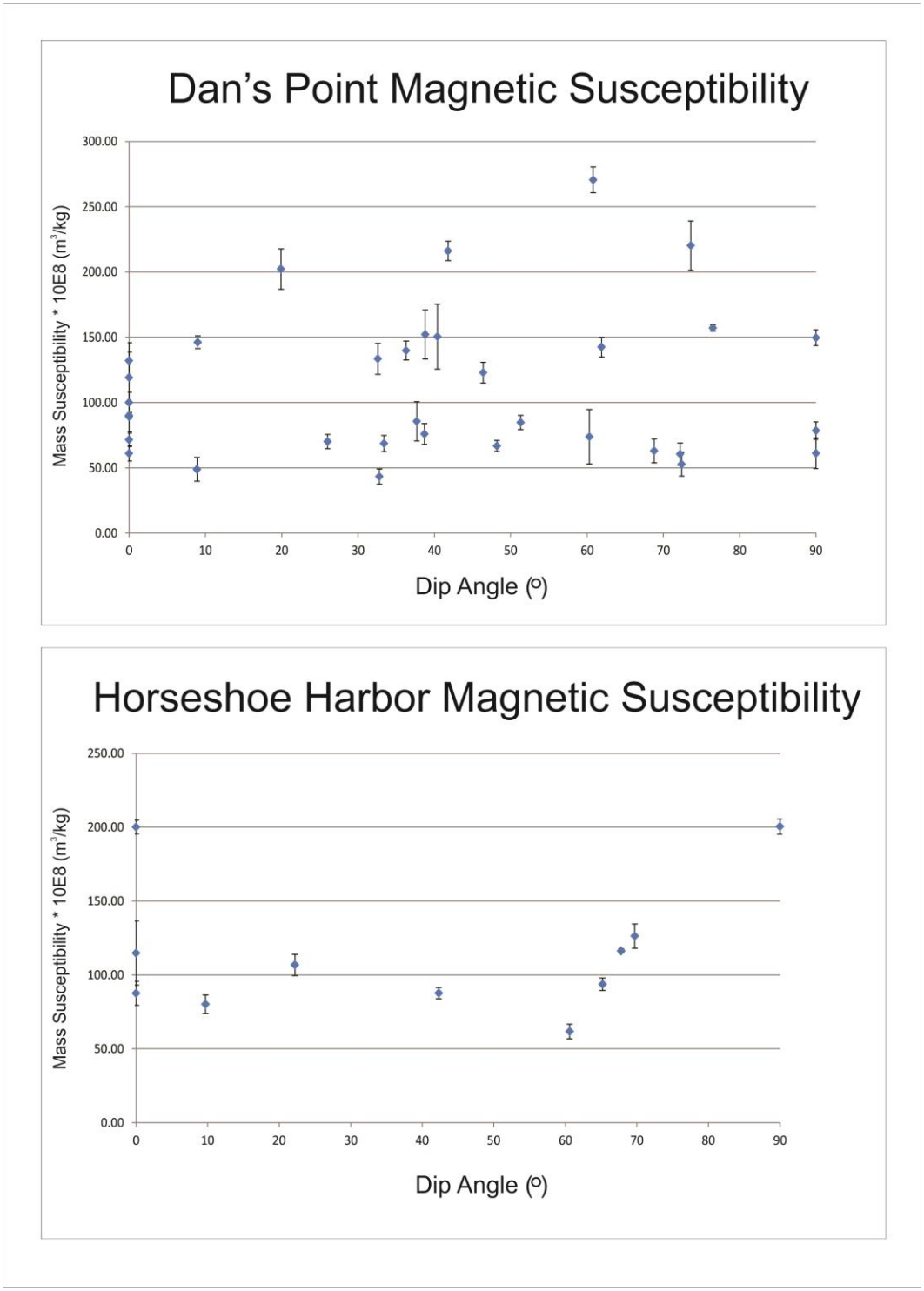

Fig. 16. Measured mass normalized susceptibility vs. dip angle of stromatolite laminae in stromatolites from both Horseshoe Harbor and Dan's Point. No clear relationship is observed between magnetic susceptibility and laminae dip angle.

siderite (Fig. 17) (Pan et al., 2000). For this reason, an AF demagnetization of the NRM and IRM acquisition were conducted to determine magnetic mineralogy without heating the samples. AF demagnetization of the samples (1 from both localities) revealed highly variable magnetization intensities in peak AF fields of 2-60 mT with a gradual decrease in magnetization intensities in fields beyond 60 mT (Fig. 18). By contrast, magnetic directions were relatively stable, but consistent with at least two antiparallel components of magnetization which may explain the variable intensities. Neither sample was fully demagnetized at 200 mT.

Results of the IRM acquisition showed that neither sample was saturated at 1T (Fig. 19). This implies a high-coercivity antiferromagnetic mineral such as hematite or goethite that has not been fully saturated is present in the samples. The HIRM ratio for the Horseshoe Harbor sample was 0.64 and 0.46 for the Dan's Point sample. The HIRM ratio reveals that the sample's magnetization is comprised of approximately half magnetically hard minerals such as hematite and half magnetically soft minerals such as magnetite or titanomagnetite. Therefore, the samples are volumetrically dominated by hematite which has a much lower susceptibility than either magnetite or titanomagnetite.

The presence of authigenic hematite means that magnetic susceptibility will not be a useful biosignature on these particular stromatolites. The test developed by Petryshyn et al. (2010) depends on a detrital magnetic component that is representative of sediment settling onto the stromatolite from above. Elmore and Van der Voo (1982) describe hematite in the Copper Harbor Conglomerate as a weathering product from magnetite grains. However, while some hematite grains may be detrital, the fact that there is laminae-specific hematite within the Horseshoe Harbor stromatolites implies that it

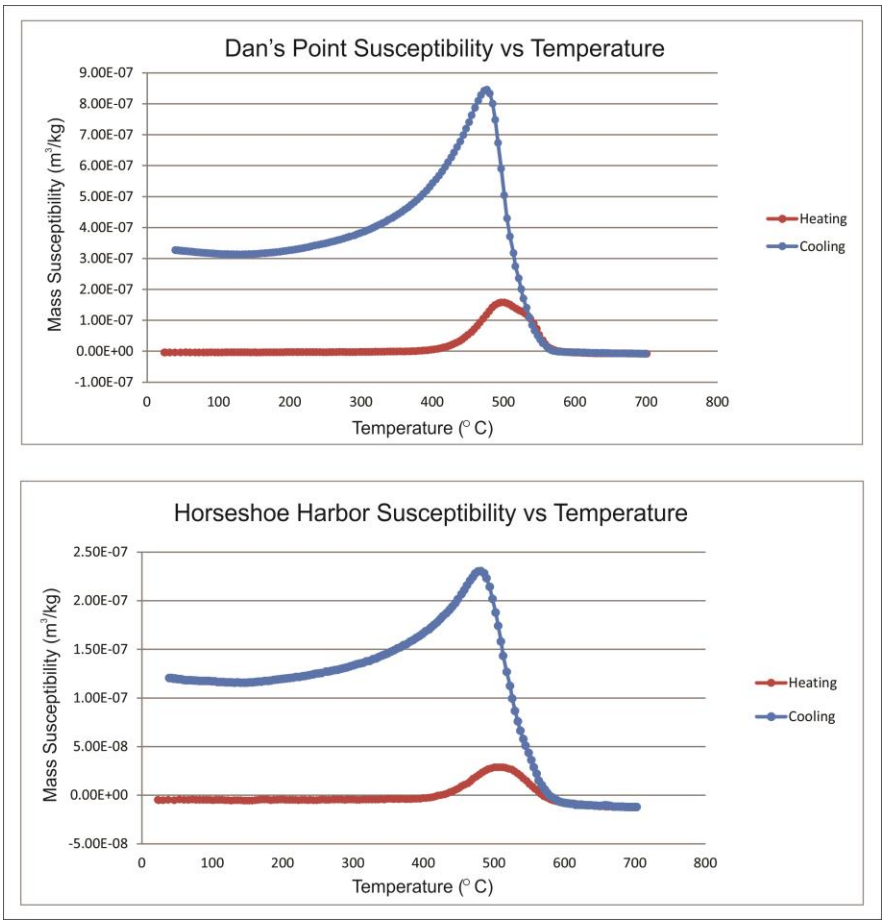

Fig. 17. Thermomagnetic curves obtained by heating samples to determine Curie temperature of magnetic minerals present.

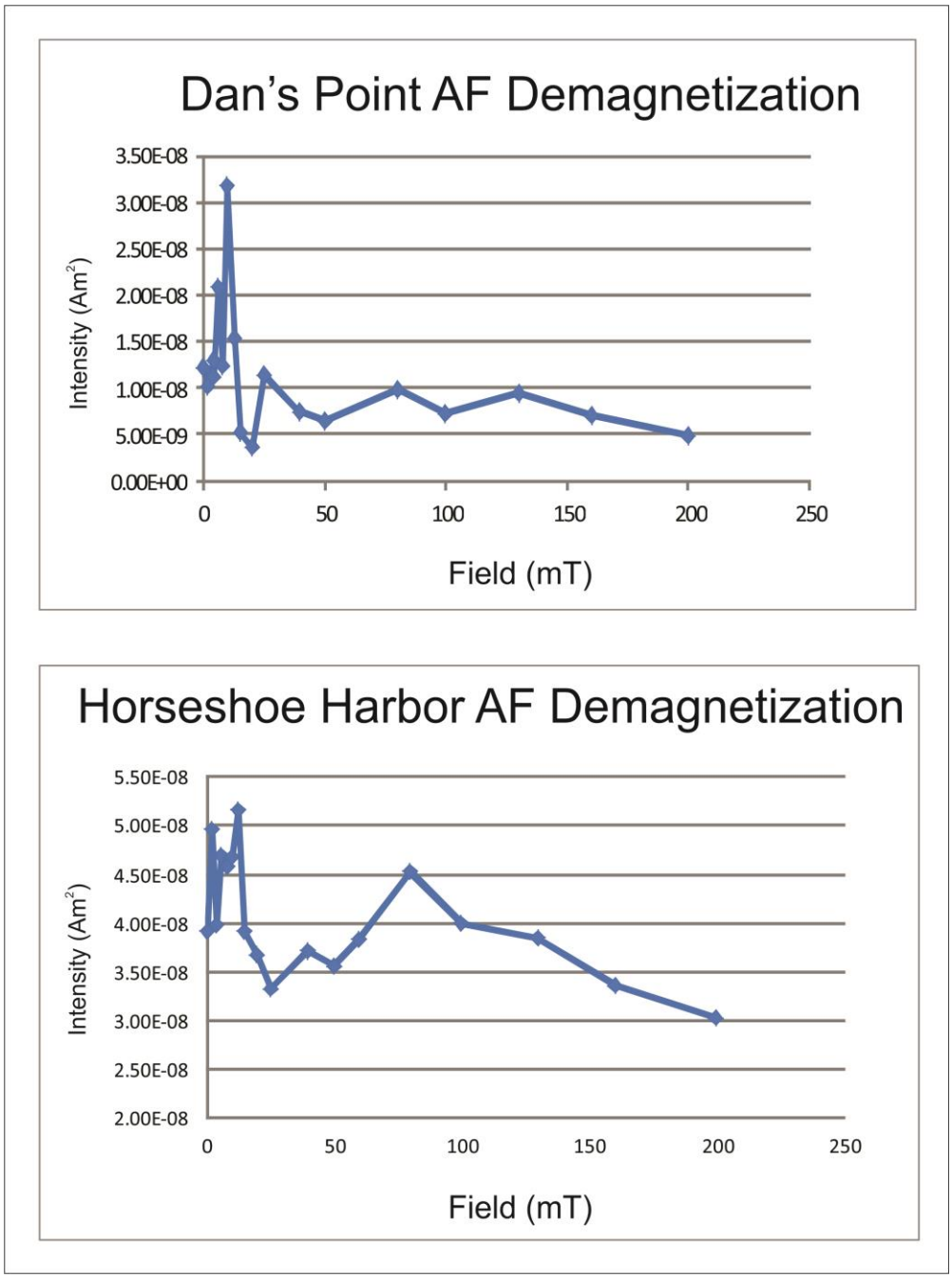

Fig. 18. Alternating field demagnetization results from both Horseshoe Harbor and Dan's Point stromatolites.

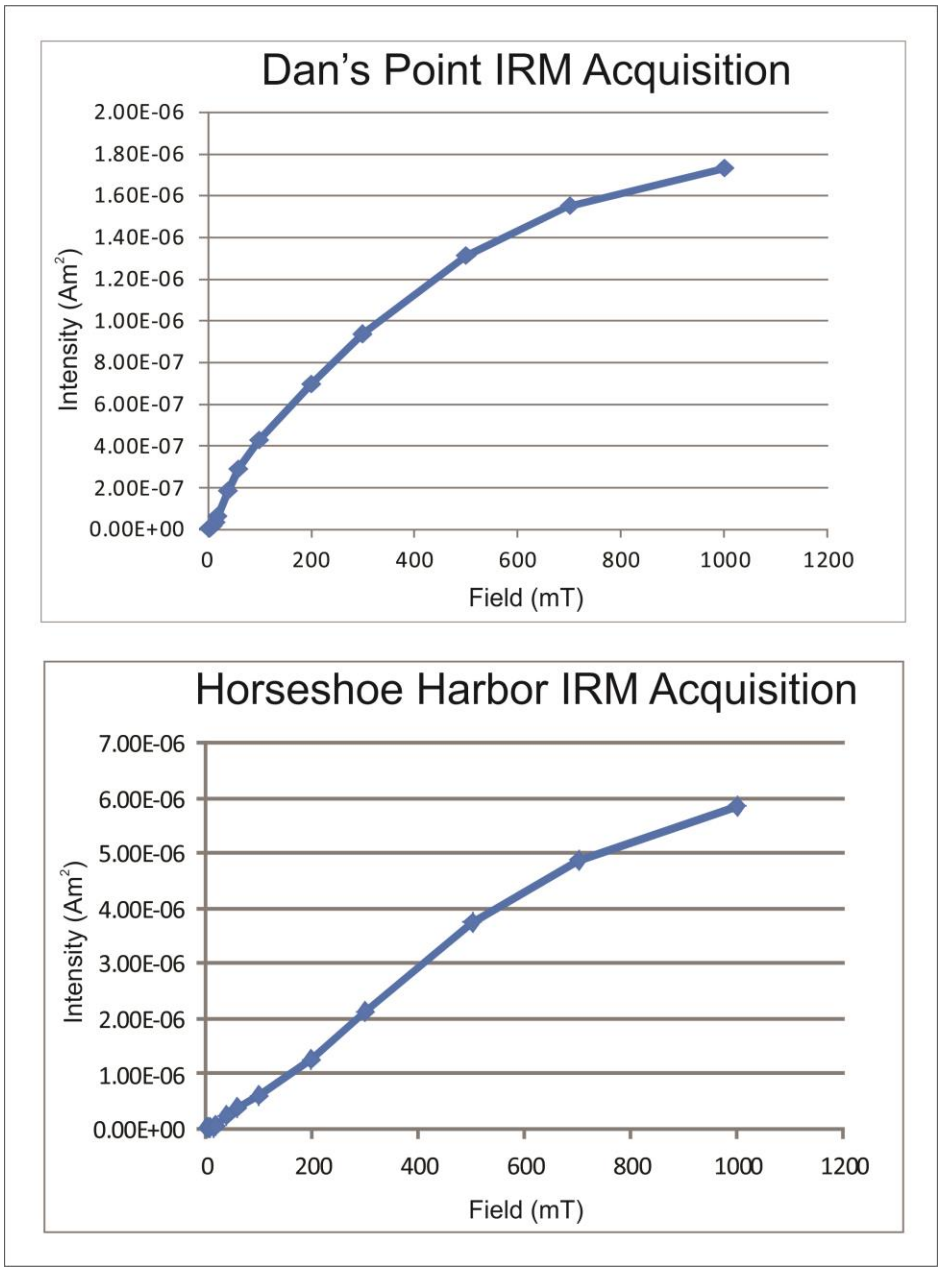

Fig. 19. Isothermal remnant magnetization acquisition results from both Horseshoe Harbor and Dan's Point stromatolites.

may be forming *in-situ* from the oxidation of siderite. An oxidation reaction that occurs over an extended period of time may explain why there are multiple overprints of NRM seen in the AF demagnetization. Additionally, the fact that there are both magnetically soft and magnetically hard minerals may explain the variability in magnetic susceptibility measurements. Various proportions of the two minerals may yield very different results when measuring mass normalized susceptibility.

6. Discussion

6.1 Depositional System

Sedimentary systems in rift basins are primarily controlled by the creation of accommodation space due to active faulting/tectonic activity (e.g. Leeder and Gawthorpe, 1987; Blair and Bilodeau, 1988; Schlische and Olsen, 1990; Leeder, 1995; Gawthorpe and Leeder, 2000; Withjack et al., 2002; Melchor, 2007). Cannon et al. (1989) created offshore seismic reflection profiles across the Keweenawan Trough, north from the tip of the Keweenawan Peninsula. The reflection profiles reveal the presence of a large, asymmetrical, central graben (Fig. 20a). The graben is bounded by the normal Keweenaw Fault, observable on the Keweenaw Peninsula, and the Douglas and Isle Royale Faults on the northern side of Lake Superior (Cannon et al., 1989). The Copper Harbor Conglomerate is part of a volcanic and sedimentary succession that was deposited on top of the graben once the basin began to fill in (Elmore, 1984). During the deposition of the Copper Harbor Conglomerate, subsidence was driven by extension, crustal sag, and sediment loading. The asymmetric nature of the central graben was the result of faster

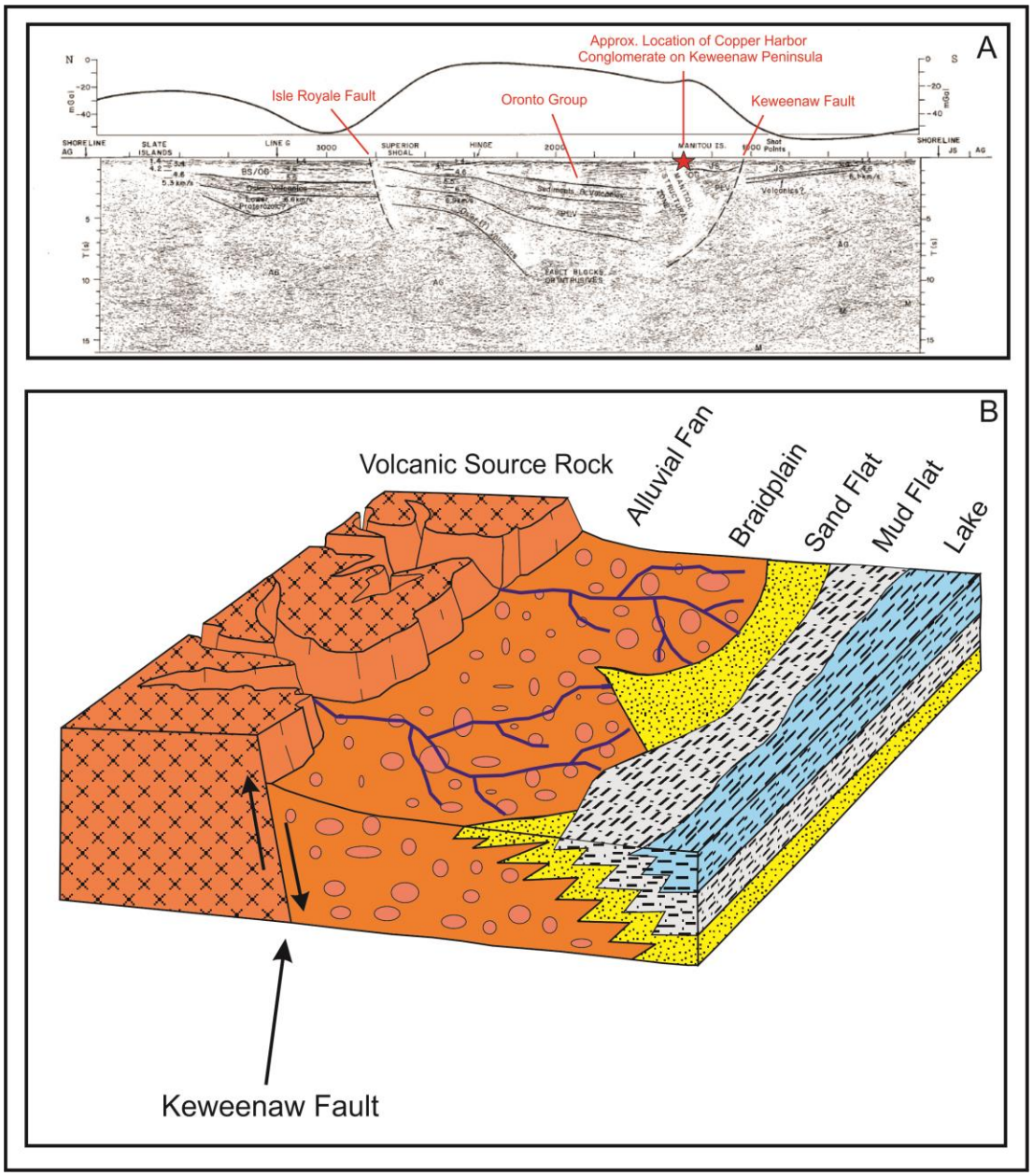

Fig. 20. (A) Offshore seismic profile across the Keweenawan Trough showing large central graben flanked by Isle Royale Fault and Keweenaw Fault. Approximate location of Copper Harbor Conglomerate on Keweenaw Peninsula marked by red star (Modified from Cannon et al., 1989). (B) Simple depositional model for facies pattern observed in Copper Harbor Conglomerate. Stromatolites are located within mudflat/sandflat setting and braidplain setting (Modified from Elmore, 1984).

subsidence rates along the Douglas Fault compared to the Keweenaw Fault (Cannon et al., 1989).

The conglomerate facies and trough-cross stratified sandstone facies are fluvial and mass-gravity flow deposits from an alluvial fan complex that occurred on the flanks of the Keweenawan Trough (Fig. 20b). The siltstone facies is both overlain and underlain by the conglomerate facies. It is interpreted as a mudflat/sandflat setting that occurred along the margin of Lake Nonesuch. A possible explanation for this facies pattern is that episodic subsidence along the Keweenaw Fault was controlling deposition. When subsidence rates exceeded sedimentation rates, accommodation space was created and the alluvial fan would step back to fill the space. This creation of accommodation space allowed Lake Nonesuch to transgress toward the basin margin and the siltstone mudflat/sandflat facies to be deposited on top of the conglomerate facies. The conglomerate facies was deposited during times when sedimentation outpaced subsidence. Therefore, we interpret the large accretionary surfaces within the conglomerate facies to represent fan lobes prograding toward the center of the basin.

At both localities, the Copper Harbor Conglomerate stromatolites occur on the top of the conglomerate facies, overlain by siltstone, or within the siltstone facies itself. This suggests that the stromatolites formed along the lake margin during times when subsidence outpaced sedimentation. The Horseshoe Harbor stromatolites grew over an erosional surface and have the characteristics of microbial mats that grew on a shallow mudflat or sandflat. This setting probably experienced occasional subaerial exposure and flooding as illustrated by the desiccation cracks, erosional surfaces, and mud intraclasts. In contrast, we hypothesize that the Dan's Point cobble-draping stromatolites formed on a

shallow flooded braidplain where the lake had transgressed over a back-stepping fan lobe.

Elmore (1983) thought that the cobble-draping stromatolites likely formed in abandoned fluvial channels that were re-flooded seasonally. However, we do not see evidence of the stromatolites forming within channel bodies. The stromatolite beds at both localities appear as laterally continuous carbonate beds whereas the channels located within the conglomerate facies are seen as lenticular sand and gravel bodies that range from 2-15 m in width. The presence of ooids and coated grains suggests a setting that would require substantial wave activity which would not exist in small abandoned channels. Additionally, standing water in shallow abandoned channels is problematic in an arid or semi-arid setting as Elmore (1983) conceded. Finally, the lack of significant detrital laminae within the stromatolite bed from Dan's Point indicates an extended period with low sedimentation rates. Based on this evidence, the cobble-draping stromatolites likely formed along the shallow shoreline of the lake itself. This flooded braidplain setting may have had restricted circulation and increased alkalinity, contributing to the growth of the cobble-draping stromatolites as well as the ooids, botryoidal lumps, and coated grains.

6.2 Stromatolite Biogenicity

6.2.1 Horseshoe Harbor Stromatolites

The results of this study indicate that the Horseshoe Harbor stromatolites likely have a biogenic origin. Carbonate filled dessication cracks, rip-up clasts, ripple marks and an eroded topography are all indicative of a mudflat or sandflat depositional

environment that experienced subaerial exposure and erosive flooding events. The Horseshoe Harbor stromatolites are interpreted to have been formed by microbial mats that colonized this setting and stabilized the substrate. This is based on the contorted appearance of the stromatolites which Elmore (1983) interpreted as post-depositional deformation. Alternatively, this study shows that they have grown over an erosive topography based on the lack of detachment blocks and the lack of deformation in overlying and underlying beds. Rip-up clasts of stromatolite fragments can also be seen floating in the overlying mudstone. The ability of microbial mats to stabilize the substrate in shallow mudflat/sandflat settings can be seen in similar modern day environments (Noffke, 1998).

The microfabrics of the Horseshoe Harbor stromatolites also strongly suggest a biogenic origin. Alternating layers of micrite, microspar and detrital material is consistent with trapping and binding activity by microbes in a mudflat/sandflat setting that experiences episodic deposition. The presence of hematite rich micritic laminae and siderite are common in stromatolites with heterotrophic microbial communities that create reducing conditions as they degrade EPS (Noffke et al., 2006; Druschke et al., 2009). Finally, secondary calcite-filled fenestrae are consistent with gas build up due to the decomposition of organic material within a microbial mat (Gerdes, 2007). The role of heterotrophic microbes in the formation of stromatolites is considered by many to be more important than cyanobacteria in alkaline lakes (Dupraz et al., 2009). The evidence presented here suggests that heterotrophic bacteria played an important role in the formation of the microfabrics seen in these stromatolites. A shallow flooded mudflat or

sandflat setting offers ideal conditions for the formation of complex layered microbial mats such as those preserved in the Horseshoe Harbor locality.

6.2.2 Dan's Point Stromatolites

The stromatolites from Dan's Point are interpreted to be from a flooded braidplain setting and to have been formed through a mix of microbial and chemical processes. The stromatolites have a microdigitate morphology which is commonly associated with abiotic carbonate crusts (Riding, 2008). The stromatolites do not have laminae comprised of detrital clastic grains that would typically be found in a stromatolite formed by trapping and binding. Instead, they have isopachous laminae with radial fibrous calcite fans and botryoids, which are all considered to be strong indicators of chemical precipitation (Grotzinger and Knoll, 1999). The individual stromatolites also show evidence of interference growth in which they grow into each other but do not become laterally linked as takes place with microbial mats (Grotzinger and Knoll, 1999; Corsetti and Storrie-Lombardi, 2003).

These cobble and boulder draping stromatolites also demonstrate surface-normal growth and they lack evidence of a phototrophic response to incident light. Surface-normal growth is commonly associated with *in-situ* mineral precipitation and abiogenic structures (Pope and Grotzinger, 2000). However, it may simply imply that sunlight was abundant in a shallow reflective setting or that space was a greater limiting factor in determining stromatolite growth direction than sunlight. It may also indicate that the stromatolites were dominated by heterotrophic microbial communities instead of photosynthetic cyanobacteria. However, this growth angle data combined with the

microfabric evidence makes a strong argument that growth was driven, at least in large part, by chemical processes.

There is also evidence that there was a microbial presence involved in the formation of the Dan's Point stromatolites. There are abundant botryoidal lumps, grapestone and aggregate grains within the stromatolite bed. Microbial binding is considered an important step in the formation of these grains (Fabricius, 1977). Some of the stromatolites also show a transition from isopachous laminae with radial-fibrous fans to more micritic laminae and cone-shaped morphologies that are common in biogenic structures (Bosak, 2009). Fenestrae and wavy laminae that are separated by blocky spar can also be found within some of the laminae from the Dan's Point stromatolites. These are similar features to lift-off structures described by Bosak (2009) that are formed by gas build-up within a microbial mat. Finally, these stromatolites (just like those from Horseshoe Harbor) contain siderite and hematite which may have originated from reducing conditions within a mat.

It is not uncommon for microbial communities to colonize abiogenic stromatolites. Allwood et al. (2009) describe Archean stromatolites from Western Australia that have laminae characteristic of both biogenic and abiogneic growth despite a persistent microbial presence. They relate the changes between microbial dominated growth and *in-situ* precipitation to shifting environmental conditions. The Dan's Point stromatolites may have formed by chemical precipitation in a shallow and possibly more restricted setting than those at Horseshoe Harbor. They also may have been colonized by microbial communities at various times during their formation.

6.3 Magnetic Susceptibility as a Biosignature

Studies conducted by Petryshyn et al. (2010) demonstrate the potential usefulness of magnetic susceptibility as a biosignature. They found evidence that supports this technique in both laboratory experiments and the measured susceptibility of ancient stromatolites. This biosignature works well when the primary magnetic signal is found in detrital grains. This study suggests that this technique may be less useful in cases when authigenic magnetic minerals (such as hematite oxidized from siderite) represent a large portion of the magnetic signal. These minerals form *in-situ* and therefore cannot be swept off the high angle sides of abiogenic stromatolites as demonstrated by Petryshyn et al. (2010). It is also possible that a mix between magnetically soft minerals like magnetite or titanomagnetite and magnetically hard minerals like hematite may make it more difficult to measure the magnetic susceptibility. Difficulty may be related to laminae-specific, variable proportions of these minerals that are found in a micro-drilled powder. For these reasons, caution should be used when applying magnetic susceptibility as a biosignature to stromatolite samples like those from the Copper Harbor Conglomerate that have Fe-rich laminae.

7. Conclusions

Deposition of the Copper Harbor Conglomerate was controlled by subsidence and sediment supply in a rift basin setting (Elmore, 1984). The stromatolites from the Copper Harbor Conglomerate are located within two distinct facies (a siltstone facies and a conglomerate facies) and were deposited during times when subsidence outpaced sedimentation. The siltstone facies corresponds to a shallow mudflat or sandflat that

experienced occasional subaerial exposure and flooding. The conglomerate facies represents a shallow flooded braidplain with restricted circulation that was part of a back-stepping alluvial fan. Both of these depositional environments were part of the marginal shoreline of Paleo-lake Nonesuch based on stromatolite bed geometries, an elevated water table and interpretations of wave energy.

Stromatolites from the Horseshoe Harbor locality have all of the characteristics of microbial mats that stabilized the mudflat/sandflat substrate (Noffke, 1998; Noffke et al., 2006). They likely had a heterotrophic microbial presence that created reducing conditions within the mat. These microbes also decomposed the mat and caused gas pockets to form below the mat surface. The laminae of these stromatolites were formed by the trapping and binding of sediment during episodic sedimentation and the precipitation of calcite (either chemically or biologically derived).

The stromatolites from Dan's Point are interpreted to have formed through a mix of biogenic and abiogenic processes. The microfabrics and growth angles suggest that chemical growth was an important factor in the formative architecture of these stromatolites (Grotzinger and Knoll 1999; Petryshyn and Corsetti, 2011). This may be related to these stromatolites forming in a more restricted or evaporitic setting than the stromatolites from Horseshoe Harbor. The lack of detrital laminae also suggests that these stromatolites did not form from the trapping and binding of episodic sedimentation like the stromatolites from Horseshoe Harbor. There is some evidence that these stromatolites were also influenced by microbial activity and that these communities may have been episodically responsible for controlling growth patterns.

Magnetic susceptibility offers a promising new way of determining stromatolite biogenicity in the absence of microfossil evidence (Petryshyn et al., 2010). This methodology works well when the primary magnetic signal comes from detrital magnetic grains that settled out of suspension. This study suggests, however, that caution should be applied when attempting to use this methodology on stromatolites with authigenic magnetic minerals. These minerals sometimes occur in Fe-rich laminae that are created by heterotrophic bacteria (Noffke et al., 2006; Druschke et al., 2009). In these cases, the magnetic susceptibility will not be representative of the detrital sediment trapped within the stromatolite laminae.

This study supports the body of work indicating that microbes had colonized the Midcontinent Rift during the Mesoproterozoic. The fact that the same fluvial-lacustrine depositional environment holds distinctly different types of stromatolites provides an interesting test case into the controls on stromatolite biogenicity. The Copper Harbor Conglomerate stromatolites demonstrate how minor environmental influences may favor either biogenic or abiogenic growth, even with a consistent microbial presence and a similar depositional setting. Despite our improved understanding of stromatolite formation, this study highlights the need to continue searching for new methodologies to determine biogenicity in the absence of microfossil evidence.

References

Allwood, A.C., Grotzinger, J.P., Knoll, A.H., Burch, I.W., Anderson, M.S., Coleman, M.L., 2009. Controls on development and diversity of Early Archean stromatolites. Proceedings of the National Academy of Sciences 106, 9548-9555.

Blair, T.C., 1987. Tectonic and hydrologic controls on cyclic alluvial fan, fluvial, and lacustrine rift-basin sedimentation, Jurassic-Lowermost Cretaceous Todos Santos Formation, Chiapas, Mexico. Journal of Sedimentary Research 57, 845-862.

Blair, T.C., Bilodeau, W.L., 1988. Development of tectonic cyclothems in rift, pull-apart, and foreland basins—sedimentary response to episodic tectonism. Geology 16, 517-520.

Bosak, T., Liang, B., Sim, M.S., Petroff, A.P., 2009. Morphological record of oxygenic photosynthesis in conical stromatolites. Proceedings of the National Academy of Sciences 106, 10939-10943.

Bull, W.B., 1977. The alluvial-fan environment. Progress in Physical Geography 1, 222-270.

Cannon, W.F., Green, A.G., Hutchinson, D.R., Lee, M.W., Milkereit, B., Behrendt, J.C., Halls, H.C., Green, J.C., Dickas, A.B., Morey, G.B., Sutcliffe, R.H., Spencer, C., 1989. The North American Midcontinent Rift beneath Lake Superior from GLIMPCE seismic reflection profiling. Tectonics 8, 305-332.

Cornwall, H.R., 1954. Bedrock Geology of the Fort Wilkins quadrangle, Michigan. U.S. geol. Surv. Quad. Map GQ-52.

Corsetti, F.A., Storrie-Lombardi, M.C., 2003. Lossless compression of stromatolite images: a biogenicity index?. Astrobiology 3, 649-655.

Davis, D.W., Paces, J.B., 1990. Time resolution of geologic events on the Keweenaw Peninsula and implications for development of the Midcontinent Rift system. Earth Planet. Sci. Lett. 97, 54-64.

Dickas, A.B., 1986. Comparative Precambrian stratigraphy and structure along the mid-continent rift. Am. Assoc. Pet. Geol. Bull. 70, 225-238.

Druschke, P.A., Jiang, G., Anderson, T.B., Hanson, A.D., 2009. Stromatolites in the Late Ordovician Eureka Quartzite: implications for microbial growth and preservation in siliciclastic settings. Sedimentology 56, 1275-1291.

Dupraz, C., Reid, R.P., Braissant, O., Decho, A.W., Norman, R.S., Visscher, P.T., 2009. Processes of carbonate precipitation in modern microbial mats. Earth-Science Reviews 96, 141-162.

Dupraz, C., Visscher, P.T., Baumgartner, L.K., Reid, R.P., 2004. Microbe-mineral interactions: early carbonate precipitation in a hypersaline lake (Eleuthera Island, Bahamas). Sedimentology 51, 745-765.

Elmore, R.D., 1984. The Copper Harbor Conglomerate: A late Precambrian fining-upward alluvial fan sequence in northern Michigan. Geological Society of America Bulletin 95, 610-617.

Elmore, R.D., 1983. Precambrian non-marine stromatolites in alluvial fan deposits, the Copper Harbor Conglomerate, upper Michigan. Sedimentology 30, 829-842.

Elmore, R.D., Milavec, G.J., Imbus, S.W., Engel, M.H., 1989. The Precambrian nonesuch formation of the North American mid-continent rift, sedimentology and

organic geochemical aspects of lacustrine deposition. Precambrian Res. 43, 191-213.

Elmore, R.D., Van der Voo, R., 1982. Origin of hematite and its associated remanence in the Copper Harbor Conglomerate (Keweenawan), upper Michigan. Journal of Geophysical Research: Solid Earth 87, 10918-10928.

Fabricius, F. H., 1977. Origin of marine ooids and grapestones. Contributions to Sedimentology 7, 1-113.

Gawthorpe, R.L., Leeder, M.R., 2000. Tectono-sedimentary evolution of active extensional basins. Basin Research 12, 195-218.

Gerdes, G., 2007. Structures left by modern microbial mats in their host sediments. In: Schieber, J., Bose, P.K., Eriksson, P.G., Banerjee, S., Sarkar, S., Altermann, W., Catuneau, O. (Eds.), Atlas of Microbial Mat Features Preserved Within the Clastic Rock Record, Atlases in Geosciences. Elsevier, Amsterdam, pp. 5-38.

Gerdes, G., Klenke, T., Noffke, N., 2000. Microbial signatures in peritidal siliciclastic sediments: a catalogue. Sedimentology 47, 279-308.

Gerdes, G., Krumbein, W.E., Reineck, H.-E., 1985. The depositional record of sandy versicolored tidal flats (Mellum Island, southern North Sea). Journal of Sedimentary Research 55, 265-278.

Grotzinger, J.P., Knoll, A.H., 1999. Stromatolites in Precambrian carbonates: Evolutionary Mileposts or Environmental Dipsticks?. Annu. Rev. Earth Planet. Sci. 27, 313-358.

Grotzinger, J.P., Rothman, D.H., 1996. An abiotic model for stromatolite morphogenesis. Nature 383, 423-425.

Hedlund, D.C., 1953. An Algal Limestone in the Keweenawan of Upper Michigan. Unpublished Masters Thesis, University of Wisconsin-Madison, 1-45.

Hofmann, H.J., Grotzinger, J.P., 1985. Shelf-facies microbiotas from the Odjick and Rocknest formations (Epworth Group; 1.9 Ga), northwest Canada. Canadian Journal of Earth Sciences 22, 1781-1792.

Kalliokoski, J., 1986. Calcium carbonate cement (caliche) in Keweenawan sedimentary rocks (~1.1 Ga), upper peninsula of Michigan. Precambrian Research 32, 243-259.

Kamennaya, N.A., Ajo-Franklin, C.M., Northen, T., Jansson, C., 2012. Cyanobacteria as biocatalysts for carbonate mineralization. Minerals 2, 338-364.

Knoll, A.H., Semikhatov, M.A., 1998. The genesis and time distribution of two distinctive Proterozoic stromatolite microstructures. Palaios 13, 408-422.

Leeder, M.R., 1995. Continental rifts and proto-oceanic rift troughs. In: Busby, C.J., Ingersoll, R.V. (eds.), Tectonics of Sedimentary Basins. Blackwell, Cambridge, Massachusetts, pp. 119-148.

Leeder, M.R., Gawthorpe, R.L., 1987. Sedimentary models for extensional tilt-block/half-graben basins. In: Coward, M.P., Dewey, J.F., Hancock, P.L. (eds.), Continental Extensional Tectonics. Geological Society of London Special Publications 28, 139-152.

Liesa, C.L., Soria, A.R., Meléndez, N., Meléndez, A., 2006. Extensional fault control on the sedimentation patterns in a continental rift basin: El Castellar Formation, Galve sub-basin, Spain. Journal of the Geological Society 163, 487-498.

Melchor, R.N., 2007. Changing lake dynamics and sequence stratigraphy of synrift lacustrine strata in a half graben: an example from the Triassic Ischigualasto-Villa Unión Basin, Argentina. Sedimentology 54, 1417-1446.

Milroy, P.G., Wright, V.P., 2002. Fabrics, facies control and diagenesis of lacustrine ooids and associated grains from the upper Triassic, southwest England. Geological Journal 37, 35-53.

Mitchell, R.L., Sheldon, N.D., 2010. The ~1100Ma Sturgeon Falls paleosol revisited: Implications for Mesoproterozoic weathering environments and atmospheric CO_2 levels. Precambrian Res. 183, 738-748.

Mitchell, R.L., Sheldon, N.D., 2009. Weathering and paleosol formation in the 1.1 Ga Keweenawan Rift. Precambrian Res. 168, 271-283.

Nemec, W., Steel, R.J., 1984. Alluvial and coastal conglomerates: their significant features and some comments on gravelly mass-flow deposits. In: Koster, R.H., Steel, R.J. (eds.), Sedimentology of gravels and conglomerates. Canadian Society of Petroleum Geologists, Memoir 10, 1-31.

Nishioka, G.K., Kelly, W.C., Elmore, R.D., 1984. Copper occurrences in stromatolites of the Copper Harbor Conglomerate, Keeweenaw Peninsula, northern Michigan. Economic Geology 79, 1393-1399.

Noffke, N., 1998. Multidirected ripple marks rising from biological and sedimentological processes in modern lower supratidal deposits (Mellum Island, southern North Sea). Geology 26, 879-882.

Noffke, N., Eriksson, K.A., Hazen, R.M., Simpson, E.L., 2006. A new window into Early Archean life: microbial mats in Earth's oldest siliciclastic tidal deposits (3.2 Ga Moodies Group, South Africa). Geology 34, 253-256.

Noffke, N., Gerdes, G., Klenke, T., 2003. Benthic cyanobacteria and their influence on the sedimentary dynamics of peritidal depositional systems (siliciclastic, evaporitic salty, and evaporitic carbonate). Earth-Science Reviews 62, 163-176.

Nordeng, S.C., 1963. Precambrian stromatolites as indicators of polar shift. In: Munyan A.C. (ed.), Polar wandering and continental drift. SEPM Special Publication 10, 131-139.

Ojakangas, R.W., Morey, G.B., Green, J.C., 2001. The Mesoproterozoic midcontinent rift system, Lake Superior region, USA. Sedimentary Geology 141, 421-442.

Petryshyn, V.A., Corsetti, F.A., 2011. Analysis of growth directions of columnar stromatolites from Walker Lake, western Nevada. Geobiology 9, 425-435.

Petryshyn, V.A., Corsetti, F.A., Lund, S., and Berelson, W., 2010. Magnetic susceptibility as a biosignature. Journal of Earth Sciences 21, 329-332.

Pan, Y., Zhu, R., Banerjee, S.K., Gill, J., Williams, Q., 2000. Rock magnetic properties related to thermal treatment of siderite: behavior and interpretation. Journal of Geophysical Research 105, 783-794.

Pope, M.C., Grotzinger, J.P., 2000. Controls on fabric development and morphology of tufa and stromatolites, uppermost Pethei Group (1.8 Ga), Great Slave Lake, Northwest Canada. In: James, N.P., Grotzinger, J.P. (eds.), Carbonate sedimentation and diagenesis in the evolving Precambrian world. SEPM Special Publication 67, 103-121.

Pope, M.C., Grotzinger, J.P., Schreiber, B.C., 2000. Evaporitic subtidal stromatolites produced by in situ precipitation: textures, facies associations, and temporal significance. Journal of Sedimentary Research 70, 1139-1151.

Pratt, L.M., Summons, R.E., Hieshima, G.B., 1991. Sterane and triterpane biomarkers in the Precambrian Nonesuch Formation, North American Midcontinent Rift. Geochim. Cosmochim. Acta 55, 911-916.

Riding, R., 2008. Abiogenic, microbial and hybrid authigenic carbonate crusts: components of Precambrian stromatolites. Geologia Croatica 61, 73-103.

Riding, R., 2000. Microbial carbonates: the geological record of calcified bacterial–algal mats and biofilms. Sedimentology 47, 179-214.

Riding, R., 1999. The term stromatolite: towards an essential definition. Lethaia 32, 321-330.

Schneider, J., Le Campion-Alsumard, T., 1999. Construction and destruction of carbonates by marine and freshwater cyanobacteria. Eur. J. Phycol. 34, 417-426.

Semikhatov, M.A., Gebelein, C.D., Cloud, P., Awramik, S.M., Benmore, W.C., 1979. Stromatolite morphogenesis-progress and problems. Canadian Journal of Earth Sciences 16, 992-1015.

Schlische, R.W., Olsen, P.E., 1990. Quantitative filling model for continental extensional basins with applications to early Mesozoic rifts of eastern North America. Journal of Geology 98, 135-155.

Schmidt, P.W., Williams, G.E., 2003. Reversal asymmetry in Mesoproterozoic overprinting of the 1.88-Ga Gunflint Formation, Ontario, Canada: non-dipole effects or apparent polar wander?. Tectonophysics 377, 7-32.

Sheldon, N.D., 2012. Microbially induced sedimentary structures in the ca. 1100 Ma terrestrial midcontinent rift of North America. In: Nofke, N., Chafetz, H.S., (Eds.), Microbial mats in siliciclastic depositional systems through time. SEPM Special Publication 101, 153-162.

Steel, R.J., Wilson, A.C., 1975. Sedimentation and tectonism (? Permo-Triassic) on the margin of the North Minch Basin, Lewis. Jour. Geol. Soc. London 131, 183-202.

Sumner, D.Y., Grotzinger, J.P., 1996. Herringbone calcite; petrography and environmental significance. Journal of Sedimentary Research 66, 419-429.

Thompson, R., Oldfield, F., 1986. Environmental Magnetism. Allen and Unwin, London.

Van Schmus, W.R., Hinze, W.J., 1985. The midcontinent rift system. Annu. Rev. Earth Planet. Sci. 13, 345.

Visscher, P.T., Stolz, J.F., 2005. Microbial mats as bioreactors: populations, processes and products. Palaeogeography, Palaeoclimatology, Palaeoecology 219, 87-100.

Walter, M.R., 1976. Introduction. In: Walter, M.R. (Ed.), Stromatolites, developments in sedimentology. Elsevier, Amsterdam, pp. 1-3.

White, W.S., Wright, J.C., 1960. Lithofacies of the Copper Harbor Conglomerate, northern Michigan. US Geol. Surv. Prof. Pap. 400-B, B5-B8.

Wilmeth, D.T., Dornbos, S.Q., Isbell, J.L., Czaja, A.D., 2014. Putative domal microbial structures in fluvial siliciclastic facies of the Mesoproterozoic (1.09 Ga) Copper Harbor Conglomerate, Upper Peninsula of Michigan, USA. Geobiology 12, 99-108.

Withjack, M.O., Schlische, R.W., Olsen, P.E., 2002. Rift-basin structure and its influence on sedimentary systems. In: Renault, R.W., Ashley, G. (eds.), Sedimentation in Continental Rifts. SEPM Special Publications 73, 57-81.

Wolff, R.G., Huber, N.K., 1973. The Copper Harbor Conglomerate (middle Keweenawan) on Isle Royale, Michigan, and its regional implications. US Geol. Surv. Prof. Pap. 754-B, B1-B15.

Zavarzin, G.A., 2002. Microbial geochemical calcium cycle. Microbiology 71, 5-22.

Appendix A:

Satellite Imagery Maps

Satellite imagery showing locations of Horseshoe Harbor and Dan's Point in relation to town of Copper harbor on Keweenaw Peninsula (modified from Google Earth).

Satellite imagery and photo showing location of Horseshoe Harbor. Measured section marked by dashed line. B represents base of section and T represents top of section (modified from Google Earth).

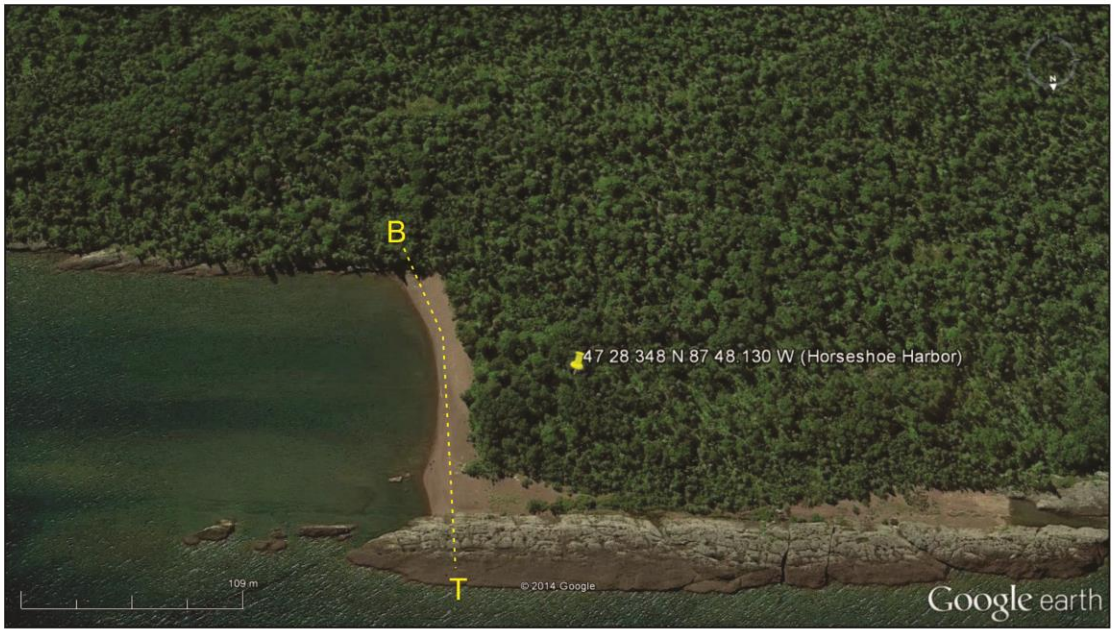

Satellite imagery and photo showing location of Dan's Point. Measured section marked by dashed line. B represents base of section and T represents top of section (modified from Google Earth).

Appendix B:

Horseshoe Harbor Field Photographs

Field assistant Dylan Wilmeth standing next to outcrop of stromatolite bearing siltstone overlain by a large conglomerate bed at Horseshoe Harbor ~64 m from base of measured section.

Interstratified sandstone, clast-supported conglomerate and matrix-supported conglomerate beds resulting from espisodic sheet-flow and debris flow deposition. Located within conglomerate facies at Horseshoe Harbor ~53 m above base of measured section.

Same outcrop as described in previous figure.

Volcanogenic clasts within conglomerate facies at Horseshoe Harbor.

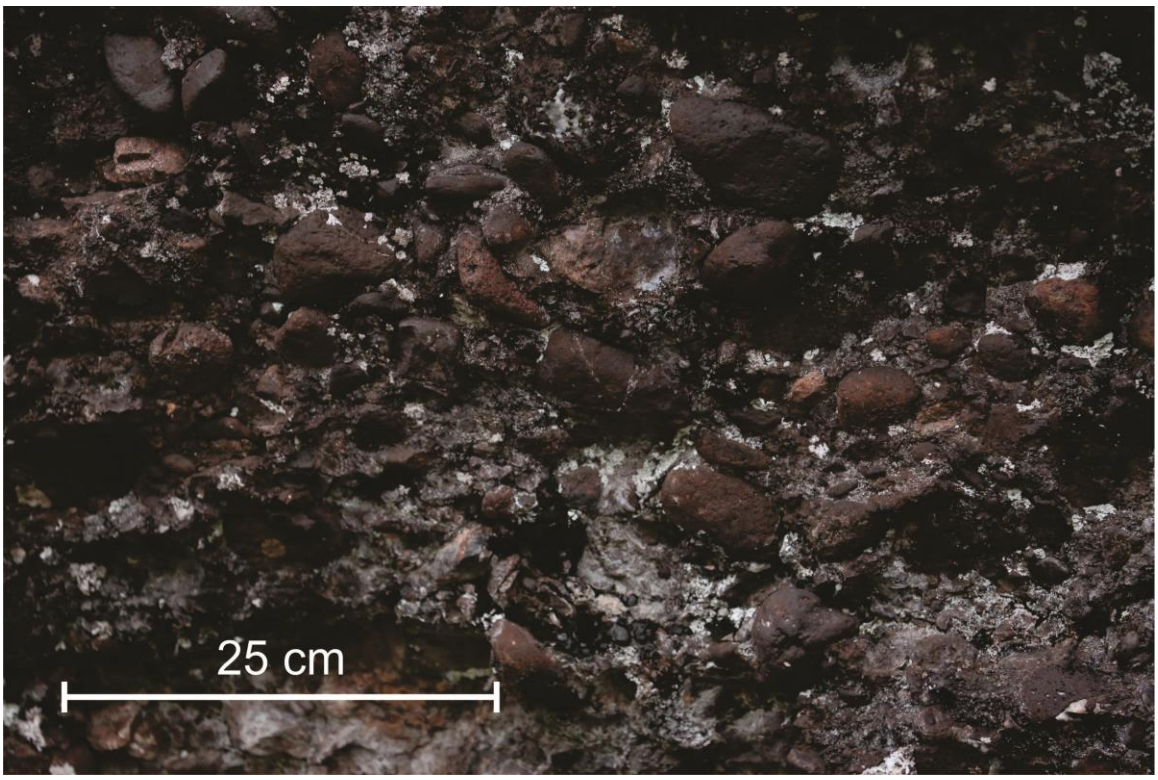

Large outcrop of conglomerate facies with accretionary surfaces marked by dotted yellow lines. Located at Horseshoe Harbor ~67 m from base of measured section. Solid yellow line denotes location of small lenticular sand body.

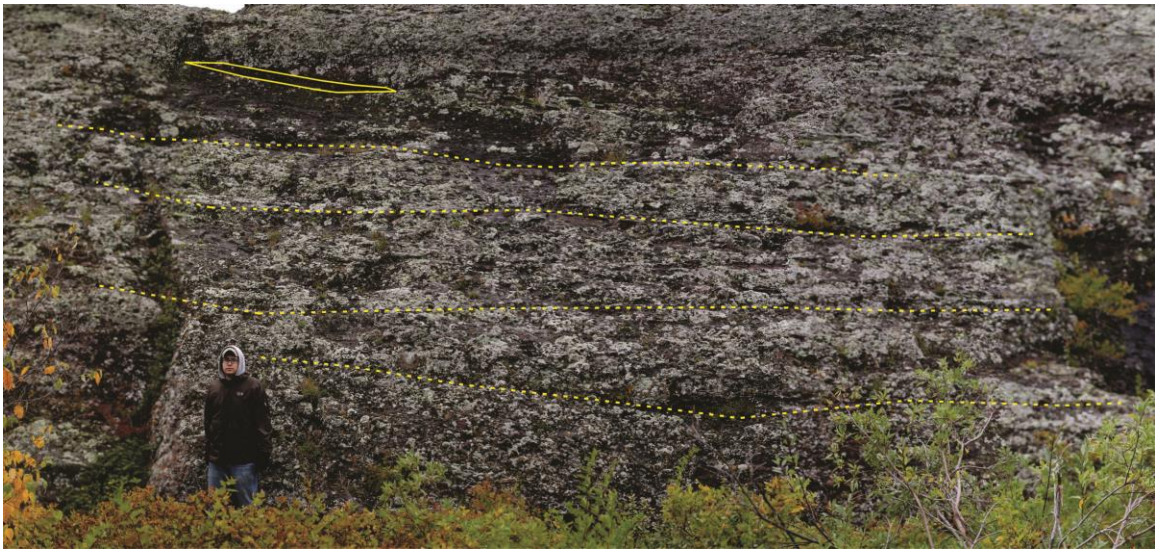

Boundary between siltstone facies and overlying conglomerate facies at Horseshoe Harbor ~67 m above base of measured section. Dashed white line represents erosional contact.

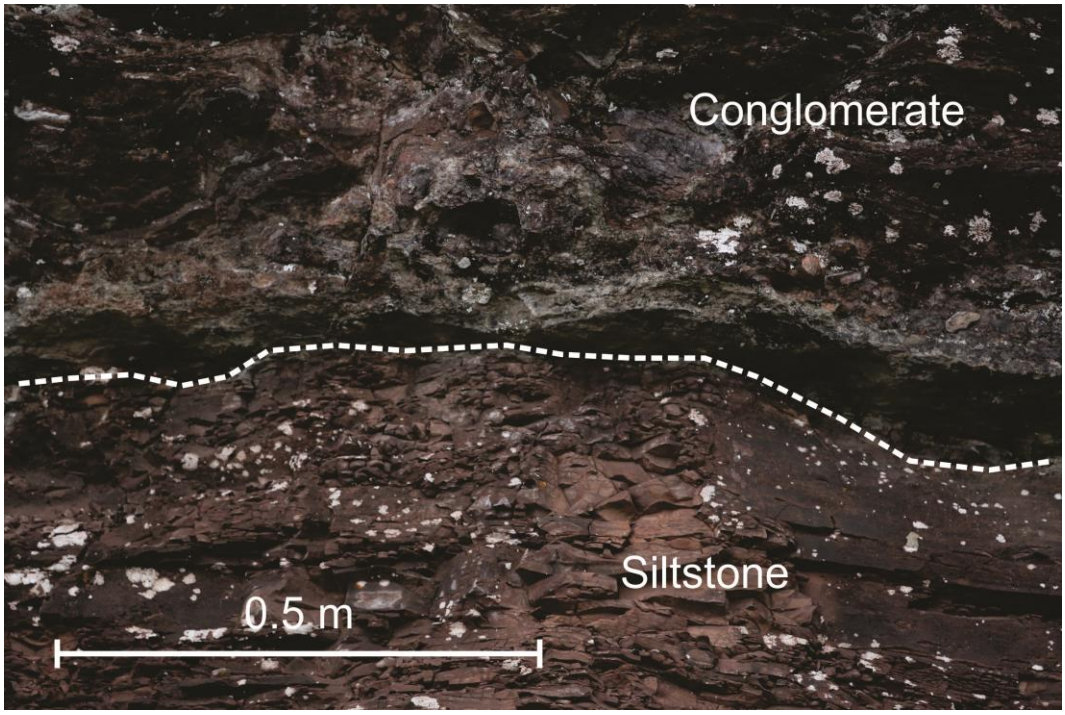

Horseshoe Harbor-type stromatolite preserved within siltstone facies at Horeshoe Harbor ~64 m above base of the measured section with characteristic contorted appearance.

Carbonate filled desiccation crack beneath stromatolite bed at Horseshoe Harbor ~64 m above base of measured section.

Stromatolite bed growing over eroded topography within siltstone facies at Horseshoe Harbor ~64 m above base of measured section.

Stromatolite bed with siltstone rip-up clast incorporated into laminae at Horseshoe Harbor ~64 m above base of measured section.

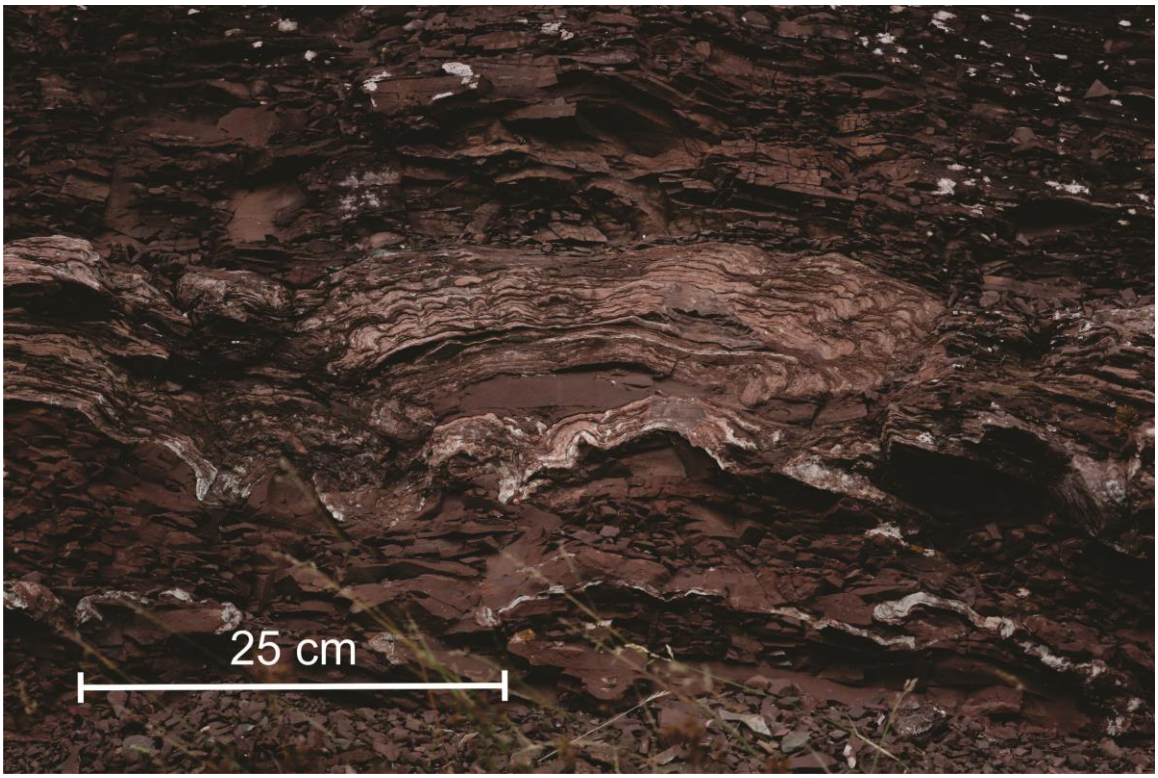

Undeformed siltstone beds overlying stromatolite bed at Horseshoe Harbor ~64 m above base of measured section. This implies post-depositional deformation is not causing contorted appearance of stromatolites.

Wave ripples from siltstone facies at Horseshoe Harbor ~63 m above base of measured section.

Appendix C:

Dan's Point Field Photographs

Field assistant Dylan Wilmeth observing stromatolite bed at Dan's Point ~11 m above base of measured section.

Dashed line denotes location of stromatolite bed at Dan's Point, ~11 m above base of measured section, which appears as a carbonate crust draping over underlying conglomerate.

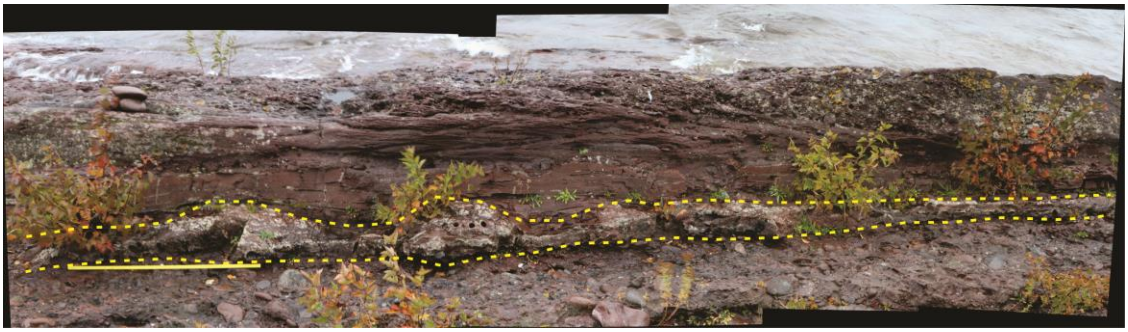

Trough cross-stratified sandstone facies at Dan's Point ~17 m above base of measured section.

Several large stromatolite mounds with siltstone drapes at Dan"s Point ~11 m above base of measured section. Each mound is comprised of many individual stromatolite domes nucleated on underlying cobbles or boulders.

Stromatolite mound with siltstone drapes at Dan's Point ~11 m above base of measured section.

Rip-up clasts within siltstone facies at Dan's Point ~6 m above base of measured section.

Coated grains and aggregate grains located within stromatolite bed at Dan's Point ~11 m above base of measured section.

Cobble-sized clast incorporated into laminae of Dan's Point-type stromatolite. Located at Dan's Point ~11 m above base of measured section.

Microdigitate mound comprised of small individual stromatolite domes at Dan's Point ~11 m above base of measured section.

Same stromatolite as previous image at Dan's Point.

Microdigitate cobble-draping stromatolite bed overlain by siltstone drape at Dan's Point ~11 m above base of measured section.

Cross-sectional view of microdigitate stromatolite mound with empty space denoting location of boulder that stromatolites nucleated on at Dan's Point ~11 m above base of measured section.

Appendix D:

Thin Section Photographs
Horseshoe Harbor Stromatolites

Thin section of Horseshoe Harbor-type stromatolite under plane polarized light with detrital laminae, opaque hematite-rich laminae, and fenestral fabrics.

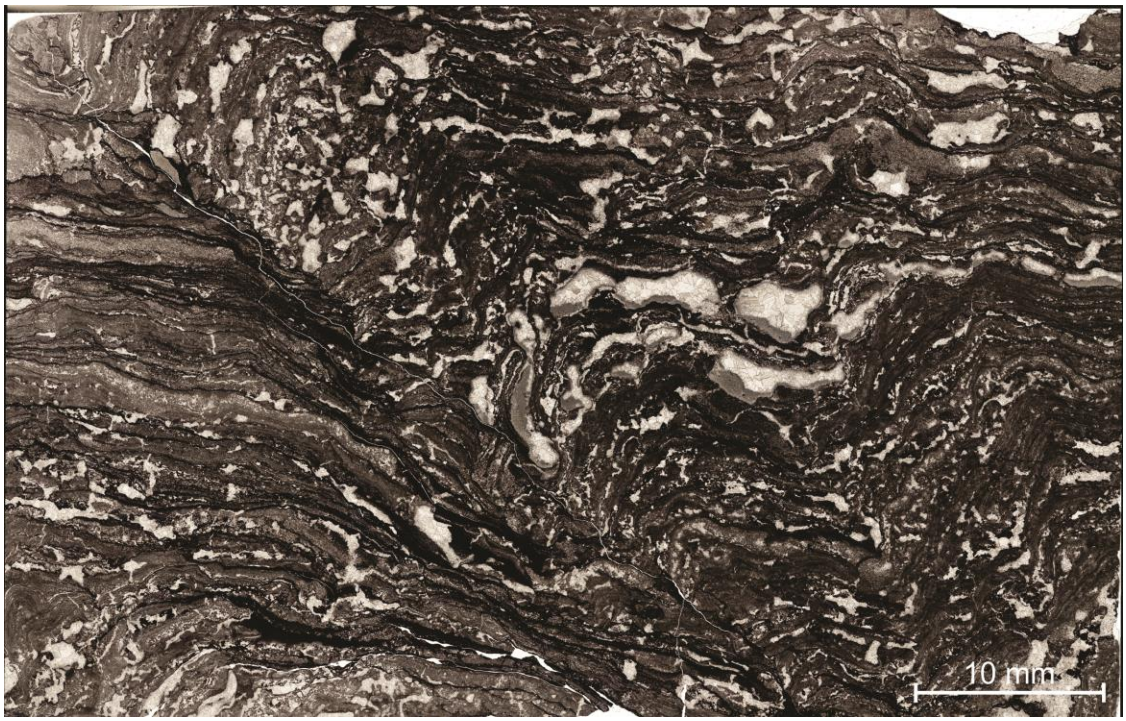

Fenestrae within Horseshoe Harbor-type stromatolites act as geopetals. Thicker accumulations of microspar located on bottom side of fenestrae while upwards side is filled in with blocky spar.

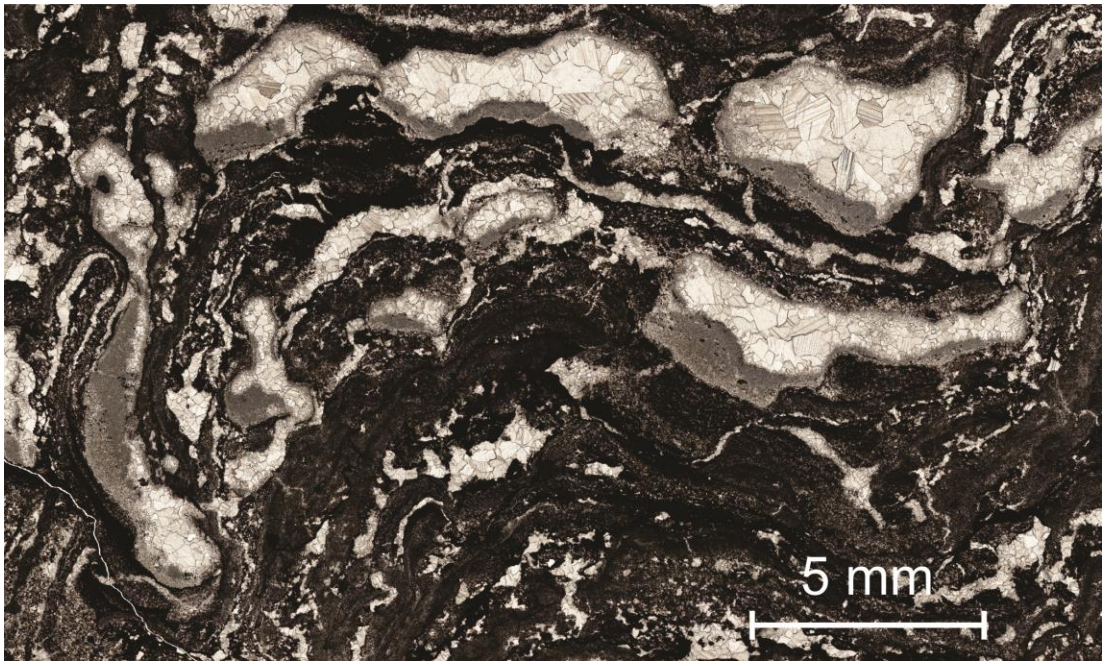

Thin section of Horseshoe Harbor-type stromatolite under reflected light. Thin dark red laminae are hematite rich.

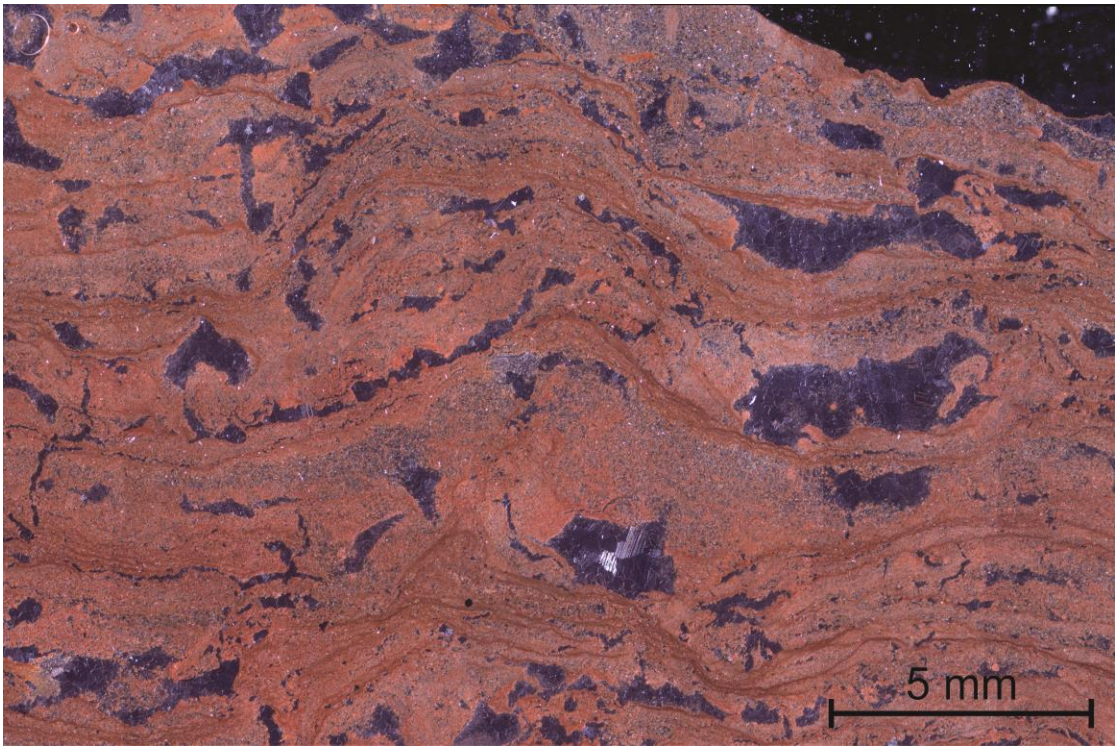

20X view under plane polarized light of opaque hematite rich laminae with clotted appearance.

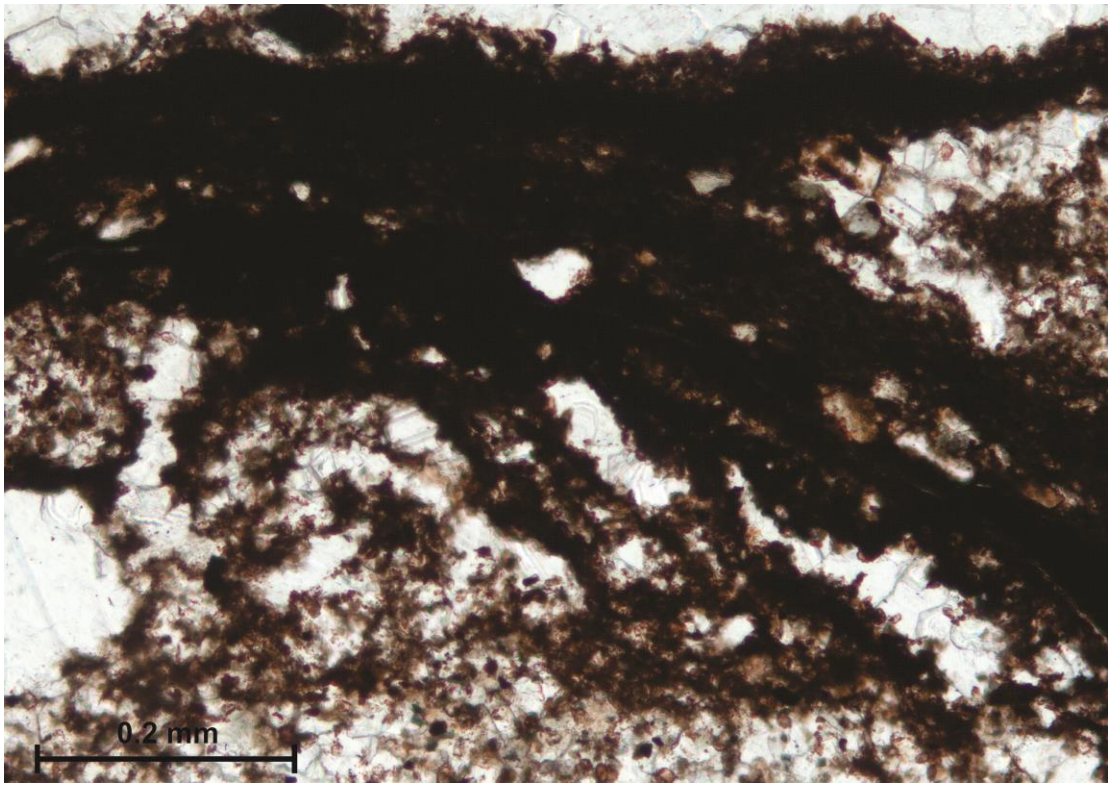

Hematite rich laminae appear opaque under plane polarized light and crossed polars.

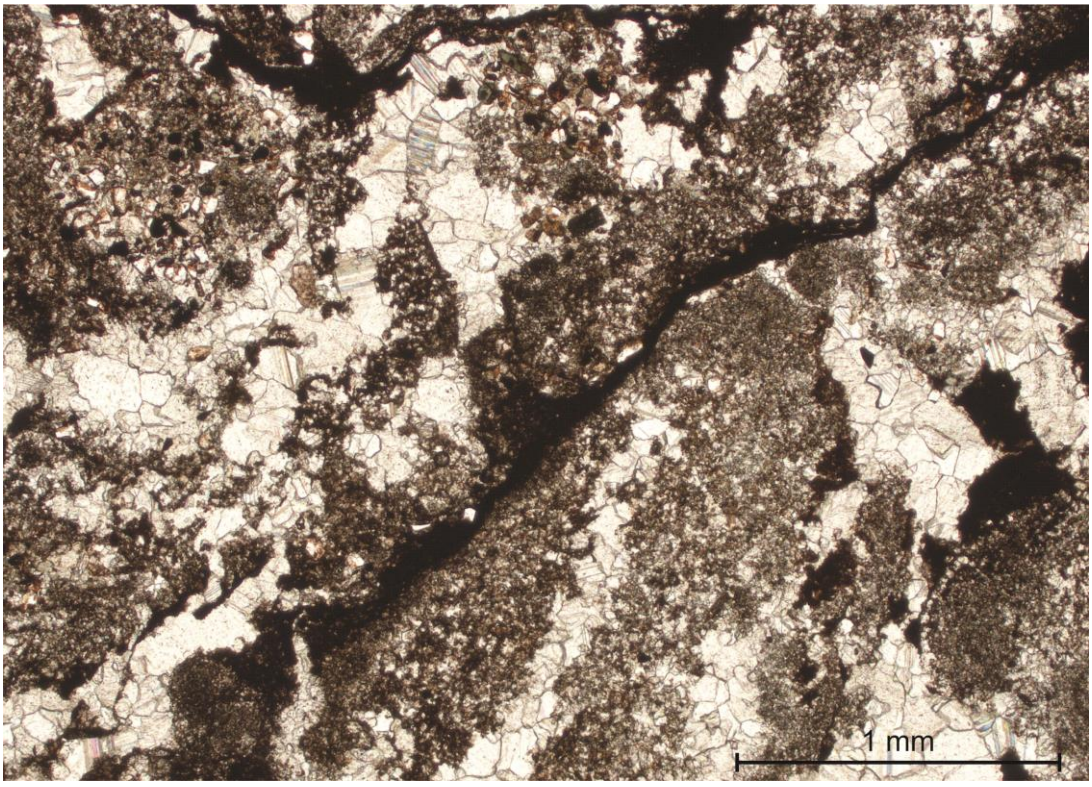

40X view of dark clotted hematite-rich laminae under reflected light.

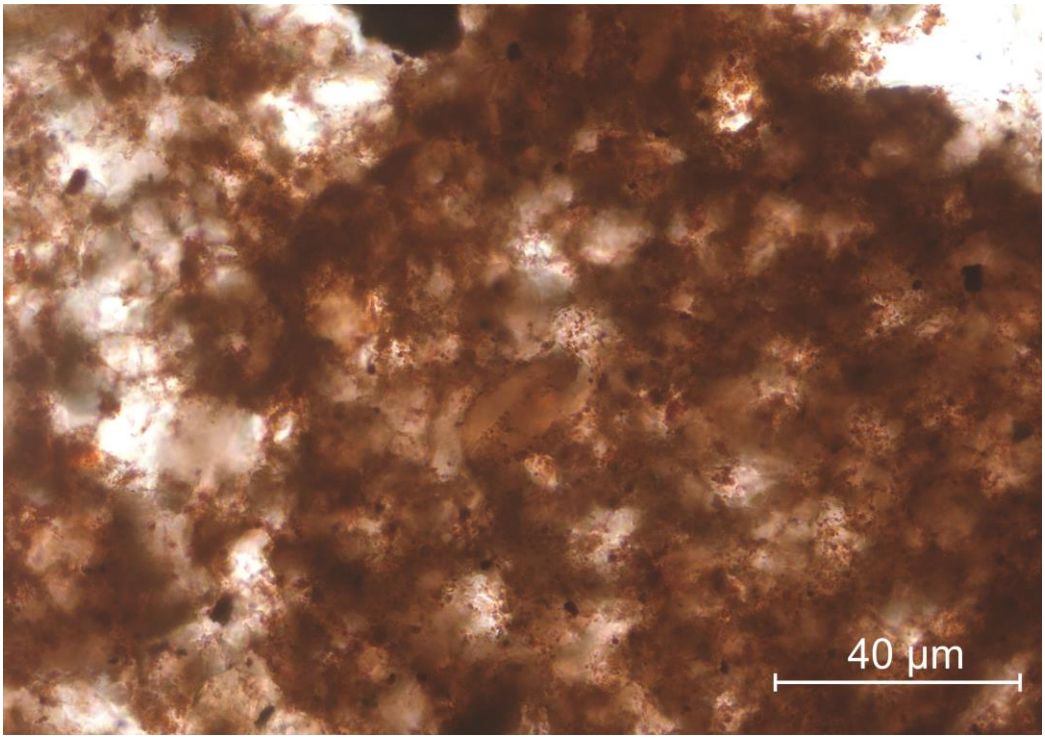

Appendix E:

Thin Section Photographs
Dan's Point Stromatolites

Microdigitate carbonate crust from Dan's Point comprised of small individual stromatolite domes under plane polarized light.

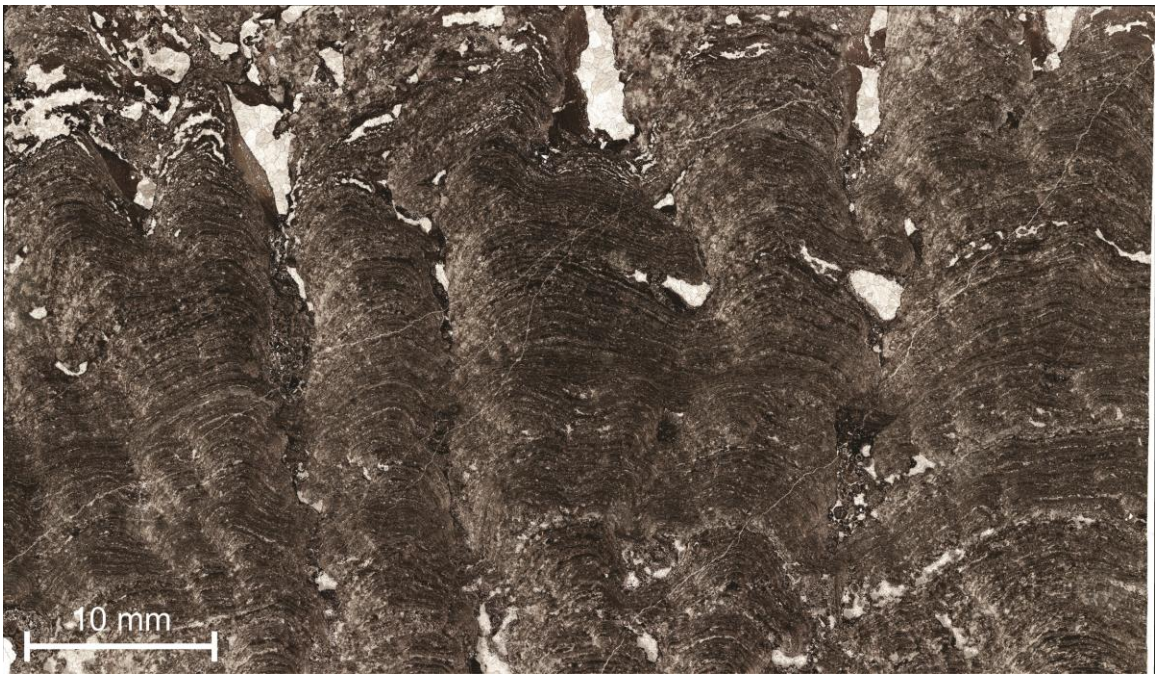

Dan's Point-type stromatolite under cross polarizing light alternating between laminae with radial fibrous fans and those without. Possibly indicative of combination of chemical and biological processes in forming stromatolites.

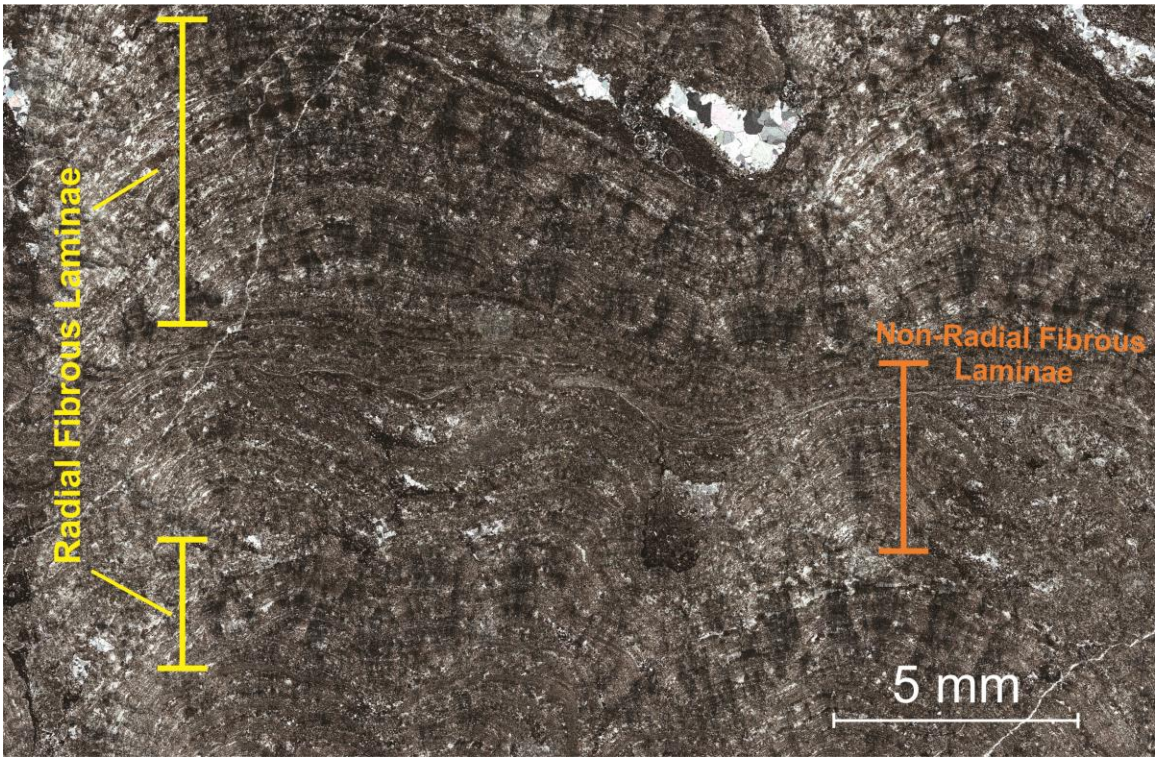

View under cross-polarizing light of ooids trapped in spacing between two stromatolite domes from Dan's Point.

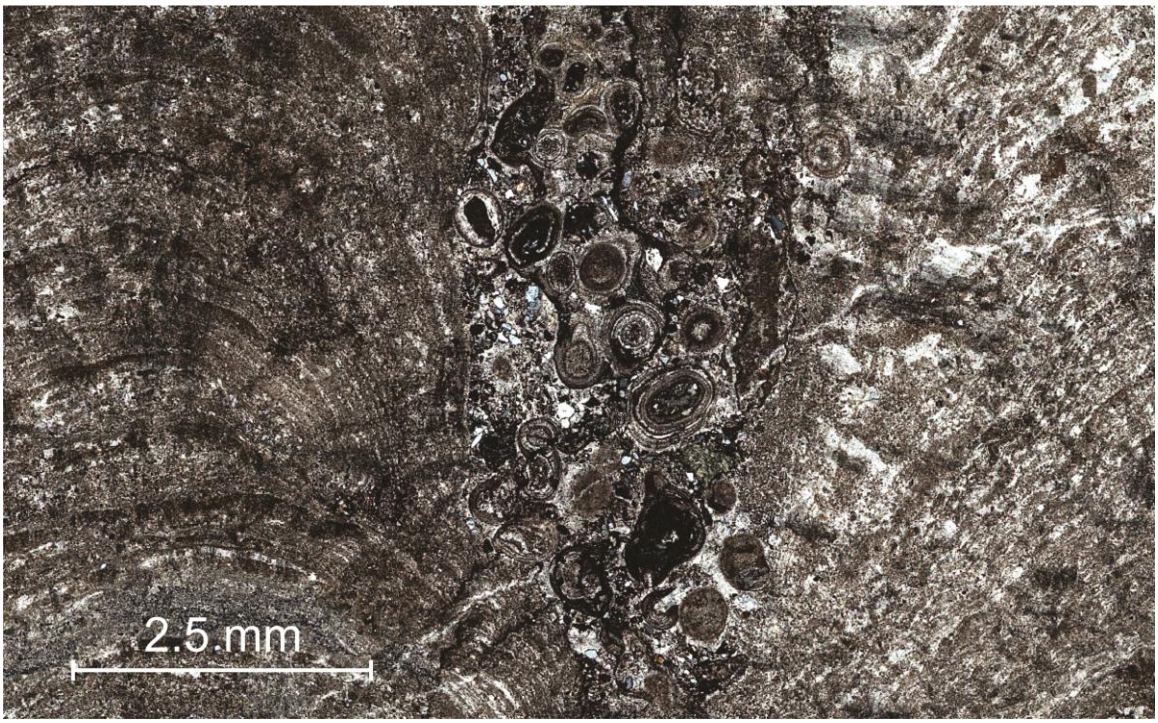

Large radial fibrous calcite fans with isopachous laminae under cross-polarizing light indicating abiogenic growth within Dan's Point-type stromatolites.

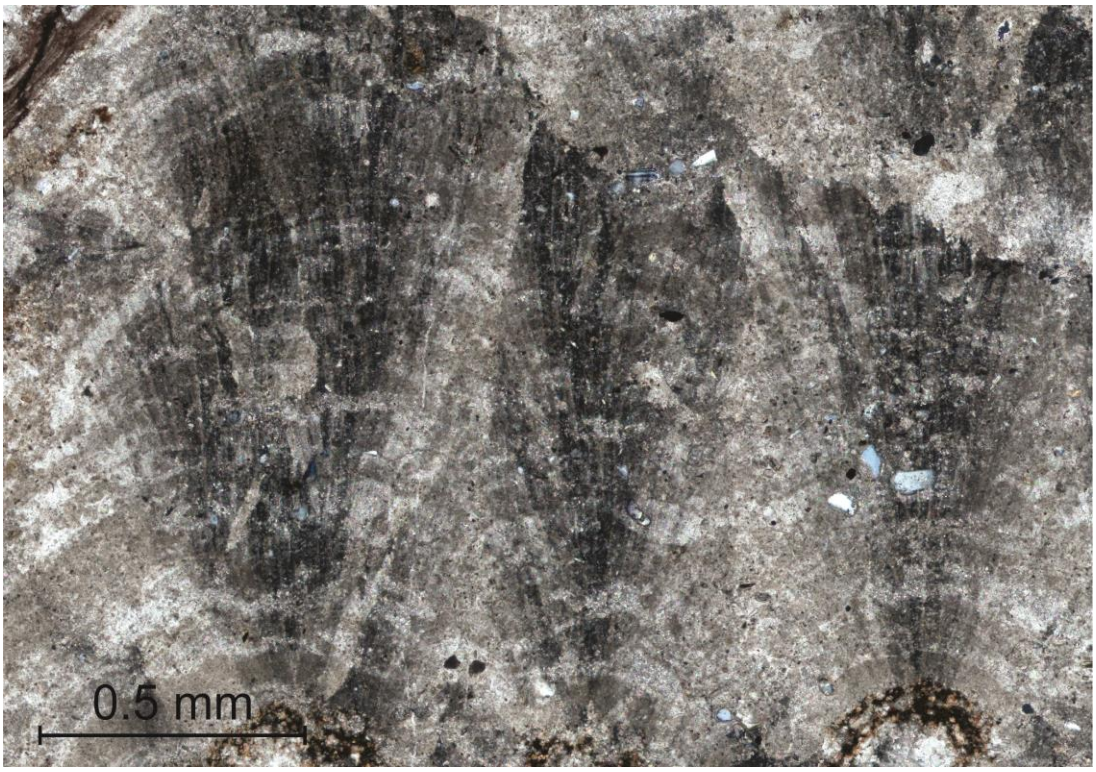

Same abiogenic isopachous laminae as previous image viewed under plane polarized light.

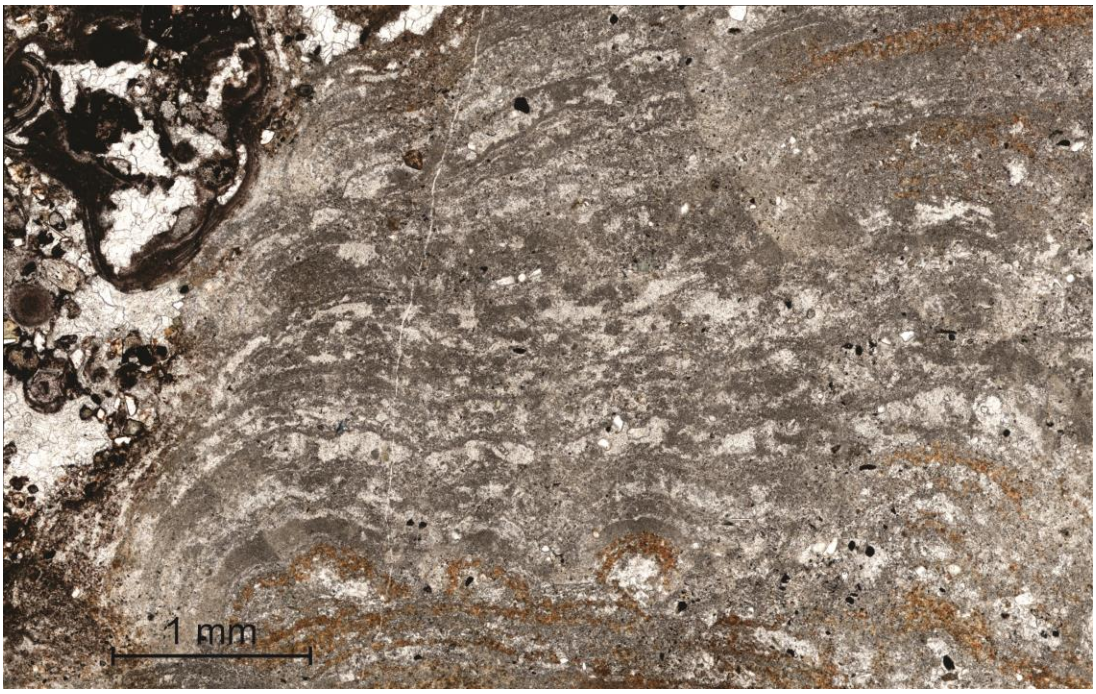

High angle flank of stromatolite dome from Dan's Point viewed under plane polarized light.

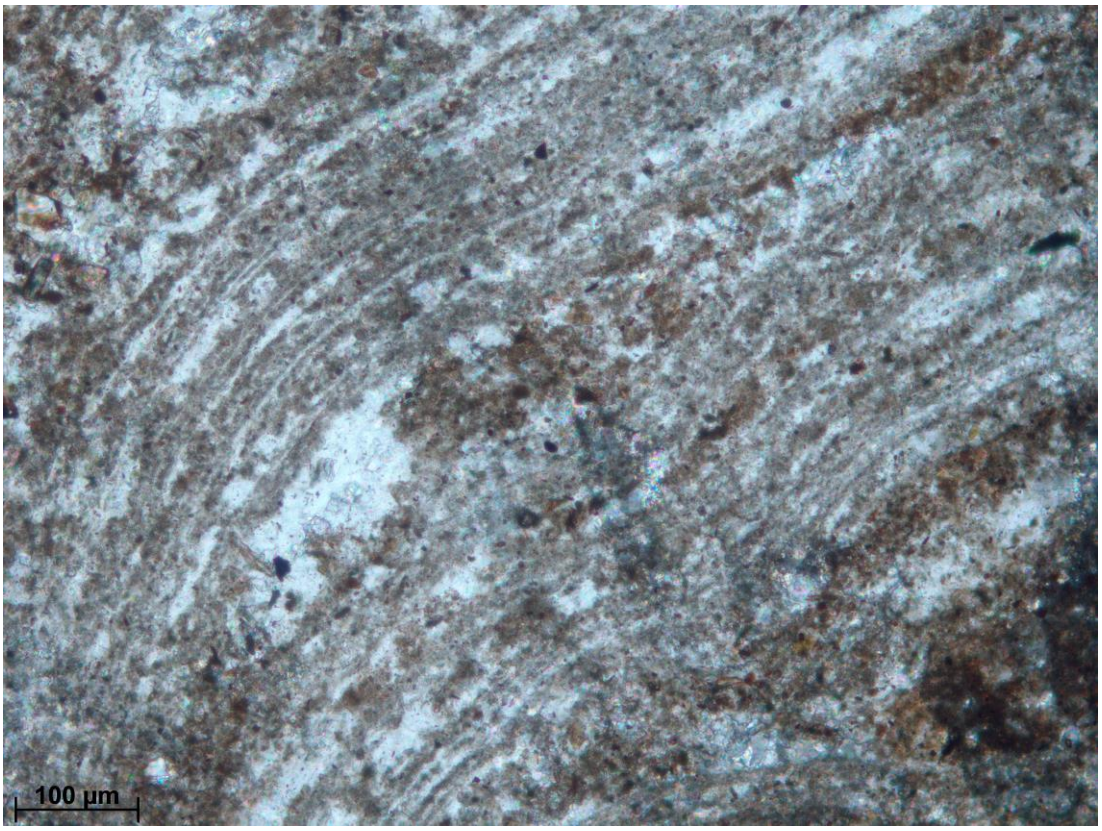

Small conical stromatolite dome from Dan's Point viewed under plane-polarized light with possible lift-off structures between laminae seen as blocky calcite. These may have formed from gas build-up within microbial mat.

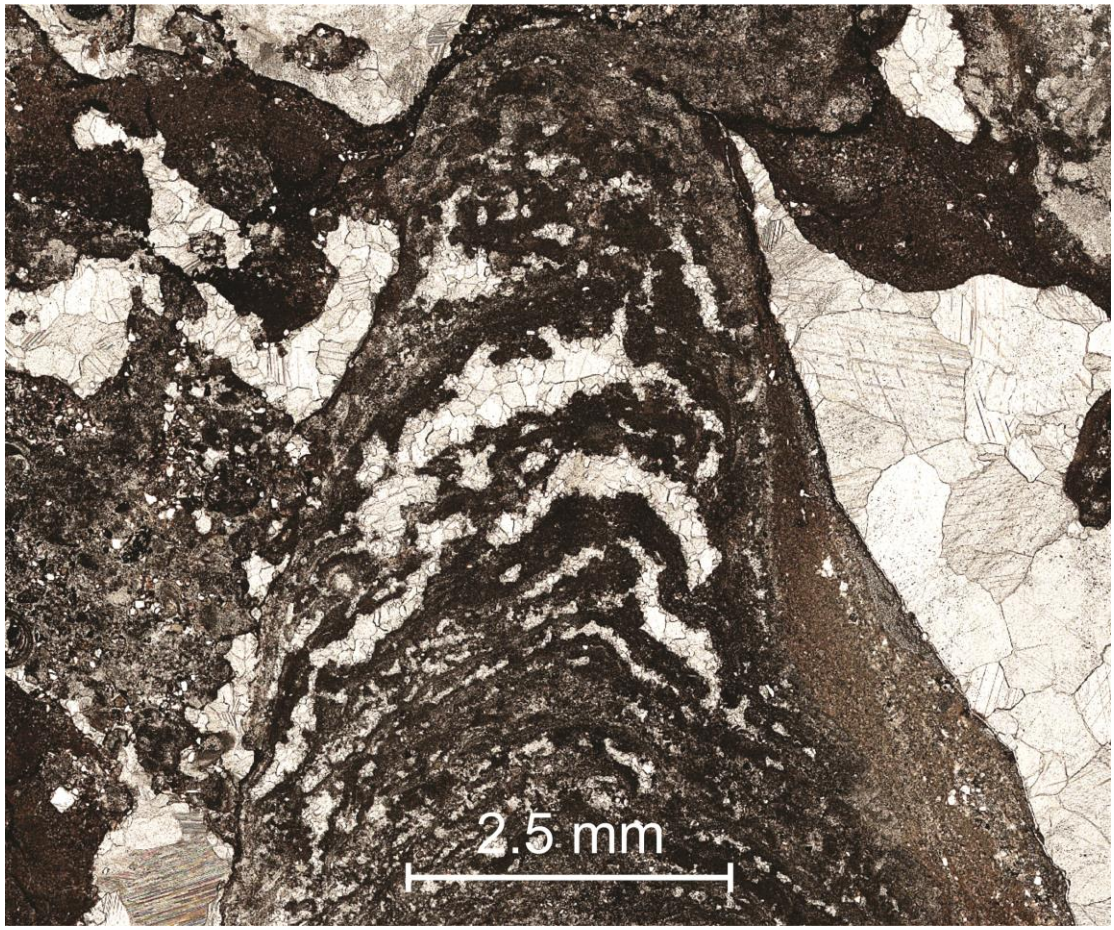

Appendix F:

Individual Laminae Transects
Horseshoe Harbor and Dan's Point Stromatolites

Very few samples could be collected from each laminae transect due to 1 mm sized drill bit and small size of individual stromatolite domes. Samples inevitably contain multiple laminae but this conforms to methodology of Petryshyn et al. (2010) as long as single laminae are consistently followed while drilling. Magnetic susceptibility should decrease to almost 0 on high-angle sides of all laminae if structure is abiogenic and magnetic component is detrital.

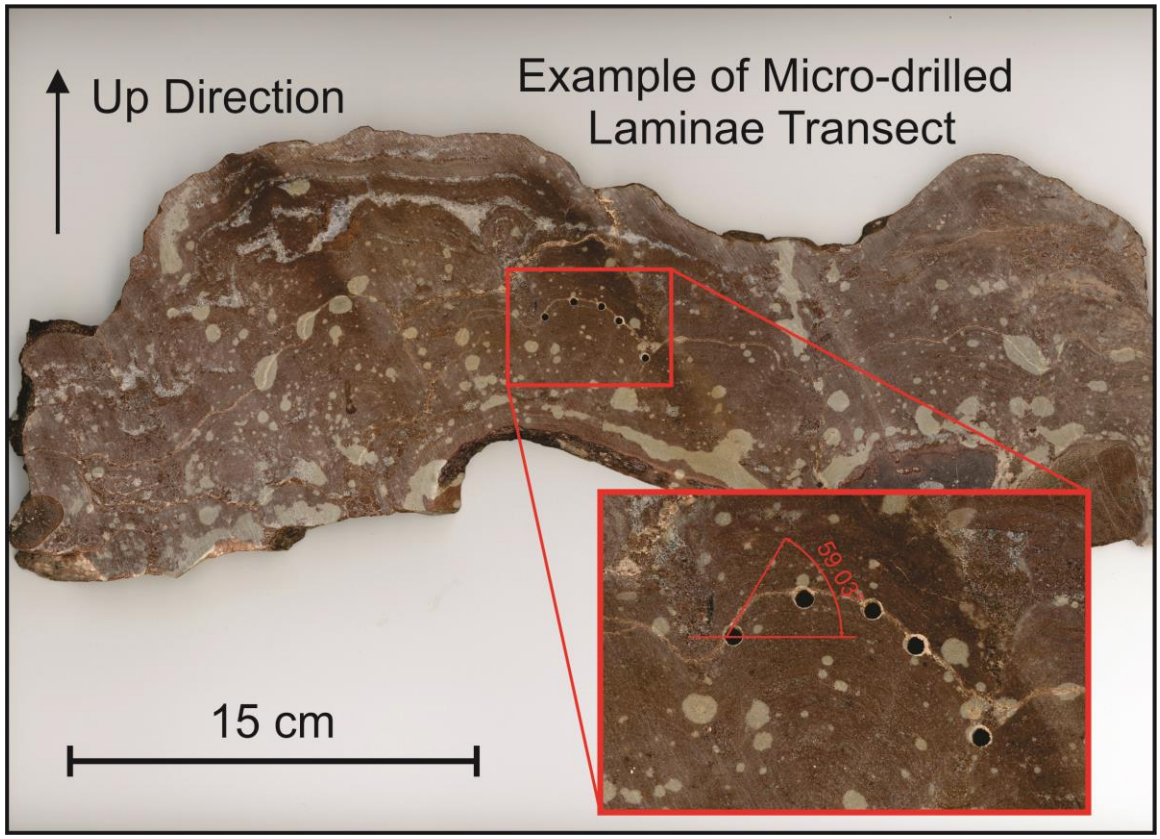

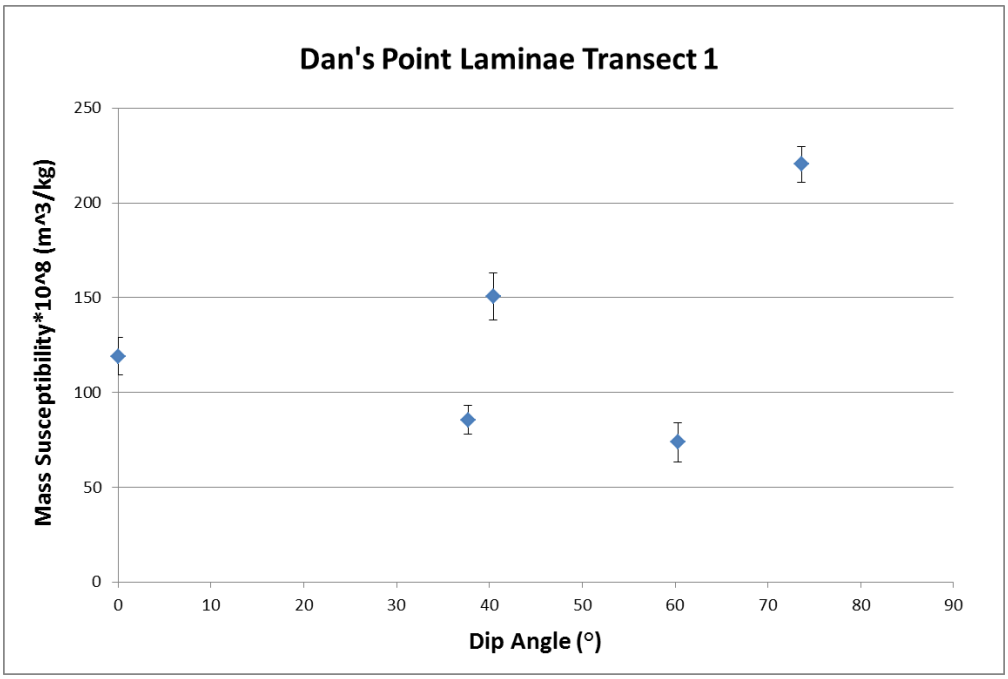
Dan's Point Laminae Transect 1
Mass Susceptibility*10^8 (m^3/kg)
250
200
150
100
50
0
0
10
20
30
40
50
60
70
80
90
Dip Angle (°)

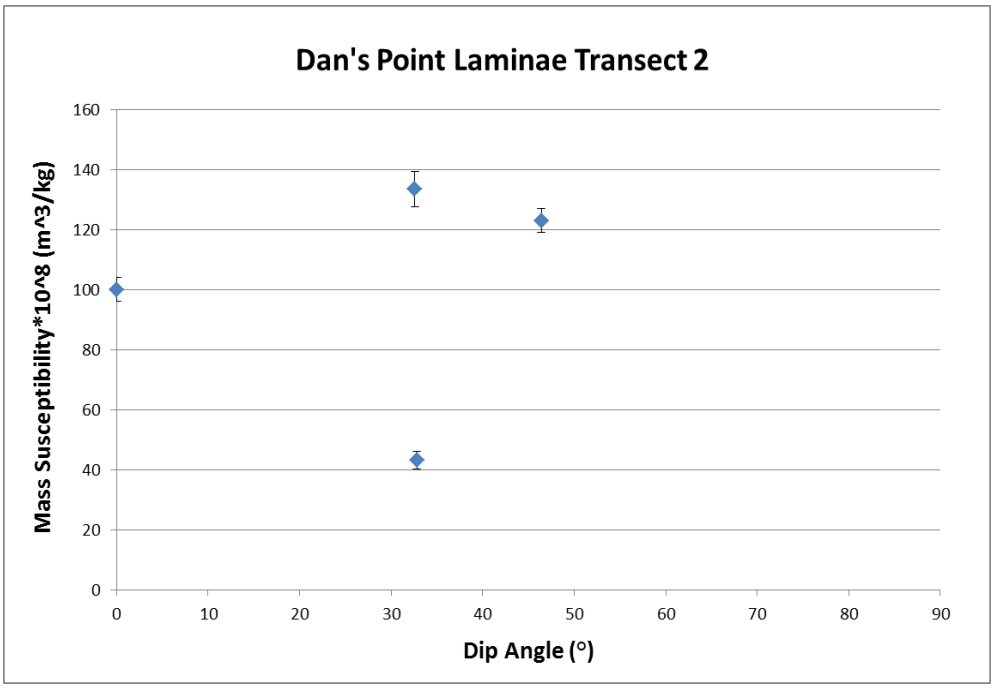
Dan's Point Laminae Transect 2
Mass Susceptibility*10^8 (m^3/kg)
160
140
120
100
80
60
40
20
0
0
10
20
30
40
50
60
70
80
90
Dip Angle (°)

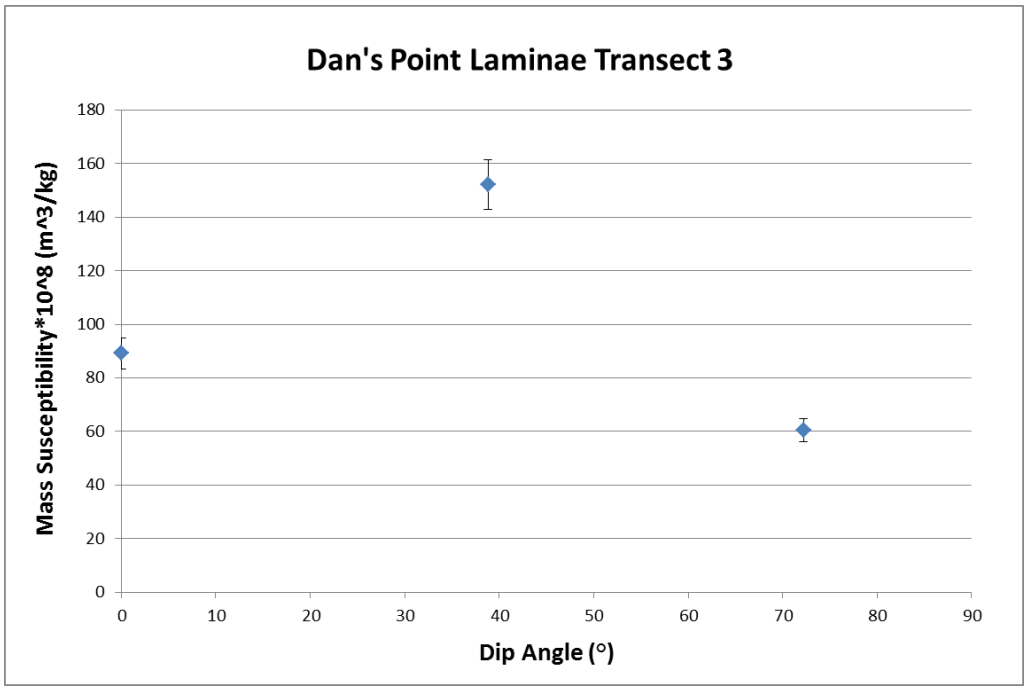
Dan's Point Laminae Transect 3
Mass Susceptibility*10^8 (m^3/kg)
180
160
140
120
100
80
60
40
20
0
0
10
20
30
40
50
60
70
80
90
Dip Angle (°)

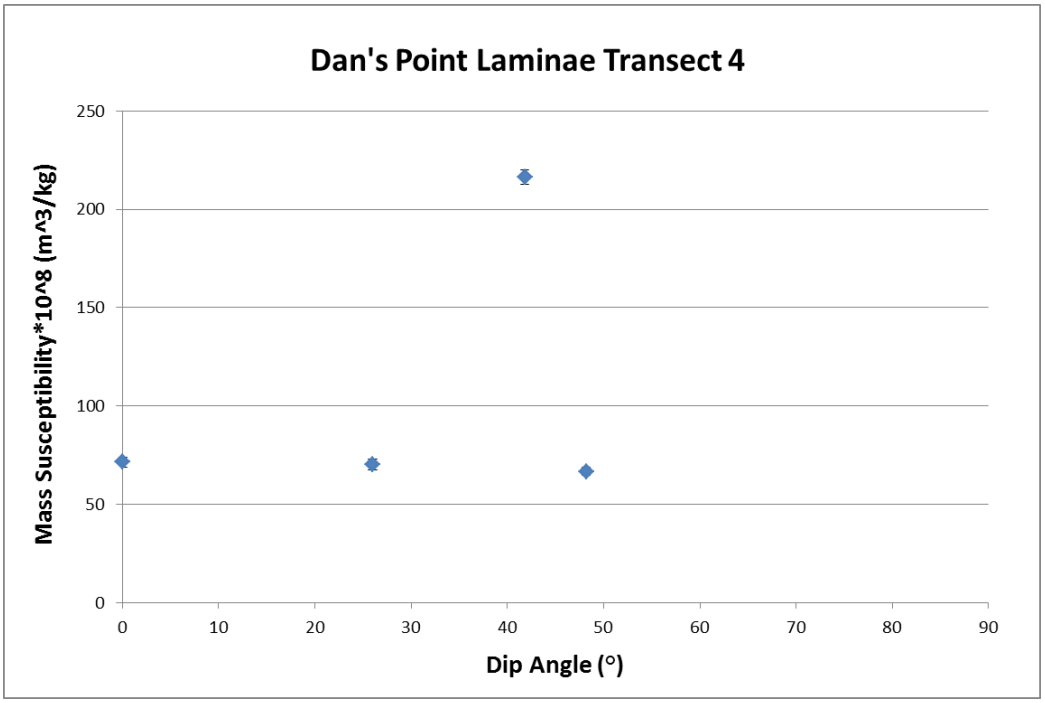
Dan's Point Laminae Transect 4
Mass Susceptibility*10^8 (m^3/kg)
250
200
150
100
50
0
0
10
20
30
40
50
60
70
80
90
Dip Angle (°)

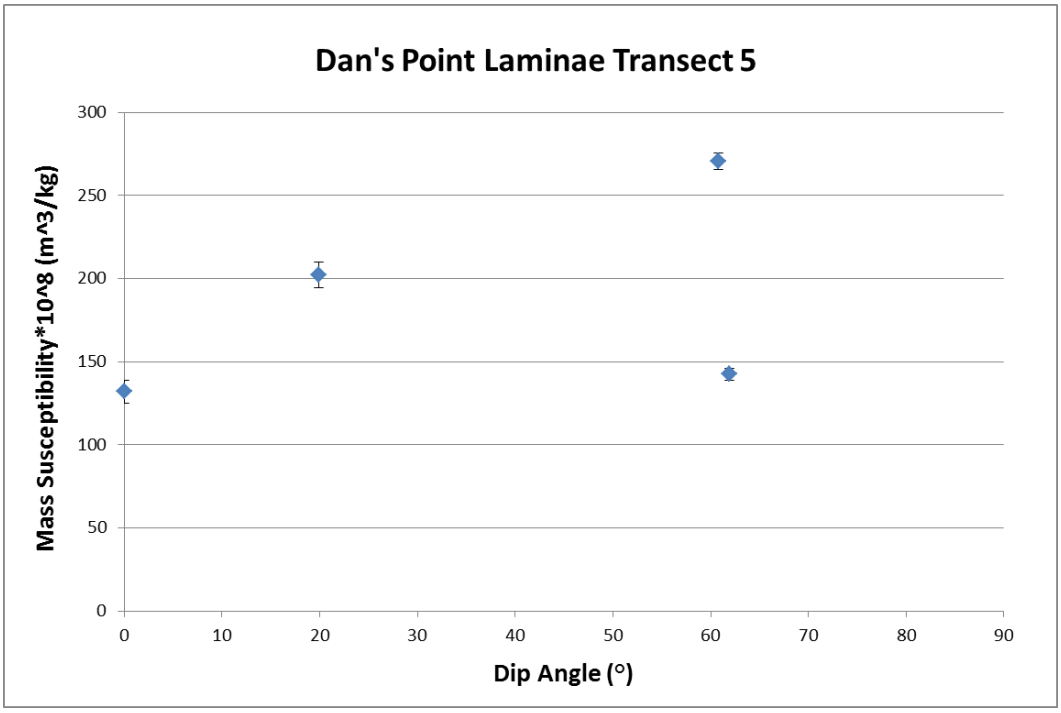
Dan's Point Laminae Transect 5
Mass Susceptibility*10^8 (m^3/kg)
300
250
200
150
100
50
0
0
10
20
30
40
50
60
70
80
90
Dip Angle (°)

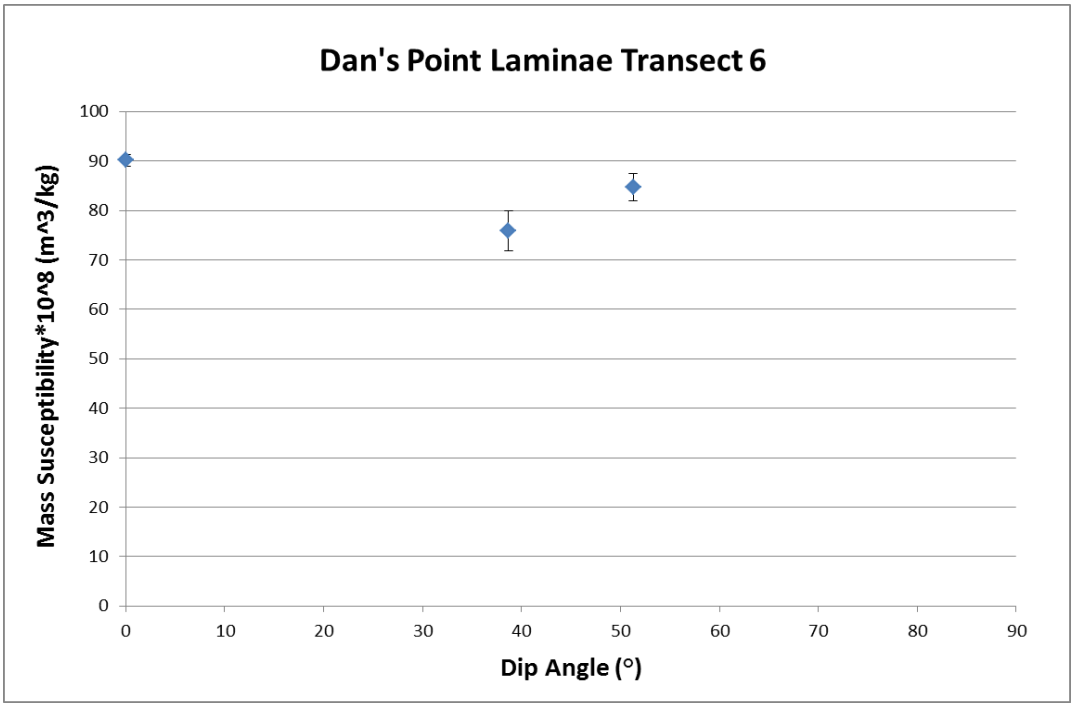
Dan's Point Laminae Transect 6
Mass Susceptibility*10^8 (m^3/kg)
100
90
80
70
60
50
40
30
20
10
0
0
10
20
30
40
50
60
70
80
90
Dip Angle (°)

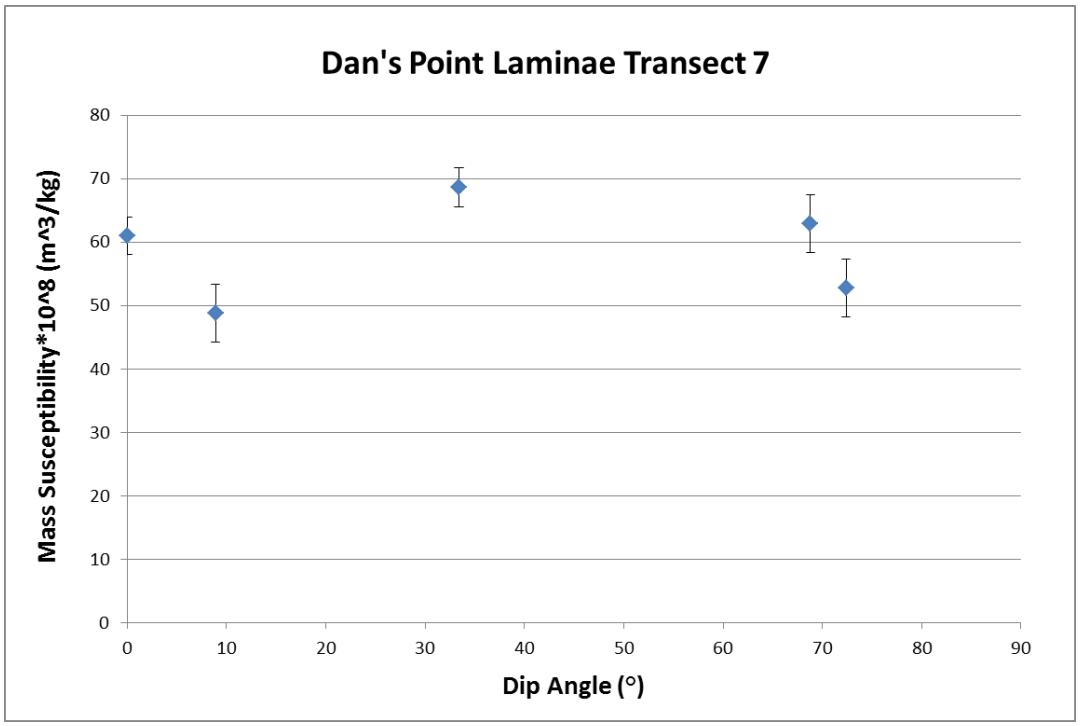
Dan's Point Laminae Transect 7
Mass Susceptibility*10^8 (m^3/kg)
0
10
20
30
40
50
60
70
80
0
10
20
30
40
50
60
70
80
90
Dip Angle (°)

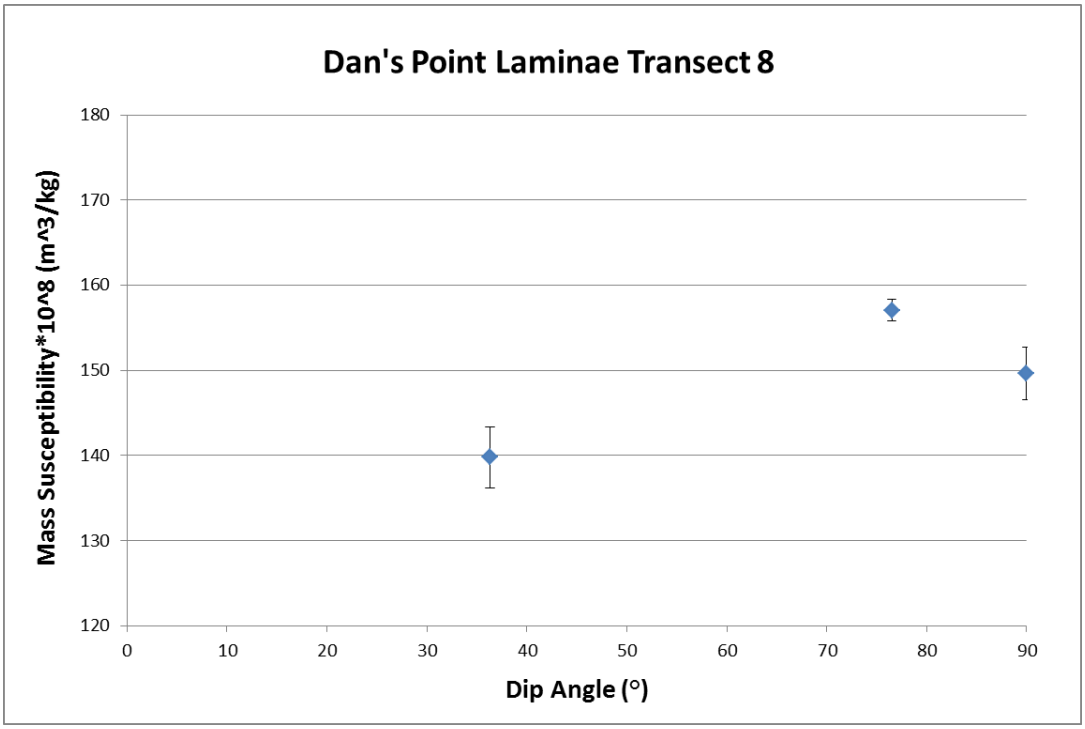
Dan's Point Laminae Transect 8
Mass Susceptibility*10^8 (m^3/kg)
120
130
140
150
160
170
180
0
10
20
30
40
50
60
70
80
90
Dip Angle (°)

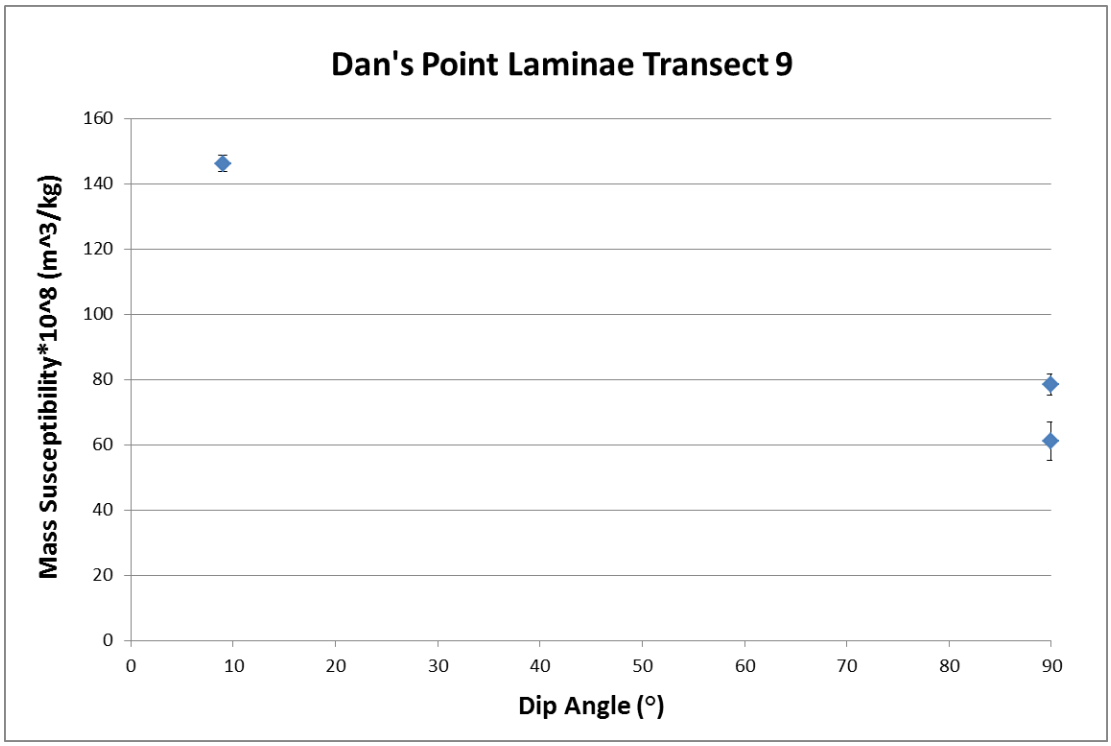
Dan's Point Laminae Transect 9
Mass Susceptibility*10^8 (m^3/kg)
160
140
120
100
80
60
40
20
0
0
10
20
30
40
50
60
70
80
90
Dip Angle (°)

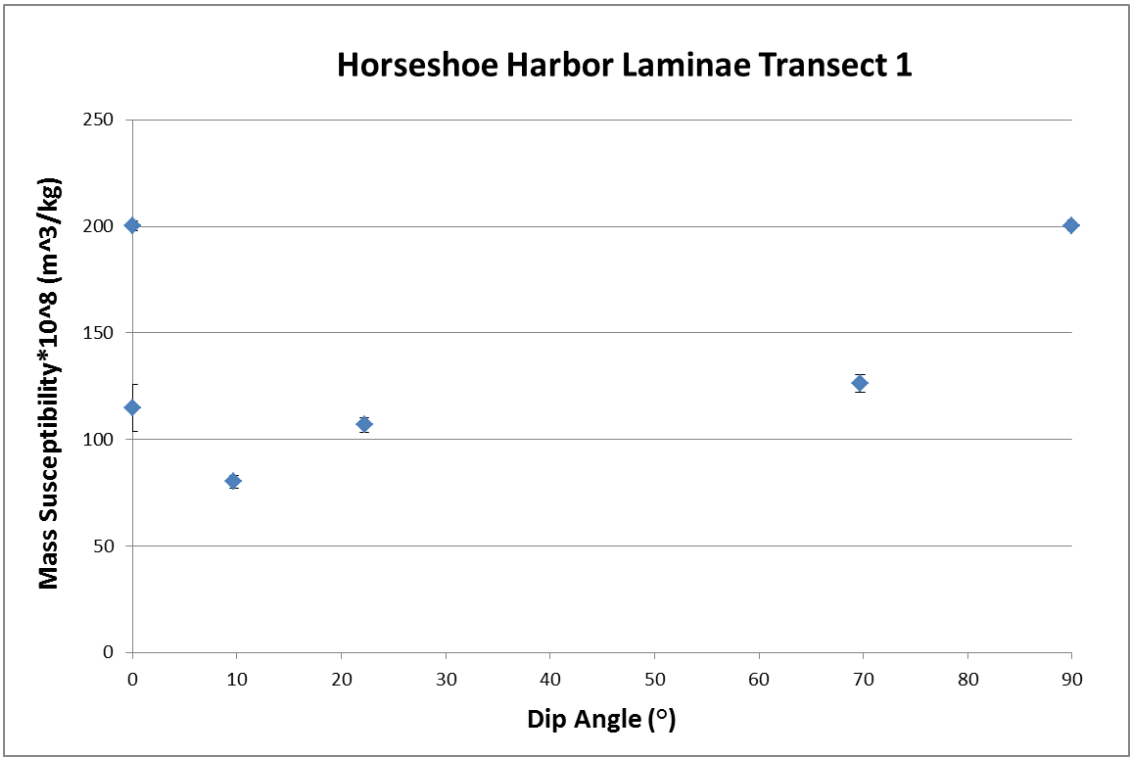
Horseshoe Harbor Laminae Transect 1
Mass Susceptibility*10^8 (m^3/kg)
250
200
150
100
50
0
0
10
20
30
40
50
60
70
80
90
Dip Angle (°)

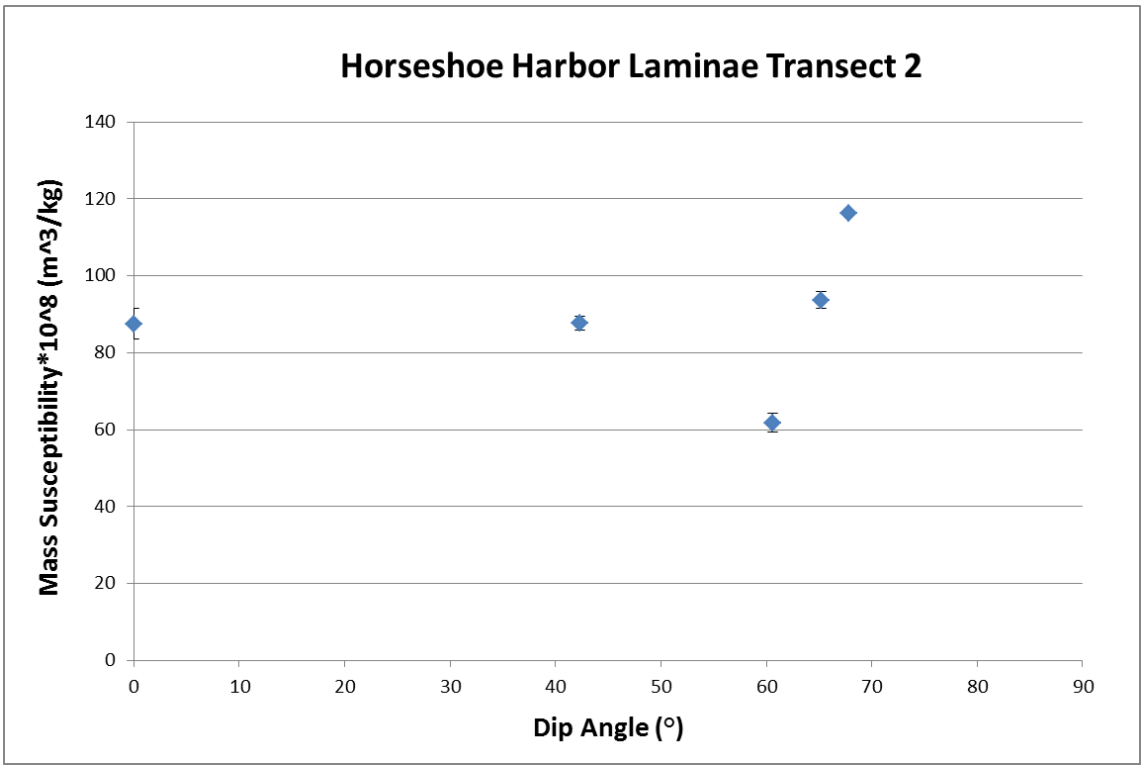
Horseshoe Harbor Laminae Transect 2
Mass Susceptibility*10^8 (m^3/kg)
140
120
100
80
60
40
20
0
0
10
20
30
40
50
60
70
80
90
Dip Angle (°)

Appendix G:

Growth Angle Measurements
Dan's Point Stromatolites

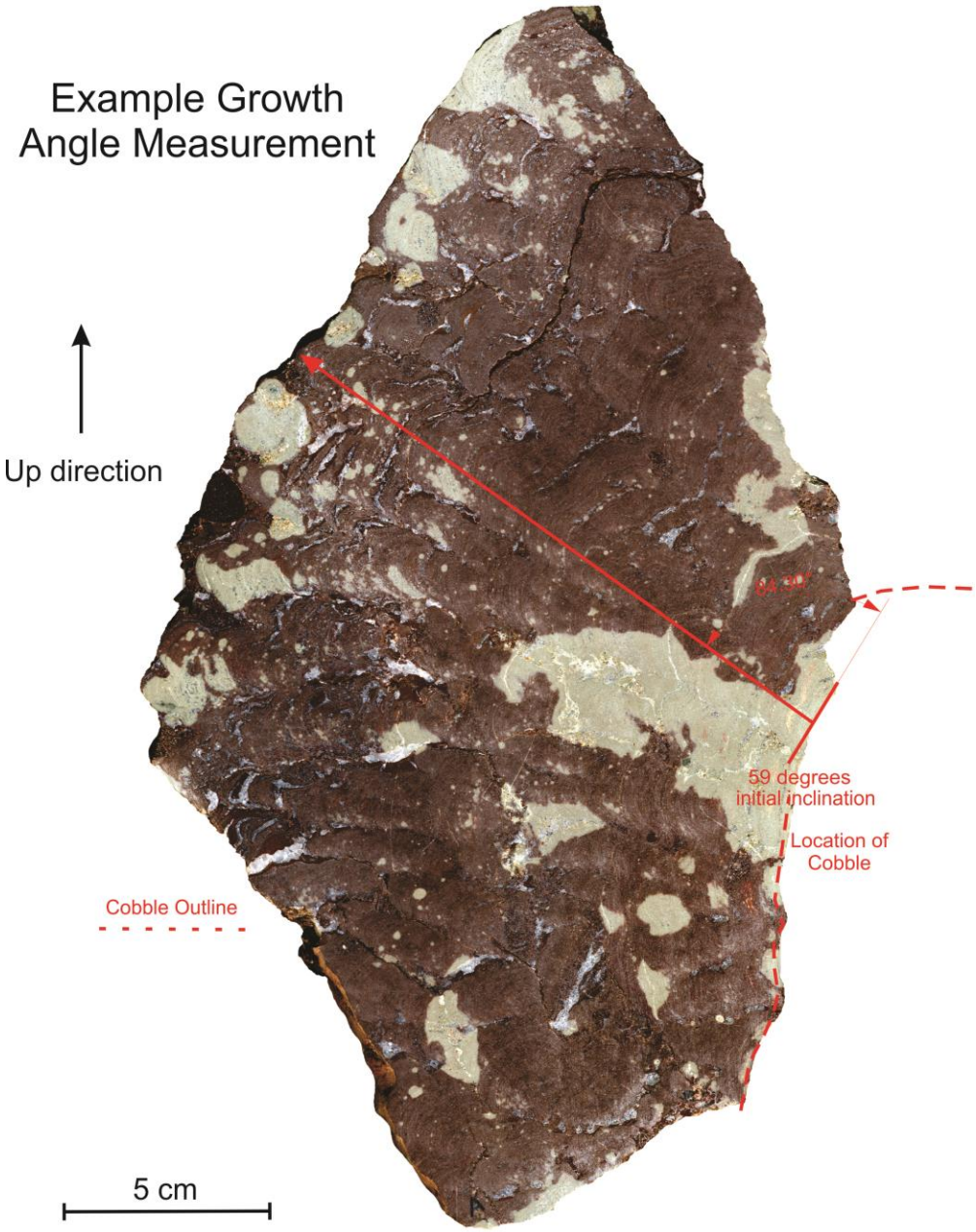
Example Growth
Angle Measurement
Up direction
59 degrees
initial inclination
Location of
Cobble
Cobble Outline
5 cm

Sample ID	Growth Angle(°)	Initial Inclination(°)
DP-IS-1-Side-1(A)	65.66	48
DP-IS-1-Side-1(B)	75.58	49.4
DP-IS-1-Side-1(C)	84.15	49.4
DP-IS-1-Side-1(D)	89.02	49.4
DP-IS-1-Side-1(E)	79.87	60.6
DP-IS-1-Side-1(F)	88.96	60.6
DP-IS-1-Side-1(G)	97.67	63.4
DP-IS-1-Side-1(H)	99.38	69.2
DP-IS-1-Side-1(I)	102.26	72.3
DP-IS-1-Side-1(J)	76.89	87.5
DP-IS-1-Side-1(K)	93.67	31.4
DP-IS-1-Side-1(L)	96.54	34.8
DP-IS-2-Side-A(A)	82.59	38.71
DP-IS-2-Side-A(B)	88.68	41.35
DP-IS-2-Side-A(C)	77.27	17.59
DP-IS-2-Side-A(D)	90.7	0
DP-IS-2-Side-A(E)	108.16	0
DP-IS-2-Side-A(F)	93.3	23.23
DP-IS-2-Side-A(G)	84.14	34.69
SS-F-1-SideB(A)	87.91	0
SS-F-1-SideB(B)	91.82	12.5
SS-F-1-SideB(C)	79.6	52.1

SS-F-1-SideB(D)	90.35	34.4
SS-F-1-SideB(E)	86.94	1.5
SS-F-1-SideB(F)	76.8	0
SS-F-1-SideB(G)	90.74	27.93
SS-F-1-SideB(H)	73.33	9.48
SS-F-1-SideB(I)	64.38	9.48
SS-F-1-SideB(J)	50.41	9.48
SS-F-1-SideB(K)	85.59	42.2
SS-F-1-SideB(L)	97.52	32.6
SS-F-1-SideB(M)	106.81	12.4
C-IS-2(A)	94.58	23.61
C-IS-2(B)	90.64	18.75
C-IS-2(C)	87.53	23.88
C-IS-2(D)	91.54	9.97
C-IS-2(E)	91.8	19.01
C-IS-2(F)	97.96	44.03
C-IS-2(G)	69.14	54.28
C-IS-4(A)	86.77	55.68
C-IS-4(B)	82.87	26.15
C-IS-4(C)	92.49	0
C-IS-4(D)	97.55	17.85
C-IS-4(E)	94.99	17.48
C-IS-3(F)	107.91	15.34

C-IS-3(G)	89.27	13.93

Appendix H:

Mass Susceptibility versus Laminae Dip Angle Measurements
Dan's Point and Horseshoe Harbor Stromatolites

Samples with the prefix SS and DP are from the Dan's Point locality while samples with the HH prefix are from Horseshoe Harbor.

Sample ID	Angle (°)	Mass Susceptibility (m^3/kg)	Stdev (m^3/kg)
SS-F-1 (1-1)	73.6	2.20E-07	1.88E-08
SS-F-1 (1-2)	60.3	7.38E-08	2.08E-08
SS-F-1 (1-3)	37.7	8.56E-08	1.51E-08
SS-F-1 (1-4)	0	1.19E-07	1.96E-08
SS-F-1 (1-5)	40.4	1.50E-07	2.49E-08
SS-F-1 (2-1)	32.6	1.33E-07	1.18E-08
SS-F-1 (2-2)	0	1.00E-07	7.85E-09
SS-F-1 (2-3)	32.8	4.32E-08	5.79E-09
SS-F-1 (2-4)	46.4	1.23E-07	7.88E-09
SS-F-1 (3-1)	72.2	6.05E-08	8.49E-09
SS-F-1 (3-2)	0	8.92E-08	1.15E-08
SS-F-1 (3-3)	38.8	1.52E-07	1.88E-08
SS-F-2 (1-1)	48.2	6.67E-08	4.21E-09
SS-F-2 (1-2)	0	7.15E-08	5.20E-09
SS-F-2 (1-3)	26	7.01E-08	5.41E-09
SS-F-2 (1-4)	41.8	2.16E-07	7.45E-09
HH-IS-3B (1-1)	0	2.00E-07	4.60E-09
HH-IS-3B (1-2)	90	2.00E-07	5.07E-09
HH-IS-3B (1-3)	69.7	1.26E-07	8.20E-09
HH-IS-3B (1-4)	9.7	8.01E-08	6.35E-09

HH-IS-3B (1-5)	0	1.15E-07	2.17E-08
HH-IS-3B (1-6)	22.2	1.07E-07	7.20E-09
HH-IS-3B (2-1)	65.2	9.37E-08	4.30E-09
HH-IS-3B (2-2)	67.8	1.16E-07	1.38E-09
HH-IS-3B (2-3)	42.3	8.77E-08	3.75E-09
HH-IS-3B (2-4)	0	8.75E-08	8.14E-09
HH-IS-3B (2-5)	60.6	6.18E-08	4.94E-09
DP-IS-1 (1-1)	19.9	2.02E-07	1.55E-08
DP-IS-1 (1-2)	0	1.32E-07	1.39E-08
DP-IS-1 (1-3)	60.8	2.71E-07	9.92E-09
DP-IS-1 (1-4)	61.9	1.42E-07	7.67E-09
DP-IS-1A (1-1)	38.7	7.59E-08	7.98E-09
DP-IS-1A (1-2)	0	9.01E-08	2.41E-09
DP-IS-1A (1-3)	51.3	8.47E-08	5.38E-09
DP-IS-1A (2-2)	0	6.10E-08	5.83E-09
DP-IS-1A (2-5)	68.8	6.30E-08	9.09E-09
DP-IS-1A (2-6)	33.4	6.86E-08	6.20E-09
DP-IS-1A (2-7)	8.9	4.88E-08	9.09E-09
DP-IS-1A (2-8)	72.4	5.28E-08	9.17E-09
DP-IS-1A (3-1)	36.3	1.40E-07	7.24E-09
DP-IS-1A (3-2)	76.5	1.57E-07	2.44E-09
DP-IS-1A (3-3)	90	1.50E-07	6.09E-09
DP-IS-1A (4-1)	9	1.46E-07	4.86E-09

DP-IS-1A (4-2)	90	7.85E-08	6.71E-09
DP-IS-1A (4-3)	90	6.11E-08	1.16E-08

Appendix I:

Thermomagnetic Data
Horseshoe Harbor Stromatolites

Temperature (°C)	Susceptibility	Corrected Susceptibility	Mass Susceptibility (m^3/kg)
24.1	-182.6	-1.7	-4.15E-09
25.7	-182.6	-1.7	-4.15E-09
31.6	-182.6	-1.6	-3.90E-09
39.1	-182.7	-1.6	-3.90E-09
47.2	-182.7	-1.6	-3.90E-09
54.2	-182.7	-1.5	-3.66E-09
60.2	-182.8	-1.7	-4.15E-09
67.2	-182.8	-1.7	-4.15E-09
72.9	-182.8	-1.6	-3.90E-09
79	-182.8	-1.6	-3.90E-09
84.5	-182.8	-1.7	-4.15E-09
89.5	-182.7	-1.5	-3.66E-09
95	-182.8	-1.6	-3.90E-09
99.7	-182.8	-1.6	-3.90E-09
104.8	-182.8	-1.6	-3.90E-09
109.8	-182.6	-1.4	-3.41E-09
113.2	-182.6	-1.4	-3.41E-09
118.2	-182.7	-1.5	-3.66E-09
122.8	-182.6	-1.4	-3.41E-09
127.5	-182.7	-1.5	-3.66E-09
131.8	-182.6	-1.4	-3.41E-09
136.1	-182.7	-1.5	-3.66E-09

140.6	-182.7	-1.5	-3.66E-09
145.1	-182.8	-1.7	-4.15E-09
150.2	-182.7	-1.5	-3.66E-09
153.7	-182.8	-1.6	-3.90E-09
158.5	-182.8	-1.6	-3.90E-09
163.4	-182.8	-1.5	-3.66E-09
168	-182.8	-1.4	-3.41E-09
172.8	-182.8	-1.4	-3.41E-09
177.4	-182.8	-1.4	-3.41E-09
181.7	-182.8	-1.5	-3.66E-09
186.6	-182.9	-1.5	-3.66E-09
191.2	-182.8	-1.4	-3.41E-09
195.5	-182.8	-1.3	-3.17E-09
200.2	-182.8	-1.3	-3.17E-09
204.8	-182.8	-1.3	-3.17E-09
210	-182.8	-1.3	-3.17E-09
213.3	-182.7	-1.2	-2.93E-09
218.2	-182.8	-1.3	-3.17E-09
223.6	-182.8	-1.2	-2.93E-09
228.3	-182.8	-1.2	-2.93E-09
232.7	-182.8	-1.3	-3.17E-09
237.4	-182.8	-1.3	-3.17E-09
242.3	-182.8	-1.3	-3.17E-09

247	-182.9	-1.4	-3.41E-09
251.7	-182.9	-1.4	-3.41E-09
256.2	-182.9	-1.3	-3.17E-09
260.3	-182.9	-1.3	-3.17E-09
265.6	-182.8	-1.2	-2.93E-09
270	-182.6	-0.9	-2.20E-09
274.8	-182.7	-1	-2.44E-09
279.2	-182.8	-1.1	-2.68E-09
284	-182.9	-1.2	-2.93E-09
288.5	-182.8	-1.1	-2.68E-09
292.9	-182.9	-1.1	-2.68E-09
298	-182.8	-1	-2.44E-09
302.2	-182.8	-1	-2.44E-09
307	-182.8	-1	-2.44E-09
310.9	-182.8	-1	-2.44E-09
315.2	-182.7	-0.9	-2.20E-09
319.7	-182.7	-0.8	-1.95E-09
323.6	-182.7	-0.8	-1.95E-09
328.5	-182.6	-0.7	-1.71E-09
333	-182.6	-0.7	-1.71E-09
337.5	-182.5	-0.6	-1.46E-09
341.5	-182.5	-0.6	-1.46E-09
345.8	-182.4	-0.5	-1.22E-09

350.4	-182.4	-0.4	-9.76E-10
354.9	-182.3	-0.3	-7.32E-10
359.5	-182.3	-0.4	-9.76E-10
363.5	-182.1	-0.2	-4.88E-10
368.1	-182.1	-0.2	-4.88E-10
371.9	-182	0	0.00E+00
376.5	-181.8	0.1	2.44E-10
380.8	-181.6	0.4	9.76E-10
385.4	-181.4	0.6	1.46E-09
389.2	-181.1	0.9	2.20E-09
393.8	-180.7	1.3	3.17E-09
398.4	-180.2	1.9	4.63E-09
402.8	-179.7	2.4	5.85E-09
407.7	-178.9	3.2	7.80E-09
411.5	-178.2	3.9	9.51E-09
415.9	-177.2	5	1.22E-08
420.6	-176.1	6.1	1.49E-08
424.7	-174.7	7.5	1.83E-08
429.1	-173	9.2	2.24E-08
433.5	-171.2	11	2.68E-08
438.2	-169.1	13.2	3.22E-08
442	-166.6	15.7	3.83E-08
445.8	-163.8	18.5	4.51E-08

450	-160.7	21.6	5.27E-08
455	-157.1	25.3	6.17E-08
458.8	-153.2	29.2	7.12E-08
463	-148.9	33.4	8.15E-08
466.9	-144.3	38	9.27E-08
471.3	-139.4	43	1.05E-07
475.8	-134.3	48.1	1.17E-07
480	-129.3	53.1	1.30E-07
484.1	-124.8	57.7	1.41E-07
488	-121.2	61.3	1.50E-07
492.8	-118.9	63.6	1.55E-07
496.4	-117.9	64.6	1.58E-07
501.2	-118	64.6	1.58E-07
505.1	-119.3	63.3	1.54E-07
509.3	-121	61.6	1.50E-07
512.7	-123.5	59.2	1.44E-07
517.8	-126.4	56.3	1.37E-07
521.7	-128.5	54.2	1.32E-07
526	-130.4	52.4	1.28E-07
529.9	-132.7	50	1.22E-07
534.2	-136	46.8	1.14E-07
537.8	-140	42.8	1.04E-07
542.4	-146.1	36.7	8.95E-08

546.7	-153.2	29.7	7.24E-08
550	-161.2	21.7	5.29E-08
555.2	-168.5	14.4	3.51E-08
558.6	-173.6	9.3	2.27E-08
562.9	-177.4	5.4	1.32E-08
566.9	-179.9	3	7.32E-09
571.5	-181.6	1.4	3.41E-09
575.5	-182.7	0.3	7.32E-10
579.9	-183.4	-0.3	-7.32E-10
584.2	-184	-1	-2.44E-09
588.2	-184.4	-1.3	-3.17E-09
592.2	-184.6	-1.5	-3.66E-09
596.3	-184.9	-1.8	-4.39E-09
600.6	-185.1	-1.9	-4.63E-09
604.7	-185.1	-1.9	-4.63E-09
608.1	-185.2	-2	-4.88E-09
611.9	-185.6	-2.4	-5.85E-09
616.6	-185.6	-2.4	-5.85E-09
620.3	-185.8	-2.7	-6.59E-09
624.4	-185.8	-2.7	-6.59E-09
628.2	-185.9	-2.8	-6.83E-09
632.3	-186	-2.8	-6.83E-09
636.7	-186	-2.8	-6.83E-09

639.5	-186	-2.8	-6.83E-09
644	-186	-2.8	-6.83E-09
647.8	-186.1	-2.9	-7.07E-09
651.6	-186.1	-2.9	-7.07E-09
656	-186.1	-2.9	-7.07E-09
659.5	-186.1	-2.9	-7.07E-09
663.3	-186.1	-2.9	-7.07E-09
667.5	-186.2	-3	-7.32E-09
671	-186.2	-3	-7.32E-09
674.8	-186.3	-3.2	-7.80E-09
678.3	-186.3	-3.2	-7.80E-09
681.9	-186.3	-3.2	-7.80E-09
686	-186.4	-3.2	-7.80E-09
689.9	-186.5	-3.3	-8.05E-09
693.8	-186.5	-3.3	-8.05E-09
697.3	-186.5	-3.3	-8.05E-09
699.6	-186.5	-3.3	-8.05E-09
700.9	-186.5	-3.3	-8.05E-09
699.3	-186.5	-3.3	-8.05E-09
697.3	-186.5	-3.3	-8.05E-09
695.4	-186.5	-3.3	-8.05E-09
692.5	-186.5	-3.3	-8.05E-09
689.6	-186.4	-3.2	-7.80E-09

686.4	-186.3	-3.2	-7.80E-09
681.9	-186.3	-3.2	-7.80E-09
680.6	-186.2	-3	-7.32E-09
677.1	-186.1	-2.9	-7.07E-09
673.5	-186.1	-2.9	-7.07E-09
670	-186.1	-2.9	-7.07E-09
666.8	-186.1	-2.9	-7.07E-09
663.3	-186	-2.8	-6.83E-09
659.8	-186	-2.8	-6.83E-09
656.3	-185.9	-2.8	-6.83E-09
652.8	-185.9	-2.8	-6.83E-09
649.3	-185.8	-2.7	-6.59E-09
645.9	-185.7	-2.5	-6.10E-09
642.4	-185.6	-2.4	-5.85E-09
638.9	-185.5	-2.3	-5.61E-09
635.1	-185.6	-2.4	-5.85E-09
631.6	-185.6	-2.4	-5.85E-09
630.4	-185.5	-2.3	-5.61E-09
625.4	-185.3	-2.2	-5.37E-09
621.3	-185.3	-2.2	-5.37E-09
617.8	-185.1	-1.9	-4.63E-09
614.1	-185	-1.8	-4.39E-09
610.9	-184.9	-1.8	-4.39E-09

605.6	-184.7	-1.5	-3.66E-09
603.1	-184.6	-1.4	-3.41E-09
599.7	-184.5	-1.4	-3.41E-09
595.7	-184.3	-1.3	-3.17E-09
591.9	-184.2	-1.2	-2.93E-09
588.8	-184.1	-1.1	-2.68E-09
584.8	-183.8	-0.9	-2.20E-09
580.8	-183.7	-0.8	-1.95E-09
577.4	-183.5	-0.7	-1.71E-09
574.6	-183.1	-0.2	-4.88E-10
570.3	-182.5	0.3	7.32E-10
566.6	-181.4	1.4	3.41E-09
562.6	-179.2	3.4	8.29E-09
560.1	-176.2	6.5	1.59E-08
554.9	-172.1	10.6	2.59E-08
551.3	-167.3	15.4	3.76E-08
547.9	-162.1	20.6	5.02E-08
543.6	-155.7	27.1	6.61E-08
540	-148	34.7	8.46E-08
536.3	-137.7	44.9	1.10E-07
532.4	-125.1	57.5	1.40E-07
527.8	-112.8	69.8	1.70E-07
524.8	-100.3	82.3	2.01E-07

521.4	-86	96.6	2.36E-07
516.6	-69.9	112.6	2.75E-07
513.9	-52.3	130.2	3.18E-07
509	-30.5	152	3.71E-07
504.8	-6.3	176.2	4.30E-07
500.9	24.4	206.8	5.04E-07
496.7	59.6	242	5.90E-07
492.2	93.7	276	6.73E-07
488.3	124.4	306.7	7.48E-07
484.7	145.9	328.2	8.00E-07
480.8	159.4	341.7	8.33E-07
476.7	164.4	346.7	8.46E-07
472.8	163	345.2	8.42E-07
468.3	157.3	339.5	8.28E-07
464.5	149.7	331.9	8.10E-07
460	140.5	322.7	7.87E-07
455.3	130.5	312.7	7.63E-07
451.7	121.3	303.5	7.40E-07
447.3	112.8	294.9	7.19E-07
443.5	104.3	286.4	6.99E-07
439.4	95.9	278	6.78E-07
434.9	88.4	270.5	6.60E-07
430.5	81.2	263.3	6.42E-07

426.7	74.8	256.9	6.27E-07
422.3	68.3	250.5	6.11E-07
418.2	62.1	244.2	5.96E-07
413.9	56.3	238.4	5.81E-07
409.5	50.8	232.8	5.68E-07
405.4	45.8	227.8	5.56E-07
400.5	40.7	222.8	5.43E-07
396.4	35.7	217.7	5.31E-07
392.1	31.1	213	5.20E-07
387.4	26.7	208.7	5.09E-07
383.4	22.7	204.6	4.99E-07
378.8	18.9	200.8	4.90E-07
374.4	15.4	197.2	4.81E-07
370.1	12	193.9	4.73E-07
366.1	8.7	190.5	4.65E-07
361.5	5.7	187.6	4.58E-07
357.2	2.6	184.5	4.50E-07
352.4	-0.2	181.7	4.43E-07
347.8	-2.8	179	4.37E-07
344.1	-5.1	176.7	4.31E-07
338.4	-7.5	174.3	4.25E-07
335	-10	171.8	4.19E-07
330.2	-12.2	169.5	4.13E-07

325.9	-14.2	167.6	4.09E-07
321.1	-16.2	165.5	4.04E-07
317.1	-18.1	163.7	3.99E-07
312.6	-20	161.7	3.94E-07
308.1	-21.7	160	3.90E-07
305	-23.3	158.5	3.87E-07
299.1	-25	156.7	3.82E-07
294.9	-26.6	155.1	3.78E-07
290.7	-28.1	153.5	3.74E-07
284.8	-29.6	152	3.71E-07
280.6	-30.9	150.7	3.68E-07
276.2	-32.3	149.3	3.64E-07
271.2	-33.6	148	3.61E-07
266.7	-34.7	146.9	3.58E-07
262.5	-35.8	145.8	3.56E-07
257.8	-36.9	144.7	3.53E-07
253.4	-38	143.5	3.50E-07
249.2	-39	142.6	3.48E-07
244.5	-39.7	141.9	3.46E-07
240.4	-40.5	141	3.44E-07
235.5	-41.4	140.1	3.42E-07
230.5	-42.6	138.9	3.39E-07
226.4	-43.4	138.1	3.37E-07

221.5	-44.3	137.2	3.35E-07
217.6	-45.1	136.4	3.33E-07
213	-45.8	135.6	3.31E-07
208.6	-46.5	134.9	3.29E-07
204	-47.2	134.2	3.27E-07
199.6	-47.8	133.6	3.26E-07
195	-48.4	133	3.24E-07
190.7	-49	132.4	3.23E-07
186.3	-49.5	131.9	3.22E-07
181.4	-50	131.3	3.20E-07
177.1	-50.4	130.9	3.19E-07
173.1	-50.8	130.5	3.18E-07
168.5	-51	130.2	3.18E-07
165	-51.4	129.8	3.17E-07
159.9	-51.7	129.5	3.16E-07
155.6	-52	129.1	3.15E-07
151	-52.2	129	3.15E-07
147	-52.4	128.7	3.14E-07
142.7	-52.6	128.6	3.14E-07
138.5	-52.7	128.4	3.13E-07
134.5	-52.8	128.4	3.13E-07
129.9	-52.9	128.2	3.13E-07
125.7	-52.9	128.3	3.13E-07

121.4	-52.8	128.4	3.13E-07
118.2	-52.8	128.4	3.13E-07
113.7	-52.6	128.6	3.14E-07
109.8	-52.6	128.6	3.14E-07
106.1	-52.5	128.6	3.14E-07
102.4	-52.3	128.9	3.14E-07
98.2	-52.1	129.1	3.15E-07
94.5	-51.8	129.4	3.16E-07
91.6	-51.6	129.5	3.16E-07
87.4	-51.4	129.8	3.17E-07
83.7	-51.1	130	3.17E-07
80.3	-50.8	130.3	3.18E-07
76.9	-50.5	130.6	3.19E-07
74	-50.3	130.8	3.19E-07
70.3	-50	131.1	3.20E-07
67.2	-49.7	131.4	3.20E-07
64.1	-49.4	131.7	3.21E-07
61.5	-49.1	132	3.22E-07
58.3	-48.9	132.2	3.22E-07
55.7	-48.7	132.5	3.23E-07
53.1	-48.5	132.7	3.24E-07
50.5	-48.3	132.8	3.24E-07
48.5	-48	133.2	3.25E-07

45.9	-47.8	133.3	3.25E-07
43.8	-47.6	133.6	3.26E-07
41.5	-47.6	133.6	3.26E-07
39.6	-47.3	133.9	3.27E-07

Appendix J:

Thermomagnetic Data
Dan's Point Stromatolites

Temperature (°C)	Susceptibility	Corrected Susceptibility	Mass Susceptibility (m^3/kg)
24.1	-182.6	-1.7	-4.15E-09
25.7	-182.6	-1.7	-4.15E-09
31.6	-182.6	-1.6	-3.90E-09
39.1	-182.7	-1.6	-3.90E-09
47.2	-182.7	-1.6	-3.90E-09
54.2	-182.7	-1.5	-3.66E-09
60.2	-182.8	-1.7	-4.15E-09
67.2	-182.8	-1.7	-4.15E-09
72.9	-182.8	-1.6	-3.90E-09
79	-182.8	-1.6	-3.90E-09
84.5	-182.8	-1.7	-4.15E-09
89.5	-182.7	-1.5	-3.66E-09
95	-182.8	-1.6	-3.90E-09
99.7	-182.8	-1.6	-3.90E-09
104.8	-182.8	-1.6	-3.90E-09
109.8	-182.6	-1.4	-3.41E-09
113.2	-182.6	-1.4	-3.41E-09
118.2	-182.7	-1.5	-3.66E-09
122.8	-182.6	-1.4	-3.41E-09
127.5	-182.7	-1.5	-3.66E-09
131.8	-182.6	-1.4	-3.41E-09
136.1	-182.7	-1.5	-3.66E-09

140.6	-182.7	-1.5	-3.66E-09
145.1	-182.8	-1.7	-4.15E-09
150.2	-182.7	-1.5	-3.66E-09
153.7	-182.8	-1.6	-3.90E-09
158.5	-182.8	-1.6	-3.90E-09
163.4	-182.8	-1.5	-3.66E-09
168	-182.8	-1.4	-3.41E-09
172.8	-182.8	-1.4	-3.41E-09
177.4	-182.8	-1.4	-3.41E-09
181.7	-182.8	-1.5	-3.66E-09
186.6	-182.9	-1.5	-3.66E-09
191.2	-182.8	-1.4	-3.41E-09
195.5	-182.8	-1.3	-3.17E-09
200.2	-182.8	-1.3	-3.17E-09
204.8	-182.8	-1.3	-3.17E-09
210	-182.8	-1.3	-3.17E-09
213.3	-182.7	-1.2	-2.93E-09
218.2	-182.8	-1.3	-3.17E-09
223.6	-182.8	-1.2	-2.93E-09
228.3	-182.8	-1.2	-2.93E-09
232.7	-182.8	-1.3	-3.17E-09
237.4	-182.8	-1.3	-3.17E-09
242.3	-182.8	-1.3	-3.17E-09

247	-182.9	-1.4	-3.41E-09
251.7	-182.9	-1.4	-3.41E-09
256.2	-182.9	-1.3	-3.17E-09
260.3	-182.9	-1.3	-3.17E-09
265.6	-182.8	-1.2	-2.93E-09
270	-182.6	-0.9	-2.20E-09
274.8	-182.7	-1	-2.44E-09
279.2	-182.8	-1.1	-2.68E-09
284	-182.9	-1.2	-2.93E-09
288.5	-182.8	-1.1	-2.68E-09
292.9	-182.9	-1.1	-2.68E-09
298	-182.8	-1	-2.44E-09
302.2	-182.8	-1	-2.44E-09
307	-182.8	-1	-2.44E-09
310.9	-182.8	-1	-2.44E-09
315.2	-182.7	-0.9	-2.20E-09
319.7	-182.7	-0.8	-1.95E-09
323.6	-182.7	-0.8	-1.95E-09
328.5	-182.6	-0.7	-1.71E-09
333	-182.6	-0.7	-1.71E-09
337.5	-182.5	-0.6	-1.46E-09
341.5	-182.5	-0.6	-1.46E-09
345.8	-182.4	-0.5	-1.22E-09

350.4	-182.4	-0.4	-9.76E-10
354.9	-182.3	-0.3	-7.32E-10
359.5	-182.3	-0.4	-9.76E-10
363.5	-182.1	-0.2	-4.88E-10
368.1	-182.1	-0.2	-4.88E-10
371.9	-182	0	0.00E+00
376.5	-181.8	0.1	2.44E-10
380.8	-181.6	0.4	9.76E-10
385.4	-181.4	0.6	1.46E-09
389.2	-181.1	0.9	2.20E-09
393.8	-180.7	1.3	3.17E-09
398.4	-180.2	1.9	4.63E-09
402.8	-179.7	2.4	5.85E-09
407.7	-178.9	3.2	7.80E-09
411.5	-178.2	3.9	9.51E-09
415.9	-177.2	5	1.22E-08
420.6	-176.1	6.1	1.49E-08
424.7	-174.7	7.5	1.83E-08
429.1	-173	9.2	2.24E-08
433.5	-171.2	11	2.68E-08
438.2	-169.1	13.2	3.22E-08
442	-166.6	15.7	3.83E-08
445.8	-163.8	18.5	4.51E-08

450	-160.7	21.6	5.27E-08
455	-157.1	25.3	6.17E-08
458.8	-153.2	29.2	7.12E-08
463	-148.9	33.4	8.15E-08
466.9	-144.3	38	9.27E-08
471.3	-139.4	43	1.05E-07
475.8	-134.3	48.1	1.17E-07
480	-129.3	53.1	1.30E-07
484.1	-124.8	57.7	1.41E-07
488	-121.2	61.3	1.50E-07
492.8	-118.9	63.6	1.55E-07
496.4	-117.9	64.6	1.58E-07
501.2	-118	64.6	1.58E-07
505.1	-119.3	63.3	1.54E-07
509.3	-121	61.6	1.50E-07
512.7	-123.5	59.2	1.44E-07
517.8	-126.4	56.3	1.37E-07
521.7	-128.5	54.2	1.32E-07
526	-130.4	52.4	1.28E-07
529.9	-132.7	50	1.22E-07
534.2	-136	46.8	1.14E-07
537.8	-140	42.8	1.04E-07
542.4	-146.1	36.7	8.95E-08

546.7	-153.2	29.7	7.24E-08
550	-161.2	21.7	5.29E-08
555.2	-168.5	14.4	3.51E-08
558.6	-173.6	9.3	2.27E-08
562.9	-177.4	5.4	1.32E-08
566.9	-179.9	3	7.32E-09
571.5	-181.6	1.4	3.41E-09
575.5	-182.7	0.3	7.32E-10
579.9	-183.4	-0.3	-7.32E-10
584.2	-184	-1	-2.44E-09
588.2	-184.4	-1.3	-3.17E-09
592.2	-184.6	-1.5	-3.66E-09
596.3	-184.9	-1.8	-4.39E-09
600.6	-185.1	-1.9	-4.63E-09
604.7	-185.1	-1.9	-4.63E-09
608.1	-185.2	-2	-4.88E-09
611.9	-185.6	-2.4	-5.85E-09
616.6	-185.6	-2.4	-5.85E-09
620.3	-185.8	-2.7	-6.59E-09
624.4	-185.8	-2.7	-6.59E-09
628.2	-185.9	-2.8	-6.83E-09
632.3	-186	-2.8	-6.83E-09
636.7	-186	-2.8	-6.83E-09

639.5	-186	-2.8	-6.83E-09
644	-186	-2.8	-6.83E-09
647.8	-186.1	-2.9	-7.07E-09
651.6	-186.1	-2.9	-7.07E-09
656	-186.1	-2.9	-7.07E-09
659.5	-186.1	-2.9	-7.07E-09
663.3	-186.1	-2.9	-7.07E-09
667.5	-186.2	-3	-7.32E-09
671	-186.2	-3	-7.32E-09
674.8	-186.3	-3.2	-7.80E-09
678.3	-186.3	-3.2	-7.80E-09
681.9	-186.3	-3.2	-7.80E-09
686	-186.4	-3.2	-7.80E-09
689.9	-186.5	-3.3	-8.05E-09
693.8	-186.5	-3.3	-8.05E-09
697.3	-186.5	-3.3	-8.05E-09
699.6	-186.5	-3.3	-8.05E-09
700.9	-186.5	-3.3	-8.05E-09
699.3	-186.5	-3.3	-8.05E-09
697.3	-186.5	-3.3	-8.05E-09
695.4	-186.5	-3.3	-8.05E-09
692.5	-186.5	-3.3	-8.05E-09
689.6	-186.4	-3.2	-7.80E-09

686.4	-186.3	-3.2	-7.80E-09
681.9	-186.3	-3.2	-7.80E-09
680.6	-186.2	-3	-7.32E-09
677.1	-186.1	-2.9	-7.07E-09
673.5	-186.1	-2.9	-7.07E-09
670	-186.1	-2.9	-7.07E-09
666.8	-186.1	-2.9	-7.07E-09
663.3	-186	-2.8	-6.83E-09
659.8	-186	-2.8	-6.83E-09
656.3	-185.9	-2.8	-6.83E-09
652.8	-185.9	-2.8	-6.83E-09
649.3	-185.8	-2.7	-6.59E-09
645.9	-185.7	-2.5	-6.10E-09
642.4	-185.6	-2.4	-5.85E-09
638.9	-185.5	-2.3	-5.61E-09
635.1	-185.6	-2.4	-5.85E-09
631.6	-185.6	-2.4	-5.85E-09
630.4	-185.5	-2.3	-5.61E-09
625.4	-185.3	-2.2	-5.37E-09
621.3	-185.3	-2.2	-5.37E-09
617.8	-185.1	-1.9	-4.63E-09
614.1	-185	-1.8	-4.39E-09
610.9	-184.9	-1.8	-4.39E-09

605.6	-184.7	-1.5	-3.66E-09
603.1	-184.6	-1.4	-3.41E-09
599.7	-184.5	-1.4	-3.41E-09
595.7	-184.3	-1.3	-3.17E-09
591.9	-184.2	-1.2	-2.93E-09
588.8	-184.1	-1.1	-2.68E-09
584.8	-183.8	-0.9	-2.20E-09
580.8	-183.7	-0.8	-1.95E-09
577.4	-183.5	-0.7	-1.71E-09
574.6	-183.1	-0.2	-4.88E-10
570.3	-182.5	0.3	7.32E-10
566.6	-181.4	1.4	3.41E-09
562.6	-179.2	3.4	8.29E-09
560.1	-176.2	6.5	1.59E-08
554.9	-172.1	10.6	2.59E-08
551.3	-167.3	15.4	3.76E-08
547.9	-162.1	20.6	5.02E-08
543.6	-155.7	27.1	6.61E-08
540	-148	34.7	8.46E-08
536.3	-137.7	44.9	1.10E-07
532.4	-125.1	57.5	1.40E-07
527.8	-112.8	69.8	1.70E-07
524.8	-100.3	82.3	2.01E-07

521.4	-86	96.6	2.36E-07
516.6	-69.9	112.6	2.75E-07
513.9	-52.3	130.2	3.18E-07
509	-30.5	152	3.71E-07
504.8	-6.3	176.2	4.30E-07
500.9	24.4	206.8	5.04E-07
496.7	59.6	242	5.90E-07
492.2	93.7	276	6.73E-07
488.3	124.4	306.7	7.48E-07
484.7	145.9	328.2	8.00E-07
480.8	159.4	341.7	8.33E-07
476.7	164.4	346.7	8.46E-07
472.8	163	345.2	8.42E-07
468.3	157.3	339.5	8.28E-07
464.5	149.7	331.9	8.10E-07
460	140.5	322.7	7.87E-07
455.3	130.5	312.7	7.63E-07
451.7	121.3	303.5	7.40E-07
447.3	112.8	294.9	7.19E-07
443.5	104.3	286.4	6.99E-07
439.4	95.9	278	6.78E-07
434.9	88.4	270.5	6.60E-07
430.5	81.2	263.3	6.42E-07

426.7	74.8	256.9	6.27E-07
422.3	68.3	250.5	6.11E-07
418.2	62.1	244.2	5.96E-07
413.9	56.3	238.4	5.81E-07
409.5	50.8	232.8	5.68E-07
405.4	45.8	227.8	5.56E-07
400.5	40.7	222.8	5.43E-07
396.4	35.7	217.7	5.31E-07
392.1	31.1	213	5.20E-07
387.4	26.7	208.7	5.09E-07
383.4	22.7	204.6	4.99E-07
378.8	18.9	200.8	4.90E-07
374.4	15.4	197.2	4.81E-07
370.1	12	193.9	4.73E-07
366.1	8.7	190.5	4.65E-07
361.5	5.7	187.6	4.58E-07
357.2	2.6	184.5	4.50E-07
352.4	-0.2	181.7	4.43E-07
347.8	-2.8	179	4.37E-07
344.1	-5.1	176.7	4.31E-07
338.4	-7.5	174.3	4.25E-07
335	-10	171.8	4.19E-07
330.2	-12.2	169.5	4.13E-07

325.9	-14.2	167.6	4.09E-07
321.1	-16.2	165.5	4.04E-07
317.1	-18.1	163.7	3.99E-07
312.6	-20	161.7	3.94E-07
308.1	-21.7	160	3.90E-07
305	-23.3	158.5	3.87E-07
299.1	-25	156.7	3.82E-07
294.9	-26.6	155.1	3.78E-07
290.7	-28.1	153.5	3.74E-07
284.8	-29.6	152	3.71E-07
280.6	-30.9	150.7	3.68E-07
276.2	-32.3	149.3	3.64E-07
271.2	-33.6	148	3.61E-07
266.7	-34.7	146.9	3.58E-07
262.5	-35.8	145.8	3.56E-07
257.8	-36.9	144.7	3.53E-07
253.4	-38	143.5	3.50E-07
249.2	-39	142.6	3.48E-07
244.5	-39.7	141.9	3.46E-07
240.4	-40.5	141	3.44E-07
235.5	-41.4	140.1	3.42E-07
230.5	-42.6	138.9	3.39E-07
226.4	-43.4	138.1	3.37E-07

221.5	-44.3	137.2	3.35E-07
217.6	-45.1	136.4	3.33E-07
213	-45.8	135.6	3.31E-07
208.6	-46.5	134.9	3.29E-07
204	-47.2	134.2	3.27E-07
199.6	-47.8	133.6	3.26E-07
195	-48.4	133	3.24E-07
190.7	-49	132.4	3.23E-07
186.3	-49.5	131.9	3.22E-07
181.4	-50	131.3	3.20E-07
177.1	-50.4	130.9	3.19E-07
173.1	-50.8	130.5	3.18E-07
168.5	-51	130.2	3.18E-07
165	-51.4	129.8	3.17E-07
159.9	-51.7	129.5	3.16E-07
155.6	-52	129.1	3.15E-07
151	-52.2	129	3.15E-07
147	-52.4	128.7	3.14E-07
142.7	-52.6	128.6	3.14E-07
138.5	-52.7	128.4	3.13E-07
134.5	-52.8	128.4	3.13E-07
129.9	-52.9	128.2	3.13E-07
125.7	-52.9	128.3	3.13E-07

121.4	-52.8	128.4	3.13E-07
118.2	-52.8	128.4	3.13E-07
113.7	-52.6	128.6	3.14E-07
109.8	-52.6	128.6	3.14E-07
106.1	-52.5	128.6	3.14E-07
102.4	-52.3	128.9	3.14E-07
98.2	-52.1	129.1	3.15E-07
94.5	-51.8	129.4	3.16E-07
91.6	-51.6	129.5	3.16E-07
87.4	-51.4	129.8	3.17E-07
83.7	-51.1	130	3.17E-07
80.3	-50.8	130.3	3.18E-07
76.9	-50.5	130.6	3.19E-07
74	-50.3	130.8	3.19E-07
70.3	-50	131.1	3.20E-07
67.2	-49.7	131.4	3.20E-07
64.1	-49.4	131.7	3.21E-07
61.5	-49.1	132	3.22E-07
58.3	-48.9	132.2	3.22E-07
55.7	-48.7	132.5	3.23E-07
53.1	-48.5	132.7	3.24E-07
50.5	-48.3	132.8	3.24E-07
48.5	-48	133.2	3.25E-07

45.9	-47.8	133.3	3.25E-07
43.8	-47.6	133.6	3.26E-07
41.5	-47.6	133.6	3.26E-07
39.6	-47.3	133.9	3.27E-07

Appendix K:

AF Demagnetization Data
Horseshoe Harbor Stromatolites

Field (mT)	Intensity (Am^2)	%Stdev	Declination (º)
0	3.91E-08	3.5	240.7
2	4.96E-08	1.9	236.5
4	3.98E-08	6.9	241.7
6	4.69E-08	1.9	240.1
8	4.57E-08	1.6	239.1
10	4.68E-08	2.3	242
12.5	5.16E-08	2.6	236.2
15	3.92E-08	3.5	243.6
20	3.68E-08	3.6	244.7
25	3.33E-08	7.5	241.7
40	3.72E-08	4.4	241.8
50	3.56E-08	5.2	238.7
60	3.83E-08	4.2	240.7
80	4.53E-08	2.8	239.7
100	4.00E-08	2.8	238.5
130	3.85E-08	2.9	239.1
160	3.36E-08	2.7	236.5
200	3.04E-08	2.2	236.3

Appendix L:

AF Demagnetization Data
Dan's Point Stromatolites

Field (mT)	Intensity (Am^2)	%Stdev	Declination (º)
0	1.22E-08	5.8	302.6
2	1.02E-08	4.5	306.2
4	1.30E-08	2.9	302.5
4	1.13E-08	5.4	302.3
6	2.09E-08	4.4	298.6
8	1.25E-08	2.4	302.6
10	3.17E-08	1.3	302.9
12.5	1.55E-08	9.8	303.5
15	5.25E-09	17.8	305.5
20	3.67E-09	10.6	313
25	1.16E-08	4.2	299.4
40	7.50E-09	10.3	297.6
50	6.54E-09	6.6	310.1
80	9.81E-09	4.6	302.4
100	7.29E-09	5.4	304
130	9.43E-09	4.4	300.3
160	7.01E-09	4.2	296.8
200	4.85E-09	5.2	294.1

Appendix M:

IRM Acquisition Data
Horseshoe Harbor Stromatolites

Field (mT)	Intensity (Am^2)	%Stdev	Declination (º)
2.5	3.25E-08	1.1	237.8
5	2.90E-08	0.5	238.3
10	2.15E-08	0.7	276.8
15	3.20E-08	2.9	319.9
20	6.78E-08	1.6	343
40	2.43E-07	1.7	354.1
60	3.88E-07	1.3	357.9
100	6.08E-07	0.8	358.4
200	1.27E-06	0.9	359.9
300	2.12E-06	0.9	1.6
500	3.73E-06	0.8	0.6
700	4.85E-06	0.9	3
1000	5.83E-06	0.9	2.2

Appendix N:

IRM Acquisition Data
Dan's Point Stromatolites

Field (mT)	Intensity (Am^2)	%Stdev	Declination (º)
2.5	8.58E-09	4.4	301.4
5	9.35E-09	3.5	314.6
10	1.79E-08	1.5	340.2
15	3.55E-08	1.6	347.3
20	6.68E-08	2.4	356
40	1.88E-07	1	351.1
60	2.92E-07	1.1	352
100	4.30E-07	0.5	353.1
200	6.99E-07	0.6	351.4
300	9.40E-07	0.9	352.3
500	1.31E-06	1	351.5
700	1.55E-06	0.8	351.6
1000	1.73E-06	0.9	352